A PHOTOMETRIC AND SPECTROSCOPIC STUDY OF SELECTED SOUTHERN, CHROMOSPHERICALLY ACTIVE STARS

A THESIS
SUBMITTED IN PARTIAL FULFILMENT
OF THE REQUIREMENTS FOR THE DEGREE
OF
DOCTOR OF PHILOSOPHY IN ASTRONOMY
IN THE
UNIVERSITY OF CANTERBURY
by
LYNDON WATSON

University of Canterbury
1999

Abstract

The results of a combined photometric and high-resolution spectroscopic study of southern active-chromosphere stars selected from the ROSAT Bright Source Catalogue are presented.

The star CS Ceti (HD 6628) is shown to be a single-lined spectroscopic binary and an orbital solution derived from radial-velocity measurements is presented. Evidence that one of the stars is an F-type dwarf and the other a highly active G-type subgiant is presented, together with information on the apparently asynchronous rotation of the latter and the spatial origin of its Hα emission.

The system BB Sculptoris (HD 9770) is shown to include a chromospherically active eclipsing binary of the BY Dra class and evidence that this is the star previously known as HD 9770B is presented. A precise orbital period is presented. Further evidence is presented to show that the star known as HD 9770A is also a binary system, one member of which dominates the absorption spectrum of BB Scl.

Two further stars selected from the Bright Source Catalogue are recommended for further study: HD 147633 in which a known binary system is found to contain a further chromospherically active, short-period, double-lined spectroscopic binary; and HD 222259, a known chromospherically active binary in the light curve of which a spot wave which persists on a time scale of years has been found and for which a precise period is presented.

In addition, the results of a continuing program of observation of the chromospherically active system GT Muscae (HR 4492) are presented. Evidence is presented that the known eclipsing binary system HD 101380 consists of A0 V and A0/2 V stars, and the period of the system is further refined. A combined photometric and high-resolution spectroscopic study of the active binary HD 101379 provides evidence that its active star is a late G-type bright giant rather than a K4 star as suggested in a previous study. Evidence that the source of its Hα emission lies in the space between the stars is discussed.

High-resolution spectra of two chromospherically active stars — CF Tucanae (HD 5303) and HD 219025 — observed for other programs are also presented and briefly discussed.

Preface

The program of research described in this thesis had its origin in a proposal by Dr D. A. H. Buckley of the South African Astronomical Observatory (hereinafter "SAAO") for a collaborative program of photometric and high-resolution spectroscopic observations of chromospherically active stars with ultraviolet excess. Medium-resolution spectra of southern stars chosen from the *ROSAT Bright Source Catalogue* were obtained at SAAO, and stars with excess emission in the H and K lines of calcium indicating chromospheric activity were selected for photometric observation at SAAO and the Mount John University Observatory (hereinafter "MJUO"), and high-resolution spectroscopy using the MJUO échelle spectrograph.

$UBV(RI)_{\rm C}$ photometry was obtained at SAAO in 1992 and 1993, and is included in the data analysed in this thesis. The balance of the photometric data which has been used was obtained by service observers at MJUO who also began $UBV(RI)_{\rm C}$ photometry in 1993 and continued to obtain data until the observational program ended in 1997. The service observers have been entirely responsible for the reduction of the photometric data to standard systems. Some high-resolution spectra were obtained by several observers during 1993. All other spectra were obtained by the writer from 1994 to 1997.

Chapters 3 and 4 relating to the binary systems CS Ceti (HD 6628) and BB Sculptoris (HD 9770) are expanded versions of papers submitted for publication in the *Monthly Notes of the Royal Astronomical Society*. Both papers were written by the present author, with the exception of the section of Chapter 4 relating to the use of a Wilson-Devinney program to fit physical stellar parameters to the photometry, and its results. The program which was used was a modification of the original Wilson-Devinney code by Dr J. D. Pritchard and the execution of the program, based on the present author's initial values of the physical parameters, was carried out entirely by Dr Pritchard who also contributed the relevant part of the paper which was submitted for publication.

In addition to the stars selected for study at SAAO, the program of research also included the active system GT Muscae (HR 4492) which has been the subject of photometric observations at MJUO since 1981. The present author made use of the $BV(RI)_C$ (and a small amount of U) photometry which has accumulated since 1981, and additionally obtained spectroscopic data on the system. Chapter 5, relating to this system, is intended for submission for publication in due course.

Contents

List of Tables

List of Figures

Chapter 1

Introduction and background

1.1 Definition of the class of chromospherically active stars

The RS Canum Venaticorum system was observed as early as 1930[1] to be an eclipsing binary system in which the light curve out of eclipse showed a variation of 0·13 magnitude amplitude. Sitterly's[2] photometry and Joy's spectroscopy[3] indicated that the secondary (cooler) component of the system was a subgiant positioned in the Hertzsprung-Russell diagram between the main sequence and the giant branch, and Popper & Ulrich[4] showed that it was likely that the RS CVn secondary was the more massive component of the binary system in the process of evolving from the main sequence to the giant branch. Hall[5] proposed a working definition of an RS CVn system as one in which the hotter star is of spectral type F–G, IV–V, at least the cooler star shows strong CaII H and K emission in its spectrum, and the orbital period of the system is between one and fourteen days.

Bopp & Fekel[6] defined a further class of chromospherically active stars, the BY Draconis class of late-type single or binary dwarfs with strong CaII H and K emission, and identified rapid rotation as a common feature of late-type active stars. Bopp & Rucinski[7] and Bopp & Stencel[8] defined a yet further class, the FK Comae Berenicis rapidly-rotating single evolved stars; and Fekel *et al*[9] identified a further class of more moderately-rotating single giant and subgiant active stars. The first catalogue of active binary stars by Strass-

[1]Sitterly B. W., 1930, *Contr. Princeton Univ.*, **11**, 21

[2]*ibid*

[3]Joy A. H., 1930, *ApJ.*, **72**, 41

[4]Popper D. M. and Ulrich R. K., 1977, *ApJ.*, **212**, L131

[5]Hall D. S., 1976, in *Proc. IAU Coll. 129, Multiply Periodic Phenomena in Variable Stars*, ed. Fitch W. S., Reidel, Dordrecht, p. 287

[6]Bopp B. W. and Fekel F. C., 1977, *AJ*, **82**, 490

[7]Bopp B. W. and Rucinski S.M., 1981, in *Proc. IAU Symp. 93, Fundamental Problems in the Theory of Stellar Evolution*, eds Sigimoto D., Lamb D. Q. and Schramm D. N., Reidel, Dordrecht, p. 177

[8]Bopp B. W. and Stencel R. E., 1981, *ApJ*, **247**, L131

[9]Fekel F. C., Moffett T. J. and Henry G. W., 1986, *ApJS*, **60**, 551

meier *et al*[10] noted that the increasing profusion of morphologically distinguished classes merely served to obscure the important common characteristic which was the chromospheric activity, and Hall[11] listed eleven classes of stars all connected by the common characteristic of chromospheric activity. Where the interest is in the syndrome and causes of chromospheric activity, as in the present project, it has now become more usual to refer to a class of active-chromosphere stars (hereinafter often referred to simply as "active" stars) which includes the RS CVn, BY Dra and FK Com classes and all other stars which meet the criteria for chromospheric activity. In the second catalogue of active binary stars, Strassmeier *et al*[12] listed stars which were not known to satisfy the formal criterion of H and K emission, but which were known to be chromospherically active by virtue of x-ray, Ca II infrared triplet and Hα emission.

Even quiet stars such as the Sun show emission in the cores of their Ca II H and K lines, but the definition of an exact level of emission which qualifies a star to be called "active" has not so far been necessary as only stars with a clearly very much stronger emission than other stars have been studied. While Ca II emission remains the *defining* characteristic of active-chromosphere stars, García López *et al*[13] proposed that the presence of a He I D_3 absorption line be adopted for the definition of active stars of early F type[14], and several other spectral and photometric characteristics, including x-ray emission[15], extreme ultraviolet emission[16], infrared excess[17], and emission in the cores of the Ca II infrared triplet[18] in emission have been used or proposed as *de facto* indicators of an excited outer atmosphere.

1.2 Evolutionary status of active stars

The survey of mass-radius, mass-colour and colour-luminosity relations by Popper & Ulrich[19] showed that RS CVn systems are following a normal evolutionary path in which the more massive component of the binary system has evolved to the subgiant or giant stage while the inactive star is still on the main sequence. Figure 1.3 is a Hertzsprung-

[10]Strassmeier K. G., Hall D. S., Zeilik M., Nelson E., Eker Z. and Fekel F. C., 1988, *Astron. Astrophys.*, **72**, 291

[11]Hall D. S., 1991, in *Proc. IAU Coll. 130, The Sun and Cool Stars: Activity, Magnetism, Dynamos*, eds Tuominen I., Moss D. and Rüdiger G., Springer-Verlag, Berlin, p. 353

[12]Strassmeier K. G., Hall D. F., Fekel F. C., and Scheck M. , 1993, *Astron. Astrophys.*, **100**, 173

[13]García López R. J., Rebolo R., Beckman J. E. and McKeith C. D., 1993, *Astron. Astrophys.*, **273**, 482

[14]Its presence implies temperatures high enough ($T > 10^4$ K) to populate the ^{3}P levels of He I, and thus the presence of an excited chromosphere. However, an absence of correlation of activity with surface structure indicates that the mechanism of excitation of these stars is fundamentally different from that of later-type active stars (possibly acoustic), and it might be more useful to classify them separately.

[15]E.g. Mathioudakis M. and Doyle J. G., 1992, *Astron. Astrophys.*, **262**, 523, and Haisch B. and Schmitt J. H. M. M., 1994, *ApJ*, **426**, 716

[16]Wood B. E., Brown A., Linsky J. L., Kellet B. J., Bromage G. E., Hodgkin S. T. and Pye J. P., 1994, *ApJS*, **93**, 287

[17]Katsova M. M. and Tsikoudi V., 1992, *Sov. Astron.*, **36**, 421

[18]Dempsey R. C., Bopp B. W., Henry G. W. and Hall D. S., 1993, *ApJS*, **86**, 293

[19]*op cit*

Russell diagram showing all of the stars listed in the second edition of the catalogue of chromospherically active binary stars by Strassmeier *et al.*[20] The list is not confined to stars classified as RS CVn. The majority are on the main sequence or in the subgiant or ascending giant branch stages, although one star (KU Pegasi, HD 218153) is listed with $M_V = -2{\cdot}0$ assumed from its spectral type.

FK Com stars have the spectral characteristics of late-type giants.[21] BY Dra systems consist of late-type dwarfs still on the main sequence.[22] The non-FK-Com class of moderately rapidly rotating single stars distinguished by Fekel & Balachandran[23] are evolved giant stars. The much-observed active star AB Doradus is a rapidly rotating pre-main-sequence star. Chromospheric emissions have also been observed from UV Ceti flare stars, W Ursae Majoris binaries, Algol-type binaries and cataclysmic variables. No active-chromosphere stars have been positively identified as AGB giants or later on the evolutionary sequence, but chromospheric activity is not particularly associated with any one evolutionary stage in the life of a pre-AGB star.

1.3 Rotation of active stars

Anomalously fast rotation for their luminosity class and spectral type is a common characteristic of active stars. Figures 1.1 and 1.2 plot the rotational $v \sin i$ of the stars listed in the second catalogue of active binary stars by Strassmeier *et al*[24] against, respectively, their absolute visual magnitude and their $(B-V)$ colour index. The sine of the unknown inclination i is a reducing factor for rotational velocities of random value between 0 and 1 with a mean value of $\frac{\pi}{8}$. Even without allowing for that effect, however, it is evident that active binary stars have rotational speeds ranging from $\geq$10 km/s to $>$ 100 km/s. The effect is not confined to binary active stars. The FK Com class of single active stars was initially identified by Bopp and Stencel[25] as a class of stars with a fast rotation which could not be explained by retention of primeval angular momentum because that would have required rotation speeds on the main sequence in excess of their break-up speeds. The explanation advanced then, and still accepted, was that stars of this class had coalesced from binary systems and still possessed the former binary systems' large angular momentum. The class of active single giants and subgiants distinguished by Fekel *et al*[26] are characterized by rotation periods which, although longer than those of the FK Com stars, are still shorter than predicted by stellar evolutionary theory for stars of their spectral type and luminosity class.

---

[20] Strassmeier, Hall, Fekel, and Scheck, *op cit*

[21] Bopp and Stencel, *op cit*, and Hünemörder D. P., Ramsey L. W., Buzasi D. L. and Nations H. L., 1993, *ApJ*, **404**, 316

[22] Bopp and Fekel, *op cit*, Vogt S. S. and Fekel F. C., 1979, *ApJ*, **234**, 958, and Bopp B. W., Noah P. V. and Klimke A., 1980, *Stellar Surface Phenomena: Stellar Rotation and the BY Draconis Syndrome in the High-Eccentricity Binary BD +24°692*, pub. Ritter Astrophys. Research Center

[23] Fekel F. C. and Balachandran S., 1993, *ApJ*, **403**, 708

[24] Strassmeier, Hall, Fekel and Scheck, *op cit*

[25] Bopp and Stencel, *op cit*

[26] Fekel, Moffett and Henry, *op cit*

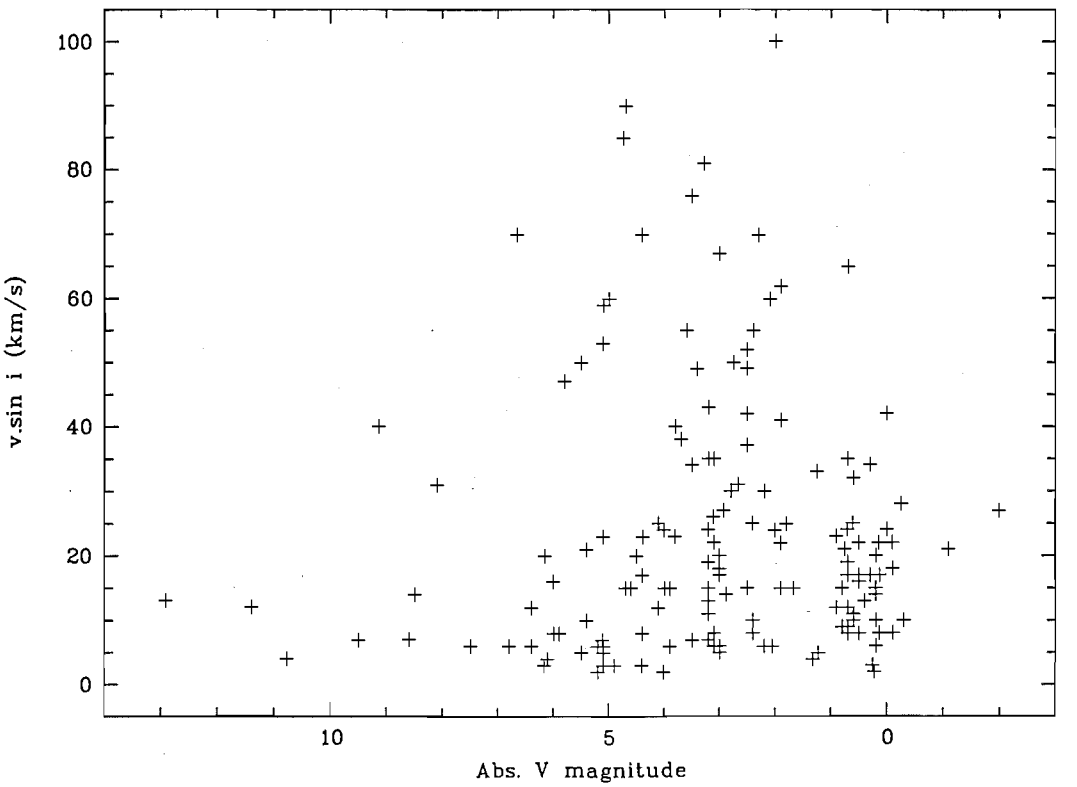

Figure 1.1: Rotational $v \sin i$ of chromospherically active binary stars listed in the second edition of the catalogue of Strassmeier K.G., Hall D. S., Fekel F. C., and Scheck M., 1993, *Astron. Astrophys.*, **100**, 173, plotted against their absolute visual magnitude. Where separate values have been listed for the hot and cool stars of a system, the cool star values have been selected. Systems for which a value is given for the hotter star only have been omitted.

1.3.1 Chromospheric activity and Rossby number

In 1986 Simon wrote[27] that a tight correlation had been found between the activity of main sequence stars and their Rossby number (the ratio of rotation period to convective turnover time) and that the relation was independent of mass for dwarfs of spectral types F to M. In 1988 Simon[28] observed that plotting chromospheric activity against Rossby number for random stellar populations generally yields a gaussian distribution having a flattened plateau on which activity changes only slowly relative to Rossby number. In the case of the Pleiades cluster where the stars are young main sequence stars which still have primeval rapid rotation, the gaussian mean occurs where the Rossby number is $N_R \approx 0{\cdot}1$, i.e. where the convective turnover time is only one tenth of the rotation

[27] Simon T., 1986, in *New Insights in Astrophysics*, ed. Rolfe E. J., E.S.A., p. 53

[28] Simon T., 1988, in *A decade of UV astronomy with the IUE satellite*, ed. Rolfe E. J., E.S.A., vol. 1, p. 279

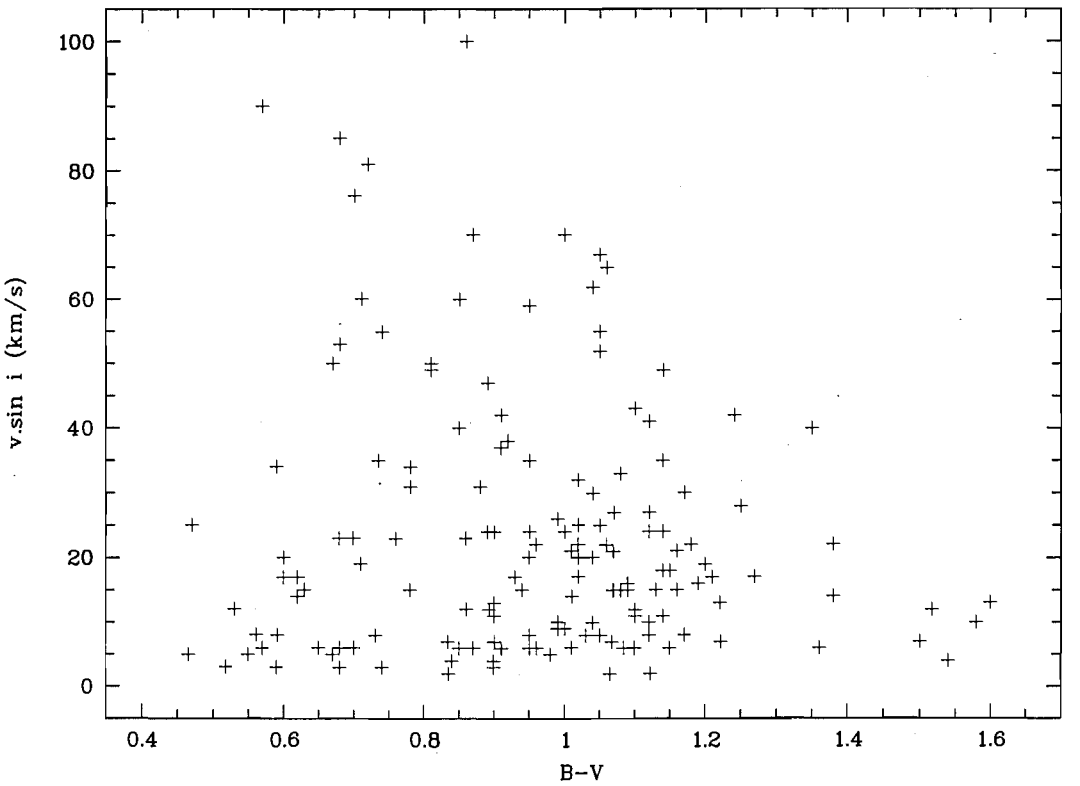

Figure 1.2: Rotational $v \sin i$ of chromospherically active binary stars listed in the second edition of the catalogue of Strassmeier K.G., Hall D. S., Fekel F. C., and Scheck M., 1993, *Astron. Astrophys.*, **100**, 173, plotted against their $(B - V)$ colour index. Where separate values have been listed for the hot and cool stars of a system, the cool star values have been selected. Systems for which a value is given for the hotter star only have been omitted.

period. Stępień[29] found that the Rossby number correlated well with activity for single dwarfs with $0{\cdot}5 \leq (B - V) \leq 0{\cdot}8$ but not well for single giants, and suggested that this difference indicated differences in structure and causes of chromospheric activity. Simon and Fekel [30] found a correlation between ultraviolet emission and rotation *simpliciter*, but Mathioudakis *et al*[31] found that the Rossby number is a better parameter than rotation period for describing levels of UV emission when the sample includes stars of differing effective temperatures, and Dobson and Radick[32] found that the Rossby number correlates better with coronal soft x-ray emission than simple rotation. The physical flows represented by the Rossby number are precisely those which are generally held to account

[29]Stępień K., 1994, *Astron. Astrophys.*, **292**, 191

[30]Simon T. and Fekel F. C., 1987, *ApJ*, **316**, 434

[31]Mathioudakis M., Fruscione A., Drake J. J., McDonald K., Bowyer S. and Malina R. F., 1995, *Astron. Astrophys.*, **300**, 775

[32]Dobson A. K. and Radick R. R., 1989, *ApJ*, **344**, 907

Orbital period (d)	Sample size	Asynchronous Number	Asynchronous % of sample	Possibly asynchronous	Total %
0–10	59	1	2	1	4
10·01–20	22	4	18	1	23
20·01–30	13	2	15	1	23
30·01–40	2	1	50	0	50
40·01–50	6	3	50	1	67
50·01–60	3	1	33	1	67
60·01–70	2	1	50	0	50
70·01–80	1	1	100	0	100
80·01–90	1	1	100	0	100
90·01–100	—	—	—	—	—
≥100·01	5	4	80	1	100

Table 1.1: Fraction of chromospherically active binaries with asynchronous rotational and orbital periods (after Fekel and Eitter, *op cit.*)

for a stellar dynamo in magnetic explanations of chromospheric excitation, and will be referred to further in Section 1.4.2 below.

1.3.2 Asynchronous rotation

Tidal theory[33] predicts that the rotation of binary stars will become synchronized with their orbits in a short time compared with the time taken to evolve to the giant stage, and generally in a shorter time than that which is required for their orbits to become circularized. Consequently it was predicted as early as 1981[34] that most RS CVn systems with periods less than 100 days should show synchronous rotation. A significant number, however, do not. Fekel & Eitter[35] investigated the distribution of asynchronously rotating stars in chromospherically active binary systems, and found asynchronous rotation (i.e. rotation having a period significantly different from the binary orbital period) in at least 15% of all systems having orbital periods from >20 to 30 days. Table 1.1 sets out their numerical analysis.

The problem of explaining asynchronously rotating stars in binary systems (in particular, in the case of active stars, stars having a rotation period *shorter* than their orbital period) is similar to that of explaining rapidly rotating evolved single stars — in both cases the anomalously fast rotation cannot be explained by tidal synchronization with orbital periods, and the explanations must be sought elsewhere. Any attempt to explain the phenomenon by attributing it to retention of primeval angular momentum actually amounts to nothing more than rephrasing the problem and leaving the questions of mechanism and history unanswered. It begs the question of how it is that some stars evolve

[33]Zahn J. P., 1977, *Astron. Astrophys.*, **57**, 383
[34]Middlekoop G. and Zwaan C, 1981, *Astron. Astrophys.*, **101**, 26
[35]Fekel F. C. and Eitter J. J., 1989, *AJ*, **97**, 1139

across the main sequence and into the subgiant stage without suffering the loss of angular momentum through mass loss that is predicted by theory and observed in most cases. The alternative is to invoke a mechanism by which a star, or at least its photosphere, gains angular momentum at a late stage of evolution on or off the main sequence.

1.3.3 Transfer of angular momentum

Pinsonneault *et al*[36] have developed models of stellar evolution wherein rotational braking on the main sequence leaves the core of a star spinning rapidly after the outer envelope has spun down, and Simon and Drake[37] suggested that the deepening of the convective zone as a star evolves towards the base of the red giant branch might bring rapidly rotating material to the surface, transferring angular momentum from the deep regions to the photosphere and creating an anomalously rapidly rotating star. Such a mechanism requires no assistance from a companion star and could explain both rapidly rotating single stars and stars in binary systems which are rotating with shorter periods than their orbital periods. The theory also has implications for the dredging-up of elements and isotopes not expected to be found in the envelope of an evolved star, and will be referred to again in Section 1.8 below.

Gray's Rotostat Hypothesis

Gray[38] distinguished a "rotation boundary" in the Hertzsprung-Russell diagram, extending from middle-F-type main sequence stars to K0 II, to the right of which rotation is seen to decrease rapidly by perhaps an order of magnitude, and argued that the sudden drop in rotation is caused by the onset of a dynamo-generated brake when the stellar convection zone deepens past a certain threshold. The hypothesis that the mechanism is magnetic in nature is supported by the observation that giant stars presumed to be subject to the brake have a small non-zero rotation — as would be expected from a magnetic brake when its driving mechanism (rotation) is reduced below a critical level. Gray also hypothesized a "rotostat" mechanism whereby deepening convention dredges up core material of high angular momentum[39] which increases the surface rotation enough to restart the dynamo and brake until the rotation is reduced to the minimum once again, the cycle possibly repeating many times. All RS CVn stars lie to the right of the rotation boundary, and Gray suggested that they are examples of stars with a large reservoir of angular momentum that the dynamo brake has not dissipated, the particularly powerful dynamo in these stars manifesting itself in magnetic activity indicators such as spots, flares, chromospheric emission, coronal x-rays and radio emission. The same account might be given of the FK Com and BY Dra stars and the active moderately-fast rotating single giants, but not of the early F active dwarfs considered by García López *et al*,[40] the chromospheres of which may be heated by acoustic mechanisms.

[36] Pinsonneault M. H., Kawaler S. D., Sofia S. and Demarque P, 1989, *ApJ*, **338**, 424
[37] Simon T. and Drake S. A., 1989, *ApJ*, **346**, 303
[38] Gray D. F., 1986, *Adv. Space Res.*, Vol. 6 No. 8, 161
[39] Cf Simon and Drake, *op cit*, and Section 1.3.3 above.
[40] *op cit*

HD No.	P_{orb} (d)	P_{rot} (d)	$i°_{orb}$	$i°_{rot}$	$\Delta i°$
352	96·44	96·32	60	69	9
1833	35·10	34·46	54	47	7
4502	17·77	17·76	71	75	4
13480	14·73	14·73	48	50	2
37824	53·58	54·10	53	61	8
37847	28·34	28·22	60	56	4
46697	13·64	13·07	20	17	3
57364	21·21	21·20	81	76	5
65626	11·08	10·16	60	65	5
101309	11·71	11·66	37	39	2
106677	64·44	63·80	65	64	1
115781	18·69	18·70	53	61	8
116204	20·62	20·70	26	24	2
119285	11·99	12·05	20	26	6
155638	27·54	27·07	80	70	10
158393	30·97	30·96	68	74	6
184398	108·57	108·80	48	47	1
185151	40·14	39·88	68	62	6
209813	24·43	24·46	59	68	9
250810	10·62	10·56	90	82	8

Table 1.2: Orbital and rotational periods and inclinations of the orbital planes and equatorial rotation planes for synchronous RS CVn systems with well-defined orbital and physical parameters (after Stawikowski A. and Głębocki R., 1994, *A.A.*, **44**, 33 and 393).

1.3.4 Co-rotation and coplanarity of orbit and rotation

It is commonly assumed[41] that RS CVn systems are coplanar, i.e. that the equatorial rotation planes (planes normal to their rotation axes) of their active stars are the same as their orbital planes. However, studies by Stawikowski and Głębocki[42] found that while none of a selection of long-period ($P > 10$ d), synchronously rotating ($P_{orb} - P_{rot} < \pm 2{\cdot}00$ d) RS CVn active stars with reliable orbital and physical parameters showed an inclination of their equatorial rotation planes relative to to their orbital planes greater than 10°, eight out of twelve *asynchronously* rotating such stars showed an inclination greater than 30°. No correlation was found between the degree of asynchronicity and the degree of non-coplanarity. Their figures are set out in Tables 1.2 and 1.3. The assumption of coplanarity is not safe when the system has asynchronous rotation, and it does not appear to be possible to predict the existence or the amount of non-coplanarity from the difference between the orbital and rotational periods.

[41] E.g. the catalogue of chromospherically active binary stars by Strassmeier, Hall, Fekel and Scheck, *op cit*

[42] Stawikowski A. and Głębocki R., 1994, *A.A.*, **44**, 33 and 393

HD No.	$P_{\rm orb}$ (d)	$P_{\rm rot}$ (d)	$i^\circ_{\rm orb}$	$i^\circ_{\rm rot}$	Δi°
7672	56·82	75·12	26	70	44
8357	14·30	12·24	26	32	6
10909	15·05	32·28	14	65	51
30050	39·28	31·40	89	85	4
34029	104·02	8·00	43	41	2
71071	16·54	21·00	17	77	60
72688	45·13	19·34	20	16	4
102509	71·69	55·00	52	68	16
181809	13·04	60·23	9	53	44
185510	20·66	25·64	83	44	39
217188	47·12	91·20	20	65	45
222107	20·52	53·95	15	70	55

Table 1.3: Orbital and rotational periods and inclinations of the orbital planes and equatorial rotation planes for asynchronous RS CVn systems with well-defined orbital and physical parameters (after Stawikowski and Głębocki, *op cit*).

1.4 Mechanisms of chromospheric excitation

It is now generally accepted, at least since the work of Eaton & Hall,[43] that the characteristic light curves of active-chromosphere stars are governed by cool spots on their photospheres, while the emissions which define the class are chromospheric in origin. (Not all emissions are necessarily chromospheric in origin. Armado & Byrne[44] found, by plotting $(U-B)_0$ against $(B-V)_0$ for a large sample of stars, that 89·50% of active giants and all active subgiants were bluer than mean zero-reddening curves, i.e. they had an ultraviolet excess. They suggested that, since chromospheric ultraviolet emissions could not account for the excess, faculae on the photosphere might be responsible.) A major unsolved problem in stellar astrophysics is that of identifying the mechanisms responsible for heating stellar chromospheres and coronae and for driving stellar winds. Observations in the near and far ultraviolet as well as the optical region, together with theoretical modelling, have led to the general conclusion that, outside the class of pulsating stars with which this project is not concerned, the possible mechanisms can be divided into two classes which correspond with different aspects of stellar structure: firstly, acoustic mechanisms and, secondly, magnetic mechanisms.

1.4.1 Acoustic mechanisms

The theoretical mechanism of acoustic heating is the upward propagation of sound waves having their origin in turbulence in the convective zone. Because of the strong density gradient and energy conservation, the amplitude of the waves increases as they propagate

[43] Eaton J. A. and Hall D. S., 1979, *ApJ*, **227**, 907

[44] Armado P. J. and Byrne P. B., 1997, *Astron. Astrophys.*, **319**, 967

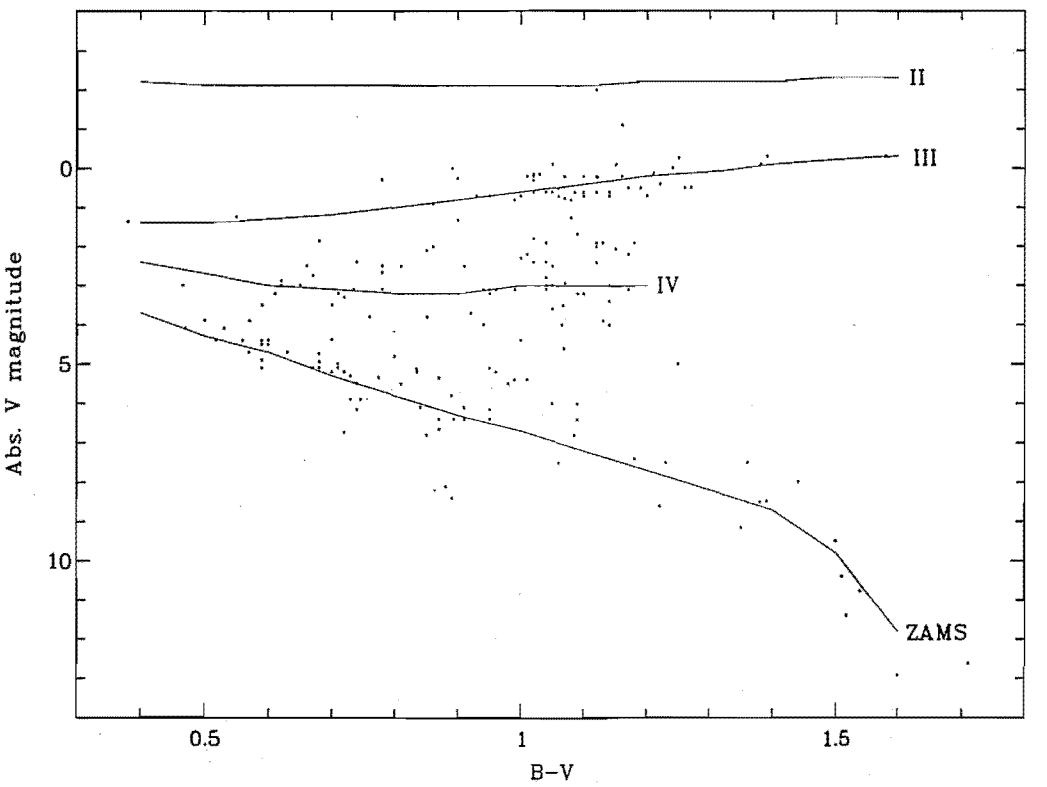

Figure 1.3: H-R diagram of chromospherically active binary stars listed in the second edition of the catalogue of Strassmeier, Hall, Fekel, and Scheck, *op cit.* Where separate values have been listed for the hot and cool stars of a system, the cool star values have been selected. Canonical values for luminosity classes II, III and IV, and for the zero-age main sequence, have been adopted from Allen C. W., 1976, *Astrophysical Quantities*, Athlone, London, at §98.

upwards to yield shocks and consequent heating in the stellar chromosphere (or, to put it another way, in a region of the atmosphere which is denoted the chromosphere by virtue of being heated relative to the atmosphere underlying it). Ulmschneider[45] has shown theoretically that the flux must increase with increasing temperature (from late-type to early-type stars) but must cease when the convective envelope disappears in stars earlier than early F-type. The effect of acoustic heating is, therefore, expected to be strongest in early F, say F0 to F5, stars, and it is in that range of spectral types that magnetic mechanisms are less favoured — "the absence of significant rotational or age dependence of chromospheric activity indicators in the range F0-F5, jointly with the low scatter observed in the chromospheric activity for these stars, implies strongly that a non-magnetic mechanism must be at work in heating the chromosphere."[46]

[45]See e.g. Narain U. and Ulmschneider P, 1990, *Space Sci. Rev.*, **54**, 377

[46]García López *et al, op cit*

Schrijver[47] and Rutten *et al*[48] statistically analysed relative fluxes and flux-colour relations in selected emission lines, from late-type stars, and separated the emission into a "basal" flux which is an intrinsic property of even quiet stars independent of stellar rotation and which might be attributable to pure acoustic heating of the chromosphere, and an additional flux which varies with rotation and age. Mathioudakis & Doyle[49] found that even in very inactive M dwarfs there is a lower limit to flux in Mg II emission which is closely related to classical stellar parameters such as effective temperature, implying that it is due to acoustic heating of the chromosphere. They found that excess flux over the basal flux in active stars, on the other hand, is closely related to coronal x-ray emission and is present mainly in the line wings, indicating that it is due to magnetic activity in the chromosphere. Strassmeier *et al*[50] examined absolute Ca II surface fluxes in the spectra of evolved G and K giants and found that, although the fluxes were linearly proportional to inverse rotation period, there was, for any given rotation period, a wide range of fluxes, suggesting that some parameter in addition to rotation was having an effect. When fluxes were plotted against effective temperature, there appeared to be a lower limit to the flux which was temperature-dependent and might represent a basal flux underlying a rotation-dependent flux. A relation

$$\log(\text{basal flux}) = 8 \log T_{\text{eff}} - 24{\cdot}8$$

was derived, but subtracting that basal flux did not improve the scatter in the observed fluxes, indicating that temperature was not the sole parameter governing the strength of the emission.

Theoretical acoustic heating models by Buchholz & Ulmschneider[51] produced model fluxes that agreed well with the observed fluxes of inactive dwarfs over the range of spectral types from F5 to M0. Carlsson & Stein[52] have developed numerical simulations of "grains" in Ca II H- and K-line images of the solar chromosphere which agree well with a theoretical model of a sub-photospheric "piston" producing upwardly propagating acoustic shock-waves which carry thermal energy to the chromosphere.

1.4.2 Magnetic mechanisms

The primary evidence for the association of starspots with magnetic phenomena comes from observation of the Sun. Nearly a century ago Hale showed that sunspot pairs are associated with strong magnetic fields, and formulated a polarity law which has been applied[53] to explain a pair of sunspots as the "footprints" of a loop of magnetic field lines

[47] Schrijver, C. J., 1987, *Astron. Astrophys.*, **172**, 111

[48] Rutten, R. G. M., Schrijver C. J., Lemmens A. F. P. and Zwaan C., 1991, *Astron. Astrophys.*, **252**, 203

[49] *op cit*

[50] Strassmeier K. G., Handler G, Paunzen E. and Rauth M., 1994, *Astron. Astrophys.*, **281**, 855

[51] Buchholz B. and Ulmschneider P., 1994, in *Cool Stars, Stellar Systems and the Sun VIII*, ed. Caillaut J.-P., ASPCS, p. 363

[52] Carlsson M. and Stein R. F., 1994, in *Chromospheric Dynamics*, ed. Carlsson M., Inst. Theor. Astrophys., Oslo, p. 47

[53] Parker E. N., 1955, *ApJ*, **122**, 293

(or "flux tube") where it emerges from and re-enters the solar photosphere. Theoretical analyses[54] attribute the magnetic flux tubes to modification of the stellar magnetic field by dynamo activity in the convective zone which in its turn depends on both convective flows and plasma flows induced by rotation, and suggest means by which the magnetic flux tubes in active stars might transfer energy from the convective zone to the chromosphere of an active star. Hall[55] provided a theoretical basis for relating spot activity to both stellar rotation and convection, predicting that the Rossby number must be less than 0·67 for spot activity to be observed. Observational evidence — correlation of chromospheric activity with rotation rate or Rossby number, correlation of chromospheric activity with spot waves, coronal activity, measurements of surface magnetic flux in active stars, helioseismological observations of solar convective flows — points to the excitation of the chromospheres of late-type and giant active stars by magnetic mechanisms connected with the processes responsible for photospheric spots.

Mullan[56] discussed the astrophysical basis of the activity of red dwarf flare stars and spotted stars in general, including AR Lacertae and RS CVn. On the assumption that the chromosphere is heated by Alfvén waves originating in convective cells in the photosphere, his model required surface magnetic fields between 1 and 3 tesla produced by a dynamo driven by the rotation of the star. The survey of BY Dra stars by Bopp and Fekel[57] found that they all had a rotational $v \sin i$ of at least 5 km/s. Simon[58] noted that a tight correlation exists between the activity of main-sequence stars and their Rossby number. Strassmeier *et al*[59] found that absolute Ca II surface fluxes calculated from the H and K lines of evolved G and K giants were linearly proportional to the inverse rotation period, albeit with the wide range of fluxes for any given rotation period which implies a basal flux of different origin.

The strength of emission lines formed in the solar chromosphere and transition region varies greatly with position across the surface of the Sun, but is tightly correlated with magnetic flux. Cool stars show a correlation of emission-line flux with rotational velocity indicating the onset of a Sun-like rotation-driven dynamo near $(B - V)$ =0·45 (sp. F6 V).[60] Ultraviolet emission has also been shown to be dependent on rotation[61] or Rossby number.[62]

[54]See generally the papers published in Tuominen I., Moss D. and Rüdiger G., eds, 1991, Proc. IAU Coll. 130 *The Sun and Cool Stars: activity, magnetism, dynamos*, Springer-Verlag, Berlin.

[55]Hall, 1991, *op cit*

[56]Mullan D. J., 1974, *ApJ*, **192**, 149

[57]*op cit*

[58]Simon, 1986, *op cit*

[59]Strassmeier, Handler, Paunzen and Rauth, *op cit*

[60]Jordan C. and Linsky J. L., 1987, in *Exploring the Universe with the IUE Satellite*, ed. Kondo Y., Reidel, Dordrecht, p. 259

[61]Simon and Fekel, *op cit*

[62]Mathioudakis, Fruscione, Drake, McDonald, Bowyer and Malina, *op cit*

1.5 Excess fluxes at non-optical wavelengths

As noted in previous sections, in addition to emissions at wavelengths corresponding to particular bound-bound transitions in the optical region and the near infrared and ultraviolet, active stars are characterized by broad-band excess fluxes in the x-ray, far ultraviolet, infrared and radio regions.

1.5.1 Excess x-ray emission

X-ray emissions occur both as "quiet" emissions and flares, sometimes both in the same star, such as HR 3922,[63] and are attributed to the corona. Mathioudakis and Doyle[64] observed that Mg II emission in active stars is closely related to coronal x-ray emission, suggesting that the same, probably magnetic, mechanism is responsible for both the chromospheric and the coronal heating, or that there is a transfer of energy from the chromosphere to the corona when the former is heated. Mullan and Johnson[65] modelled the coronal heating of x-ray flare stars using magnetic coronal loops heated by resonant magneto-hydrodynamic absorption so that the loops extending into the corona acts as a resonant cavity. They noted that the coronal loops of flare stars appear to have resonance times which are matched to their convection time-scales, which may explain how they are particularly efficient at coronal heating.

The relation between x-ray emission and spot waves is well established[66] and the prevailing magnetic model of chromospheric and coronal heating accommodates the relation by postulating magnetic flux tube loops intersecting the photosphere in regions which are cooled by loss of energy (and are therefore observed as spots) and passing through the chromosphere in regions, not necessarily exactly above the spots, which are heated in the rearrangement of the energy budget in the presence of localized magnetic fields (and are therefore observed as bright plages in the emission wavelengths) to have their summits in the stellar corona.

1.5.2 Excess ultraviolet emission

The ROSAT wide-field camera (WFC) operating in the extreme ultraviolet (EUV) detected excess fluxes from stars having photospheres insufficiently hot to emit in that wavelength region. Such stars must have heated atmospheres outward of the photosphere (otherwise the EUV would be absorbed), and those atmospheres must be abnormally hot to emit at wavelengths corresponding to transitions downward from highly excited electronic states. Thus, Mulliss and Bopp[67] suggested that late-type ROSAT WFC sources

[63] Haisch B. and Schmitt J. H. M. M., 1994, *ApJ*, **426**, 716

[64] *op cit*

[65] Mullan D. J. and Johnson M., 1995, in *IAU Symposium No. 176, Poster Proceedings*, ed. Strassmeier K. G.,Institut für Astronomie, Vienna, p. 206

[66] See, for example, Kürster M., 1996, in *Proc. IAU Symp. 176, Stellar Surface Structure*, eds Strassmeier K. G. and Linsky J. L., Kluwer, Dordrecht, p. 477.

[67] Mullis C. L. and Bopp B. W., 1994, *PASP*, **106**, 822

were good candidates in a search for chromospherically active stars, and that suggestion was followed in the present project.

Armado and Byrne[68] (see Section 1.4) found that 89·5% of active giants and all active subgiants in a sample of active stars had an ultraviolet excess which could not be accounted for by chromospheric emission, and suggested that faculae on the stellar photospheres might be responsible. Wood *et al*[69] established a relation between coronal EUV emission and and bolometric luminosity for 220 non-degenerate stars within 10 pc, and found that known RS CVn stars have excess coronal EUV emission according to that relation. Based on observations of AR Lac, they suggested that the magnetic fields of RS CVn systems might interact in such a way as to produce an extended corona which fills a larger volume of space than normal coronae.

1.5.3 Excess infrared emission

Katsova and Tsikoudi[70] reported that K and M stars with surface activity have been found to have an infrared excess which correlates with magnetic fluxes, and offered three possible explanations of the phenomenon: (a) absorption at short wavelengths and re-emission in the infrared by dust grains surrounding the star or, in the case of binary stars, accumulating at a Lagrangian point, (b) synchrotron or other high-energy radiation from accelerated particles originating in flare-type processes, and (c) emission by relatively cool regions (spots) in the stellar photospheres.

1.5.4 Excess radio emission

The average radio emission from RS CVn stars is about 10^{20} W compared with about 10^{13} W for the Sun.[71] Steady radio emissions from late-type active coronae can roughly be divided[72] into gyroresonance emission from thermal, optically thick plasma in strong magnetic fields in the lower corona, and gyrosynchrotron emission from accelerated, magnetically trapped electrons, both being ultimately due to the same magnetic mechanism that heats the chromosphere. The presence of large loops has been confirmed by microwave observations of AB Dor,[73] but no correlation has been found between the rotational phase of the radio source on the one hand and the chromospheric plages and photospheric spots on the other. The RS CVn star CF Tucanae which was briefly observed during the present program (Chapter 6) is a moderately active radio source which occasionally flares.[74]

---

[68] *op cit*

[69] *op cit*

[70] *op cit*

[71] Zeilik M. and Smith E. v P., 1987, *Introductory Astronomy and Astrophysics*, Saunders, Philadelphia

[72] Güdel M., 1996, in *Proc. IAU Symp. 176, Stellar Surface Structure*, eds Strassmeier K. G. and Linsky J. L., Kluwer, Dordrecht, p. 485

[73] Budding E., Burgess A., Chan S. and Slee O. B., 1992, in *Surface inhomogeneities on late-type stars*, eds Byrne P. B. and Mullan D. J., Springer Lect. Notes Phys., **397**, at p. 253

[74] Slee O. B., Nelson G. J., Stewart R. T., Wright A. E., Innis J. L., Ryan S. G. and Vaughan A. E., 1987, *MNRAS*, **229**, 659

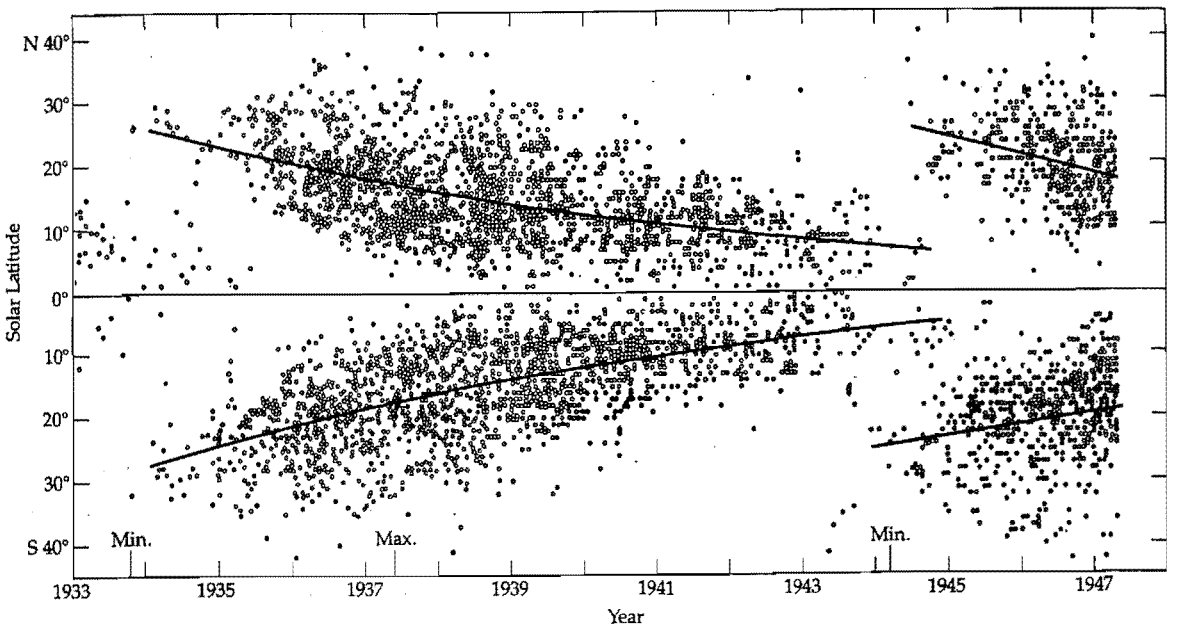

Figure 1.4: The latitude of sunspots during the interval 1933–1947 (after Abetti, G., 1969, *The Sun*, Faber and Faber, London).

1.6 Differential rotation and spot size, lifetime and location

The Sun, a "quiet" star, has a well-observed 11-year (22 years if the orientation of magnetic poles is also taken into account) cycle of spot formation and apparent migration, the spots initially forming at relatively low latitudes (~30–40°) and having a lifetime from a few days to a few months depending on the size, and subsequent spots forming at lower latitudes until the cycle ends with the spots being concentrated at ~8–15°. Figure 1.4 plots the latitudes of the sunspots observed from 1933 to 1947 against time. Solar spots are rarely more than ~60,000 km in diameter.

At any given time, the spots appear in a narrowly defined longitudinal zone of the Sun, the so-called "active longitude". Gaizauskas *et al*[75] found that active longitudes typically persist for a few rotations, and Castenmiller *et al*[76] found that such zones can reactivate after lapsing into inactivity for up to $2\frac{1}{2}$ rotation periods.

1.6.1 Size of spots on active stars

The amplitude of light curves attributed to spots on active stars typically implies that the spots cover a much larger fraction of the stellar photosphere than is covered by sunspots. Hall[77] has shown that there are two types of convective star: (a) inactive or weak-dynamo

[75] Gaizauskas V., Harvey K. L., Harvey J. W. and Zwaan C., 1983, *ApJ*, **265**, 1056
[76] Castenmiller M. J. M., Zwaan C. and van der Zalm B. J., 1986, *Solar Physics*, **105**, 237
[77] Hall, 1991, *op cit*

stars such as the Sun which have only small spots, and (b) active or strong-dynamo stars with spots which can be large enough to cover half a visible hemisphere (e.g. XX Tri[78]). What is not known is whether such very large spots are one hugely magnified version of a solar spot with an umbra and a surrounding penumbra, or a pair of spots with magnetically north and south components, possibly accommodating both "legs" of the one coronal loop, or a clump of spots of similar size to sunspots, or a clump of spots of some intermediate size.

The physical factors determining the sizes of spots are not known. Correlation of spot coverage with activity[79] implies a relation between spottedness and Rossby number and suggests a dependence of spot size on the strength of the magnetic fields associated with coronal loops, but no connection between the physical conditions in the photosphere and convective zones of active stars and the size and number of their spots has been established.

1.6.2 Differential rotation of active stars

The solar rotation period increases with the square of the sine of the latitude, being about 25 days at the equator, about 27 days at 40° latitude, and about 30 days at 70°. It has been observed[80] that some active stars have surface rotation which differentiates in the opposite sense to the that of the Sun, i.e. the rotation period *decreases* with increasing latitude, and that for very short rotation periods the differential rotation decreases with rotation period[81] so that the fastest-rotating stars approach rigid-body rotation, a condition not predicted by linear dynamo theory.

1.6.3 Lifetime of spots on active stars

Hall and Henry[82] subjected several dozen spotted stars to continuous photometric observation for ten years, and found that the lifetimes were proportional to their sizes, similar to the relation which governs the lifetime of solar spots, subject to an upper limit (therefore affecting the larger spots) equal to the time required for them to be disrupted by differential surface rotation (Hall and Henry cautiously avoided claiming that differential rotation actually *was* the mechanism limiting the spot lifetimes).

1.6.4 Location of spots on active stars

Donahue *et al*[83] have found evidence for the existence of *chromospheric* active longitudes (located by CaII H and K emission) in a survey of 35 late-type stars. The existence of

[78]Nolthenius R., 1991, *IBVS* No. 3589

[79]Hall, 1991, *op cit*

[80]*ibid*

[81]Hall D. S., *ibid*, and Rodonò M., 1986, in *Cool Stars, Stellar Systems and the Sun, Fourth Cambridge Workshop*, eds Zeilik M. and Gibson D. M., Springer-Verlag, Berlin, p. 475

[82]Hall D. S. and Henry G. W., 1994, *IAPPP Comm.*, **55**, 51

[83]Donahue R. A., Dobson A. K. and Baliunas S. L., 1996, *Harvard-Smithsonian Center for Astrophysics Preprint series* No. 4423

photospheric active longitudes in active stars might be inferred from that finding, but has not yet been proved.

The main questions associated with the location of spots on active stars arise out of attempts to model the spots and, especially out of attempts to map stellar photospheres using Doppler imaging technique.

1.7 Modelling star spots

Techniques for modelling starpots range in complexity of method and detail of result from modelling a simple, regular light curve by a single circular spot[84] to methods of constructing a stellar image from sets of rotationally modulated line profiles (Doppler imaging). Purely photometric methods include parameter-fitting methods and the methods of Vogt,[85] Gershberg *et al*[86] and Strassmeier & Olah[87] for determining the temperatures of spots from variations in V and $(V-I)$, from which the fractional area of the star covered by the spot or spots may be calculated. Mixed photometric and spectroscopic techniques include the cross-correlation method of Eaton *et al*[88] for determining the number of spots on a star and the use of photometry and ultraviolet spectra by Olah *et al*[89] to reconstruct the flux of the immaculate star.

Doppler-imaging techniques require a moderately high rotational $v \sin i > 36$ km/s, high resolving power $\lambda/\Delta\lambda \geq 60\,000$, and very high S/$N \geq 400 : 1$[90] For spectra with $15 < v \sin i < 40$ km/s, Dempsey *et al*[91] developed a method of cross-correlating the spectra with spectra of inactive narrow-line stars of similar spectral type and inverting the cross-correlation function to obtain information about the latitude and evolution of the spots from spot-induced line profile asymmetries.

1.7.1 High-latitude spots

Simple light-curve analysis (see, for example, the treatments of HD 101379 and CF Tuc in this project) has shown that some active stars must have a spot coverage so extensive that it cannot be confined to low latitudes as sunspots are. So it is not a surprise that Doppler imaging techniques produce maps of active stars showing spots at high, even polar, latitudes. However, it is, perhaps, surprising that the maps of fast-rotating stars tend to produce polar spots and high-latitude spots on stars with no or few low-latitude spots, and polar and high-latitude spots which are long-lived while low-latitude spots

[84] E.g. Banks T. and Budding E., 1990, *Ap&SS*, **167**, 221

[85] Vogt S. S., 1981, *ApJ*, **250**, 327

[86] Gershberg R. E., Il'in I.V. and Sharkhovskaya N. I., 1991, *Sov. Astron.*, **35**, 479

[87] Strassmeier K. G. and Olah K, 1992, *Astron. Astrophys.*, **259**, 595

[88] Eaton J. A., Gregory W. H., Bell C. and Okorogu A., 1993, *AJ*, **106**, 1181

[89] Olah K, Budding E., Butler C. J., Houidebine E. R., Gimenez A. and Zeilik M., 1992, *MNRAS*, **259**, 302

[90] Dempsey R. C., Bopp B. W., Strassmeier K. G., Granados A. F., Henry G. W. and Hall D. S., 1992, *ApJ*, **392**, 187

[91] *ibid*

are transient (for example UX Arietis,[92] EI Eridani,[93] HU Virginis[94] and HR 1099[95]). The longer life of high-latitude spots might be explained by differential rotation and the observed phenomenon of differential rotation decreasing with rotation period for fast-rotating stars (Section 1.6.2 above), but the omnipresence of polar spots when none are observed on the Sun does raise questions about the mechanisms responsible for them. A more extensive spot coverage than on the Sun might be explained by more complex and powerful dynamo processes produced by the combination of fast rotation and deep convection, and polar spots might be explained by postulating an Earth-like dynamo, possibly close to the stellar core, producing a magnetic field directed along the axis of rotation.

1.8 Lithium excess

The resonance doublet of neutral lithium at 6707·8 Å is an important diagnostic of mixing in late-type stars. Since lithium is easily destroyed by nuclear reactions at temperatures $\geq 2{\cdot}5 \times 10^6$ K, the surface layers of a star are progressively depleted in lithium as a result of convection, microscopic and turbulent diffusion, and meridional circulation. The λ6708 line is strongly enhanced in sunspots relative to the quiet solar photosphere by as much as a factor of ~ 50 because of lower temperatures and hence ionization levels.[96] In plage spectra, on the other hand, it is weakened by a factor of up to 2 because of non-radiative heating and ionization. Giampapa[97] suggested that the strength of disc-integrated Li lines in stellar spectra should therefore be significantly affected by surface activity, and Pallavicini *et al* (1987)[98] suggested that very extensive spots could be responsible for the strong Li line sometimes observed in RS CVn binaries. However Pallavicini *et al* (1992)[99] also recognized that it is not characteristic of RS CVn stars as a class and there is no obvious relationship between its strength and the spottedness of the stars, and Pallavicini *et al* (1993)[100] found that the strength of the Li line did not vary with the light curves of four active stars.

It appears likely, therefore, that the lithium enhancement observed in some active stars is not due directly to the same mechanism or stellar features as the activity, but to some other mechanism, possibly one which is connected with the evolutionary status of the stars. Fekel & Balachandran[101] found lithium excess in all of a sample of moderately

[92] Vogt S. and Hatzes A., in *Proc. IAU Coll. 130, The Sun and Cool Stars: Activity, Magnetism, Dynamos*, eds Tuominen I., Moss D. and Rüdiger G., Springer-Verlag, Berlin, p. 297

[93] Strassmeier K. G., Rice J., Wehlau W., Vogt S., Hatzes A., Tuominen I., Piskunov N., Hackman T. and Poutanen M., 1991, *Astron. Astrophys.*, **247**, 130

[94] Strassmeier K. G., 1994, *Astron. Astrophys.*, **281**, 395

[95] Donati J.-F., Brown S., Semel M., Rees D., Dempsey R., Matthews J., Henry D. and Hall D. S., 1992, *Astron. Astrophys.*, **265**, 682

[96] Grevesse N., 1968, *Solar Phys.*, **5**, 159, Traub W. and Roesler F. L., 1971, *ApJ*, **163**, 629, and Giampapa M. S., 1984, *ApJ*, **277**, 235

[97] Giampapa, 1984, *ApJ*, **277**, 235

[98] Pallavicini R., Cerruti-Sola M. and Duncan D. K., 1987, *Astron. Astrophys.*, **174**, 116

[99] Pallavicini R., Randich S and Giampapa M, 1992, *Astron. Astrophys.*, **253**, 185

[100] Pallavicini R., Cutispoto G., Randich S. and Gratton R., 1993, *Astron. Astrophys.*, **267**, 145

[101] *op cit*

rapidly rotating ($v \sin i$ = 6–46 km/s) chromospherically active single giants, not strongly correlated with the amount of activity, and proposed a mechanism whereby lithium produced by the reaction chain

$$^3\mathrm{He}(\alpha,\gamma) \rightarrow {}^7\mathrm{Be}(,\mathrm{e}^+\nu) \rightarrow {}^7\mathrm{Li}$$

at the bottom of the convective envelope of a star on the ascending red giant branch is dredged up to the surface by movements associated with the transfer of angular momentum from a rapidly rotating core to the atmosphere of the star as proposed by Simon & Drake.[102] Since the excited envelope produced by the coalescence of a binary system would be expected to preclude the survival of surface lithium, Fekel and Balachandran suggested the use of the presence of lithium as a test to distinguish true FK Com stars produced by binary coalescence from less rapidly rotating single giants which are the product of a dredge-up of angular momentum, and suggested that, indeed, the only true FK Com stars might be FK Com itself and HD 199178.

De la Reza *et al*[103] proposed an evolutionary model wherein every star with a mass between 1 and 2·5 $M_\odot$ becomes lithium-rich while a K giant, and the internal mechanism responsible for the enrichment also initiates a mass-loss event which produces an infrared excess. If this model holds, then excess lithium will be observed in the spectra of slow-rotating stars and synchronously rotating binary stars, and not just in the spectra of anomalously rapidly rotating single stars.

1.9 Hα emission

Irregular and variable Hα emission, usually partially filling the photospheric absorption line but sometimes seen in strong emission[104] is also characteristic of active stars and has been associated with non-thermal flaring at radio wavelengths. Bopp & Talcott,[105] Feldman *et al*,[106] Fraquelli,[107] Furenlid & Young,[108] Hearnshaw,[109] Hobbs *et al*,[110] Popper[111] and Weiler *et al*[112] observed flaring by the RS CVn system HR 1099 in radio, optical and ultraviolet wavelengths.

The sources of chromospheric emission are bright regions ("plages") in Hα which have been observed in RS CVn systems to overlie photospheric spots, although the alignment of

[102] *op cit*

[103] de la Reza R., Drake N. A. and da Silva L., 1996, *ApJ*, **456**, L115

[104] See e.g. Jetsu L., Huovelin J, Savanov I. and Tuominen I, 1991, *Astron. Astrophys.*, **248**, 574 on the FK Com star HD 199178.

[105] Bopp B. W. and Talcott J. C., 1978, *AJ*, **83**, 1517

[106] Feldman P. A., Taylor A. R., Gregory P. C., Seaquist E. R., Balonek T. J. and Cohen N. L., 1978, *AJ*, **83**, 1471

[107] Fraquelli D. A., 1978, *AJ*, **83**, 1535

[108] Furenlid I. and Young A., 1978, *AJ*, **83**, 1527

[109] Hearnshaw J. B., 1978, *AJ*, **83**, 1531

[110] Hobbs R. W., Kondo Y. and Feibelman W. A., 1978, *AJ*, **83**, 1525

[111] Popper D. M., 1978, *AJ*, **83**, 1522

[112] Weiler E. J., Owen F. N., Bopp B. W., Schmitz M., Hall D. S., Fraquelli D. A., Piirola V., Ryle M. and Gibson D. M., 1978, *ApJ*, **225**, 919

the plages and the spots is not perfect: Catalano *et al*[113] modelled a cool spot (from *BV* photometry) and a region of enhanced Hα flux (from variations in Hα equivalent width) on UX Ari, HR 1099 and HK Lac using V and colour photometry and Hα equivalent width, and found a phase difference of 2° to 57° longitude between spot and plage, as well as less precisely determined differences in latitude. Butler[114] noted that the association between plages located using Mg II lines and spots has been firmly established only for RS CVn stars, and not for BY Dra systems, but this may be due to a lack of clear rotational modulation data caused by frequent flaring and filling in of the Mg II lines.

In a theoretical exercise on coronal magnetic loop structures with lengths comparable to or greater than a stellar radius on rapidly rotating main sequence stars, Collier Cameron[115] found that numerical models for static loops in thermal and hydrostatic equilibrium yielded two classes of solution: (a) stable "hot" loops with temperature maxima at their summits, and (b) unstable "cool" loops with temperature minima at their summits. Such loops extending outside the Keplerian co-rotation radius of the star could concentrate trapped plasma in prominence-like concentrations outside the co-rotation radius. Collier Cameron & Robinson[116] reported that AB Dor had cool, dense, neutral hydrogen clouds embedded in and co-rotating with the hot, extended corona between 3 and 4 stellar radii from the stellar rotation axis and ranging in projected area between 3% and 20% of the stellar surface area. In the case of AB Dor, the co-rotation radius was calculated as $2{\cdot}7\,R_\star$. Collier Cameron & Woods[117] reported observations of time-series transients in Hα spectra of four rapidly rotating G dwarfs of the α Persei cluster from which the presence of similarly extended hydrogen clouds in the corona was deduced. Doyle & Collier Cameron[118] and Jeffries[119] reported similar phenomena in the Hα profiles of the rapidly rotating M dwarf HK Aquarii and the rapidly rotating field star HD 197890, respectively. Jeffries[120] has also presented a model explaining dips in the x-ray light curve of XY UMa as the product of cool condensations forming in plasma in extended coronal loop apexes. It should be noted, however, that the mechanism suggested by Collier Cameron is doubted by van den Oord & Zuccarello.[121]

The Hα line of FK Com is observed as a broad emission feature with a double peak. Hünemörder *et al*[122] suggested that the rotationally-broadened emission may have its source in co-rotating material extending to several stellar radii while the the central absorption may be due to less extended, high-latitude material. Welty *et al*[123] suggested

[113] Catalano S., Rodonò M., Frasca A. and Cutispoto G, 1996, in *Proc. IAU Symp. 176, Stellar Surface Structure*, eds Strassmeier K. G. and Linsky J. L., Kluwer, Dordrecht, p. 403

[114] *op cit*

[115] Collier Cameron, A., 1988, *MNRAS*, **233**, 235

[116] Collier Cameron, A. and Robinson R. D., 1989, *MNRAS*, **236**, 57

[117] Collier Cameron A. and Woods J. A., 1992, *MNRAS*, **258**, 360

[118] Doyle J. G. and Collier Cameron A., 1990, *MNRAS*, **244**, 291

[119] Jeffries R. D., 1993, *MNRAS*, **262**, 369

[120] Jeffries R. D., 1996, in *Proc. IAU Symposium No. 176, Stellar Surface Structure*, eds Strassmeier K. G. and Linsky J. L., Kluwer, Dordrecht, p. 461

[121] van den Oord G. H. J. and Zuccarello F., 1996, in *Proc. IAU Symp. 176, Stellar Surface Structure*, eds Strassmeier K. G. and Linsky J. L., Kluwer, Dordrecht, p. 433

[122] *op cit*

[123] Welty A. D., Ramsey L. W., Iyengar M., Nations H. L. and Buzasi D. L., 1993, *PASP*, **105**, 1427

that the broad emission feature may be due to a circumstellar shell of excited material while the central absorption is a result of viewing the photosphere through the shell.

Astronomers of the former Soviet Union have proposed the "roundchrom" theory wherein very close (i.e. $a \leq 2{\cdot}7\,R_{\odot}$) binaries have a common chromosphere surrounding both stars such that the source of chromospheric emissions may be the region between the stars. The theory is supported[124] by an observed correlation between emission in the Mg II λ2800 ultraviolet doublet and the separation of the stars. In some stars the inverse correlation is linear (e.g. CF Tuc) and in some the relation is quadratic (e.g. GT Muscae).

[124]Gurzadyan G. A. and Cholakyan V. G., 1995, *A&SS*, **229**, 185

Chapter 2

Observations and reduction of data

The present program of research was not directed particularly at any of the unsolved problems of active star theory; it was rather a general study, within the limitations of the instruments available at the Mount John University Observatory (MJUO), of chromospherically active stars with extreme-ultraviolet excess. Selection of stars from the ROSAT Bright Source Catalogue[1] automatically ensured selection of stars of interest.

Observed correlations of levels of EUV flux with Rossby number[2] and coronal EUV flux with rotation speed[3] suggest that chromospherically active stars in the Bright Source Catalogue will be fast rotators, or at least have low Rossby numbers. One motivation for this program was, accordingly, the measurement of rotational $v \sin i$ of AC stars from the Bright Source Catalogue using high-resolution spectra obtainable with the échelle spectrograph at MJUO.

The availability of high-resolution échelle spectra also facilitated the examination of Hα spectra in detail with a view to finding evidence of the spatial location of Hα emission.[4]

A further use envisaged for high-resolution spectra was the measurement of stellar radial velocities and derivation therefrom of orbital parameters of RS CVn, BY Dra and moderately fast-rotating active binary systems.

The combination of high-resolution spectroscopy and single-channel $UBV(RI)_C$ photometry by permanent service observers at MJUO also raised the possibility of obtaining information about spot extent and location using the methods mentioned in Section 1.7, and another aim of the program was the extraction of such information if data of suffi-

[1]Pounds, K. A., Allan, D. J., Barber, C., Barstow, M. A., Bertram, D., Branduardi-Raymont, G., Brebner, G. E. C., Buckley, D., Bromage, G. E., Cole, R. E., Courtier, M., Cruise, A. M., Culhane, J. L., Denby, M., O'Donoghue, D., Dunford, E., Georgantopoulos, I., Goodall, C. V., Gondhalekar, P. M., Gourlay, J. A., Harris, A. W., Hassall, B. J. M., Hellier, C., Hodgkin, S., Jeffries, R. D., Kellett, B. J., Kent, B. J., Lieu, R., Lloyd, C., McGale, P., Mason, K. O., Matthews, L., Mittaz, J. P. D., Page, C. G., Pankiewicz, G. S., Pike, C. D., Ponman, T. J., Puchnarewicz, E. M., Pye, J. P., Quenby, J. J., Ricketts, M. J., Rosen, S. R., Sansom, A. E., Sembay, S., Sidher, S., Sims, M. R., Stewart, B. C., Sumner, T. J., Vallance, R. J., Watson, M. G., Warwick, R. S., Wells, A. A., Willingale, R. R., Willmore, A. P., Willoughby, G. A., and Wonnacott, D., 1993, *MNRAS*, **260**, 77

[2]Mathioudakis *et al, op cit*

[3]Wood *et al, op cit*

[4]Collier Cameron, 1988, *op cit*, Collier Cameron, and Robinson, *op cit*, Collier Cameron and Woods, *op cit*, Doyle and Collier Cameron, *op cit*, Jeffries, 1993, *op cit*

BSC Name RE...	Identification	Sp.	m_V
0030−48	HD 2726	F1	5·7
0106−22	HD 6628	G5 V	7·7
0135−29	HD 9770	K3 + K4	7·8 + 8·0
0254−05	HD 18131	K0	7·2
0312−44	HD 20121	F7 III + ?	5·9 + 9
0402−00	HD 25457	F5 V	5·4
0420+13	HD 27483	F7 V	6·2
0515−19	HD 34274	F0	7·8
0527−11	HD 35850	F7 V	6·4
0604−48	HD 41824	G6 V + G	6·6 + 6
0637−61	HD 48189	G1 V + ?	6·3 + 8·3
0650−00	HD 49933	F2 V + ?	5·8 + 11
0653−43	HD 51062	G0	8·9
0707−34	HD 54579	G0	8·0
0825−34	HD 71285	G5	7·9
0925−53	HD 81734	F8	7·0
0930+10	HD 82159	G5 + G5	7·6 + 8·2
0951−14	HD 85444	K0	4·1
1219+16	HD 107146	G2 V	7·1
1553−42	HD 141943	G1 V	7·5
1625−49	HD 147633	K1	7·1
1834+18	HD 171488	G0 V	7·3
2000−33	HD 189245	F5	5·7
2055−17	HD 199143	F8 V	7·1
2339−69	HD 222259	G5 IV + K?	8·0 + 10
2244+17	BD +17 4799	K0	8·8

Table 2.1: Initial list of chromospherically active stars selected from the ROSAT Bright Source Catalogue, as prepared by SAAO

ciently high S/N could be obtained.

2.1 Selection of target stars

The target stars initially selected at the South African Astronomical Observatory (SAAO) from the Bright Source Catalogue[5] for échelle spectroscopy at MJUO are listed in Table 2.1. Twenty stars were selected from the list in Table 2.1 for inclusion in the present program. Those excluded were HD 34274 because its relatively early spectral type made it unlikely to be a "normal" active star,[6] HD 51062, HD 54579, HD 82159 and BD +17 4799

[5]Pounds *et al, op cit*

[6]See García López *et al, op cit*

Target	Reason for selection
HD 2726	Partially filled Hα, possible double-lined sp. binary
HD 6628	Very strong and variable Hα emission
HD 9770	Partially filled Hα, eclipse seen in photometry
HD 27483	Partially filled Hα, double-lined sp. binary
HD 81734	Partially filled and variable Hα
HD 147633	Partially filled Hα, double-lined sp. binary
HD 199143	Very broad and shallow Hα
HD 222259	Partially filled Hα, good amplitude light variations

Table 2.2: Final selection of target stars from the list in Table 2.1.

because of their dimness, and HD 85444 because its brightness was likely to require the photometrists to use neutral density filters not required for the other stars. The known active system GT Mus which has been observed photmetrically at MJUO since 1981 was added to the program.

It was intended to reduce the target list to six to eight stars after initial photometric observations and spectroscopy, both of the Hα region using the MJUO échelle spectrograph and of the Ca II H and K lines using the new MJUO medium resolution spectrograph ("MRS") which was expected to be comissioned at about the commencement of this program. In the event, the MRS was not able to be used until nine months after the start of observations, and not in the highest resolution required to measure H and K emission until a further six months elapsed, and the final selection of stars had to be made on the basis of the photometry and Hα spectroscopy alone. The stars finally selected, and reasons for selection, were as set out in Table 2.2, together with GT Mus. Some observations of the excluded stars continued to be made, time permitting, throughout the three-year observing program.

2.2 Photometric observations

$UBV(RI)_C$ and differential Hα photometry was carried out by the service observers using both of the 61-cm telescopes and EMI 9558 (S20) single-channel photometers at MJUO. The check and comparison stars were as listed in Table 2.3.

The observational practice at MJUO was to observe the stars in the order (1) comparison star, (2) target star, (3) check star, (4) target star (5) comparison star. A canonical value having been assigned for the magnitude of the comparison star (based on comparison with E-region standards) in each filter passband, the mean observed magnitude of the comparison star in each filter passband was adjusted to match the canonical value, and the observed magnitudes for the check and comparison stars were then subjected to the same adjustment. The entire reduction process was performed by the observers, usually at the time of observation, and the reduced data supplied for use by the requesting astronomers in the form of both printed sheets (for all stars except GT Mus) and data files on magnetic discs.

Target Star	Comparison Star	Check Star
HD 2726	HD 3302	HD 2529
	F8 V	K0 III
	V =5·51	V =6·3
HD 6628	HD 6559	HD 6504
	G5 IV	F8
	V =6·14	V =8·1
HD 9770	HD 9849	HD 9576
	G8 IV	K2
	V =6·62	V =8·1
HD 27483	HD 27397	HD 25414
	F5 V	F5 V
	V =7·1	V =8·0
HD 81734	HD 81803	HD 81720
	F5 V	K2 III
	V =7·09	V =6·7
HD 147633	HD 147707	HD 148044
	K0	F5
	V =7·0	V =7·9
HD 199143	HD 199197	HD 198730
	K0 III	G5
	V =7·6	V =7·9
HD 222259	HD 222551	HD 222350
	G5 IV	F8
	V =7·8	V =9·1

Table 2.3: Target, comparison and check stars.

When supplying the initial list of active stars from SAAO, Dr D. A. H. Buckley noted that "the activity cycles (timescale for spot formation/decay) will also possibly be shorter than average, which has already been shown to be the case for a few ROSAT active stars. This means that it would be difficult to determine periods from spot waves, or the like, if the data covered too long a time base... we should attempt to get light curves over a time scale shorter than ~2 months, preferably ~1 month, and then look for periodicities. This will mean that we should concentrate on a few stars at any one time, and be as well coordinated as possible (i.e. between SAAO and MJUO)." In the event, a delay of over a year between that proposal and the commencement of this program meant that the program proceeded as an MJUO project alone without continued photometry at SAAO, and the pressures on the photometric observers' time at MJUO meant that it was never possible to obtain light curves in the envisaged short time periods. In general, the stars were observed at approximately weekly intervals.

Periodicity in the photometry was analysed with the aid of VMS/Fortran77 code

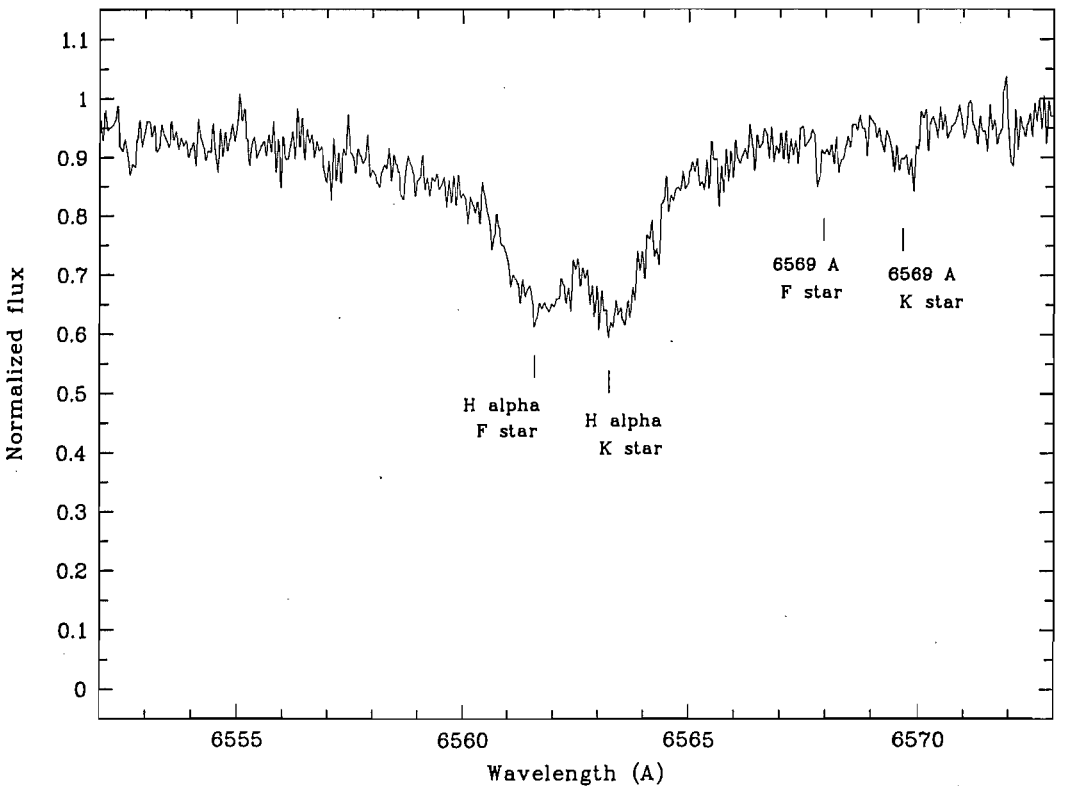

Figure 2.1: Hα spectrum of HD 147633, obtained at MJUO on JD244940·94227. The labels denote the preliminary identification of the spectral types of the stars responsible for the indicated absorption lines.

written by Dr W. A. Lawson embodying the Lomb-Scargle period-finding program[7] which uses a fast Fourier transform to generate power spectra in the frequency domain.

2.3 High-resolution échelle spectroscopy

All high-resolution spectra were obtained using the MJUO échelle spectrograph mounted at the Cassegrain focus of the MJUO 1-m McLellan telescope. The spectrograph was used in its original configuration, with the Thomson 584 × 376 pixels CCD and 9-track data-tape recorder. Short (~30 Å) sections of four orders of the échelle were recorded in each observation. The Hα line appeared in order 35 of the spectrograph in which the recorded wavelength range was 30·375 Å, with a dispersion on the CCD of 0·0520 Å/pixel. The spectrograph was used with a slit width of 100 μm, giving a resolving power of $\lambda/\Delta\lambda = 40\,000$.

Integration times ranged from 30 minutes for GT Mus in good conditions to at least 120 minutes for HD 222259. Each stellar observation was immediately followed by a

[7]Lomb, N. R., 1976, *A&SS*, **39**, 447 and Scargle, J. D., 1982, *ApJ*, **263**, 835

Échelle order	Line wavelength (Å)	Origin
34	6768	Ni I
	6750	Fe I
	6705	Fe I
	6704	Fe I
35	6569	Fe I
	6499	Fe I
36	6394	Fe I
	6344	Fe I
	6337	Fe I
	6335	Fe I
	6328	Ni I
37	6219	Fe I
	6200	Fe I
38	6027	Fe I
	6024	Fe I
41	5589	Ca I
42	5507	Fe I
	5506	Mn I
	5503	Fe
	5501	Fe I
	5497	Fe I

Table 2.4: Spectral lines in orders 34 to 42 of the MJUO échelle spectrograph used, where available, for measuring radial velocities.

spectrum of the spectrograph's internal thorium-argon lamp with the telescope in the same position. Each exposure was reduced to four or five separate wavelength-calibrated spectra, one for each order, using the European Southern Observatory MIDAS software, initially on a Vax/VMS system and later, using the 94NOV version of MIDAS, on a Sun Unix system. Cosmic-ray filtering was necessary for all target-star spectra except for some of GT Mus, and was performed using the standard MIDAS median-filtering procedure. Dispersion solutions were computed from the thorium-argon spectra using the standard MIDAS *ident/echelle* procedure and tables of laboratory wavelengths made up from the CRC lists[8] and checked against the MJUO thorium-argon spectrum. The reduced spectra were stored in FITS form on floppy discs. It was discovered at a late stage that many of the early spectra reduced under Vax/VMS had been corrupted in the process of transfer onto floppy discs by way of NFT connection to a personal computer controlling the disc drive, and it was necessary to repeat the reduction process for those exposures.

[8]Reader J. and Corliss C. H., 1982, *Line Spectra of the Elements* in *CRC Handbook of Chemistry and Physics*, 63rd ed., ed. Weast R. C., CRC Press, Boca Raton

Échelle order	Line wavelength (Å)	Origin
43	5383	Fe I
	5381	Ti I
	5380	Fe I
	5378	Mn I
	5374	Fe I
	5371	Fe I
	5367	Fe I
	5363	Fe I
	5362	Fe I
44	5255	Cr I
	5252	Ti I
	5244	Fe I
	5242	Fe I
	5240	Sc I
	5235	Fe I
	5233	Fe I
45	5142	Fe I
	5134	Fe
	5127	Fe I
	5126	Fe I
	5124	Fe I
	5122	Fe I

Table 2.5: Spectral lines in orders 43 to 45 of the MJUO échelle spectrograph used, where available, for measuring radial velocities.

Solar system barycentric corrections were computed at the time of reduction and recorded in the FITS headers. The standard MIDAS procedures *compute/precess* (which does not take the stars' proper motions into account) and *compute/barycorr* were used. After the switch to the 94NOV version of MIDAS, corrected radial velocities were also derived and recorded in the headers. Further analyses were carried out using the recorded FITS spectra and either MIDAS procedures or programs in MIDAS command language or, more usually, in VMS/Fortran77. MIDAS command language programs written for this purpose included programs for fitting one or two Gaussian curves to absorption and emission lines in radial-velocity space,[9] and for computing and displaying a plot of data points phased according to successive periods.[10] Fortran programs by the writer included programs for finding the model Hα lines which best fitted spectral lines,[11] and for

[9] Appendix A
[10] Appendix B
[11] Appendix C

Échelle order	Line wavelength (Å)	Origin
46	5031	Sc I
	5030	Fe I
	5026	Ti I
	5025	Ti I
	5022	Fe I
	5020	Ti I
	5018	Ni I
	5016	Ti I
	5015	Fe I
	5014	Ti I
	5012	Fe I
47	4924	Fe I
	4921	Fe I
	4917	Fe I
	4909	Fe I
	4908	Fe I

Table 2.6: Spectral lines in orders 46 and 47 of the MJUO échelle spectrograph used, where available, for measuring radial velocities.

subtracting appropriately scaled absorption spectra selectively of third light, companion stars and the active stars from the observed spectrum.[12]

Approximately 30 Hα observations, more or less depending on the accessibility of the object for observation, were made of each target star. In addition, each star was observed in the D-lines region to check for the presence of a He I D_3 line, and, in most cases several times, in the region of the Li I 6707·8 line. For some stars with weak metal lines in the Hα region, additional spectra were obtained in the metal-line-rich region around 5000 Å for the more precise measurement of radial velocities.

2.3.1 Measurement of radial velocities

Radial velocities were measured on a line-by-line basis using lines which were, in the MJUO spectra, free of known or apparent blending. The lines which were used, subject to the quality of the spectra, are listed in Tables 2.4, 2.5 and 2.6. Orbital solutions of the radial velocities were found with the *Orbsol* program as modified and supplied to MJUO by Tsevi Mazeh.

[12] Appendix D

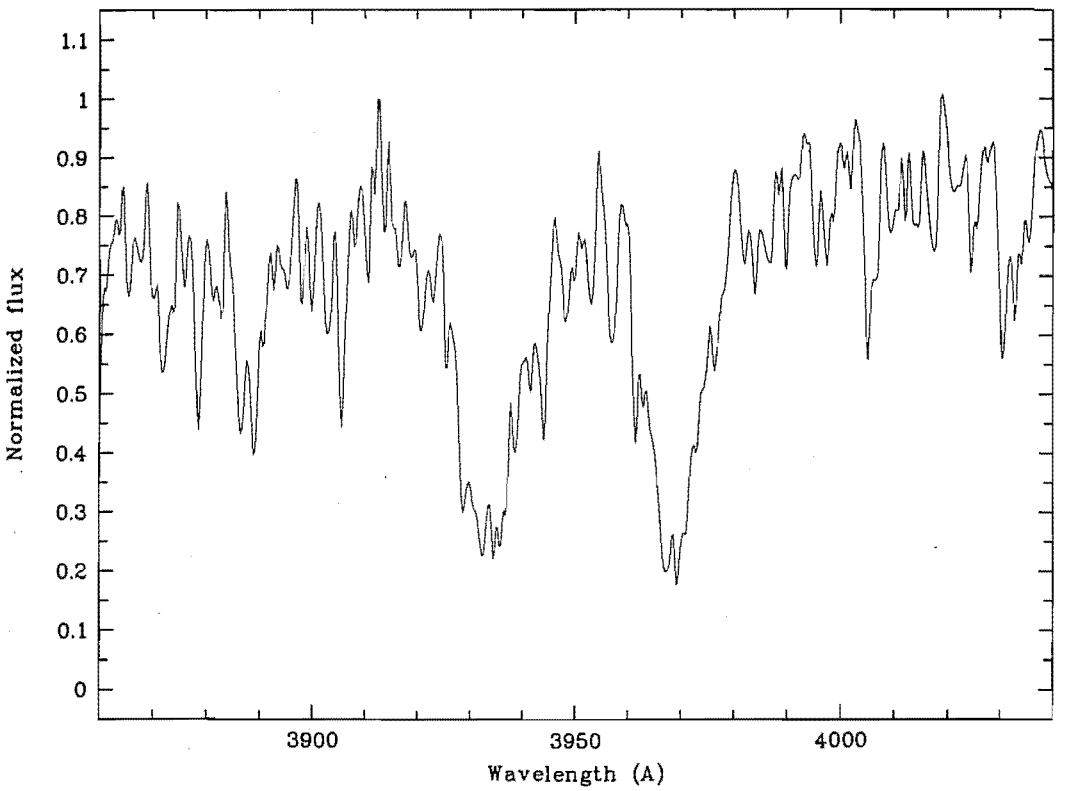

Figure 2.2: Spectrum of the CaII H and K lines of HD 147633, obtained at MJUO.

2.3.2 Measurement of rotational broadening

The rotational $v \sin i$ of stars was calculated from the Doppler broadening of the most noise-free available metal lines. In each case a corresponding metal line of a star of known zero or low rotational $v \sin i$ was convolved with the rotational-broadening function of Gray[13]

$$G(\Delta\lambda) = \left\{ \frac{2(1-\epsilon)[1-(\Delta\lambda/\Delta\lambda_L)^2]^{\frac{1}{2}}}{\pi\Delta\lambda_L(1-\epsilon/3)} \right\} + \left\{ \frac{\epsilon[1-(\Delta\lambda/\Delta\lambda_L)^2]}{2\Delta\lambda_L(1-\epsilon/3)} \right\}$$

where $\Delta\lambda_L$ is the maximum half-width of the function dependent on the $v \sin i$, over a range of values of $v \sin i$ until the FWHM matched that of the stellar line. The limb-darkening coefficient ϵ was obtained in each case from Figure 17.6 of Gray[14], using the measured or calculated $(B-V)$ colour index and a canonical value of $T_{\rm eff}$.

Initially, the MIDAS procedure *center/gauss* was used to fit gaussians to both the lines the broadening of which was to be measured and the broadened lines with which they were to be compared. However, some parameters, including both the width of a fitted gaussian and the FWHM, proved to be very sensitive to where the line-fitting routine placed the

[13] Gray D. F., 1992, *The Observation and Analysis of Stellar Photospheres*, 2nd ed., Cambridge
[14] *ibid*

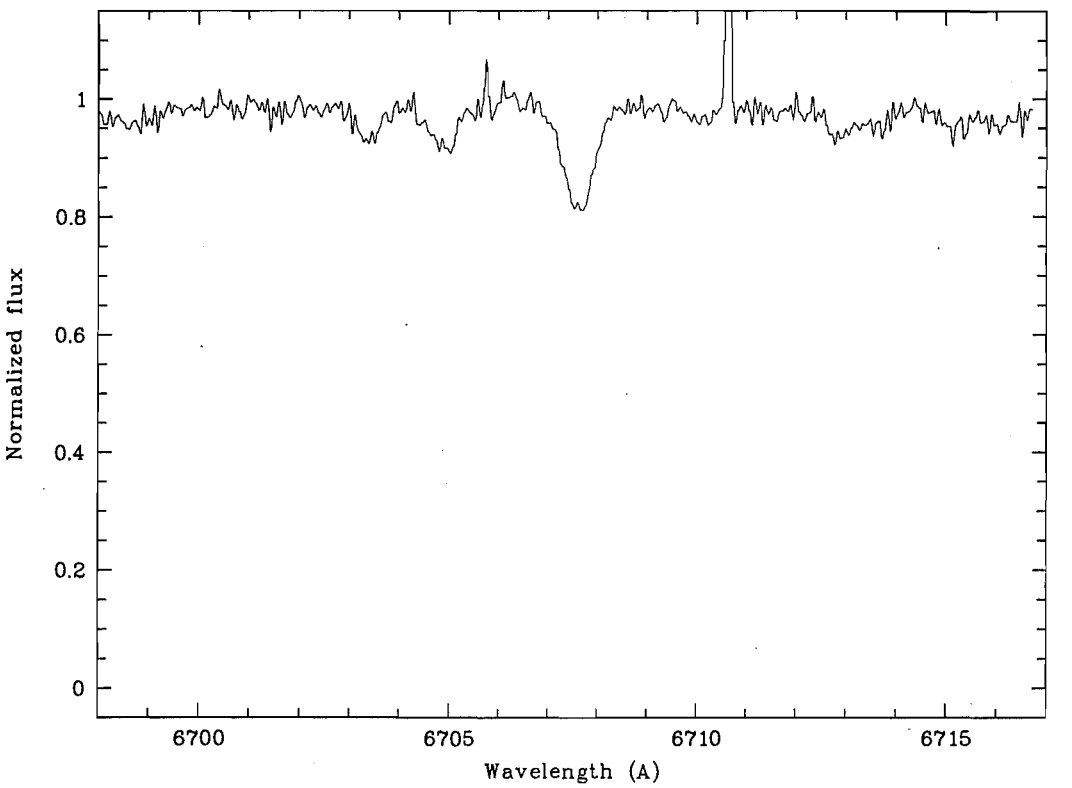

Figure 2.3: Lithium λ6708 spectrum of HD 147633, obtained at MJUO on JD2449860·89699.

continuum. The *center/gauss* procedure required the user to mark off the segment of continuum to be included in the fit, and both the slope and the height of the continuum fitted to the data by the procedure varied according to how much of the spectrum was included in the fit. For that reason, the use of the *center/gauss* procedure was abandoned except when nothing else would work, and the FWHMs of lines were measured with a fitting routine[15] which assumed a normalized spectrum with a continuum flux value of unity. That effectively transferred the continuum-locating problem to the normalization step and the amount of line-blanketing in the regions which were observed was such as to make it to some extent an arbitrary choice at all times. The relatively large uncertainty in the rotational broadening measurements is directly due to that uncertainty in locating the continuum.

2.4 Medium-resolution spectra

The MJUO medium-resolution spectrograph and 600 lines/mm grating became available for use in the middle of the observation program, and was used to observe the CaII H

[15] A modified version of the program listed in Appendix A, which was not kept.

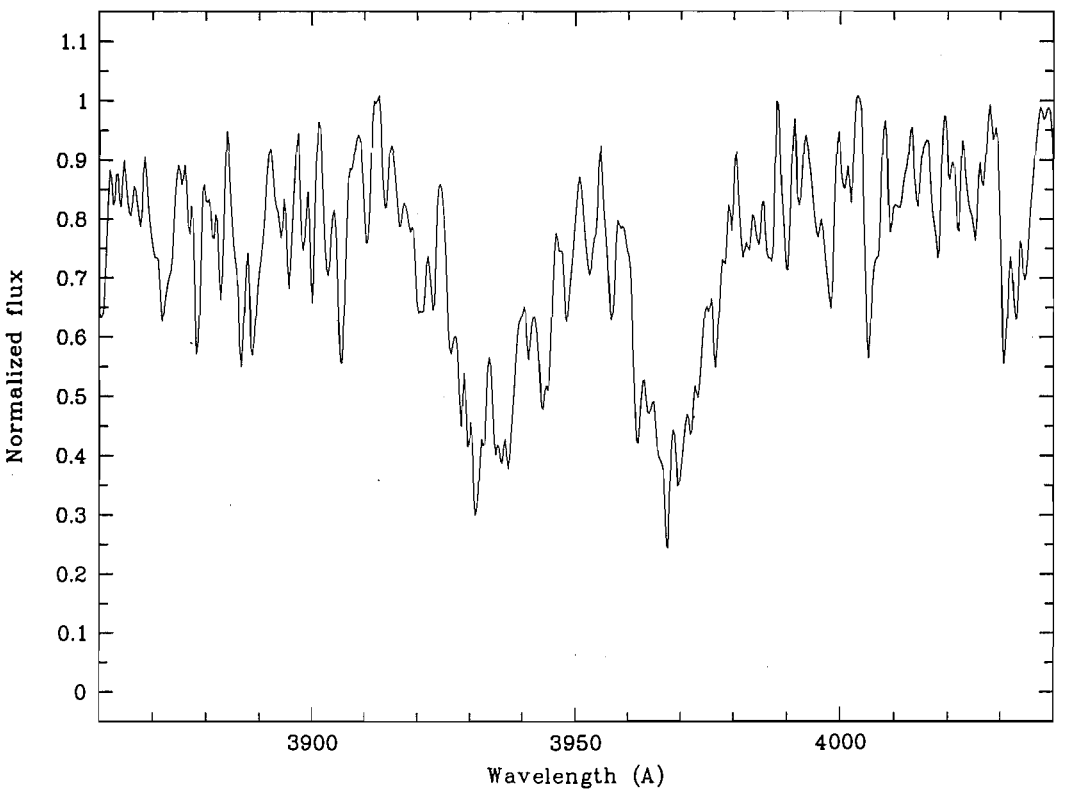

Figure 2.4: Medium-resolution spectrum of the Ca II H and K lines of HD 222259, obtained at MJUO.

and K lines of each target star. The spectrograph is used in orders 2 or 3, selected by order-separating filters. With a constant grating-tilt setting of ~640 (arbitrary units), the Fraunhofer D lines can be observed in order 2 with a yellow GG475 filter and the H and K lines, as well as the Hδ Balmer line, can be observed in order 3 with a BG28 blue filter. A calibration lamp exposure (helium-argon lamp for order 3 observations) was made after each observation, as with the échelle observations.

The same CCD and data tape were used on both of the spectrographs. MRS spectra were recorded in a narrow band on the CCD to minimize storage space. It was found that the MIDAS software was unable to fit dispersion solutions to the raw MRS spectra (the MIDAS context *echelle* required more than one order in the CCD image, and procedures in the context "long" which was advertised as appropriate for single-order spectra were unable to work on the MJUO CCD images), but use was made of a program kindly supplied by Jovan and Ljiljana Skuljan for generating a "quasi-échelle" image with the order repeated so that the context *echelle* could work, and reductions were accordingly successful.

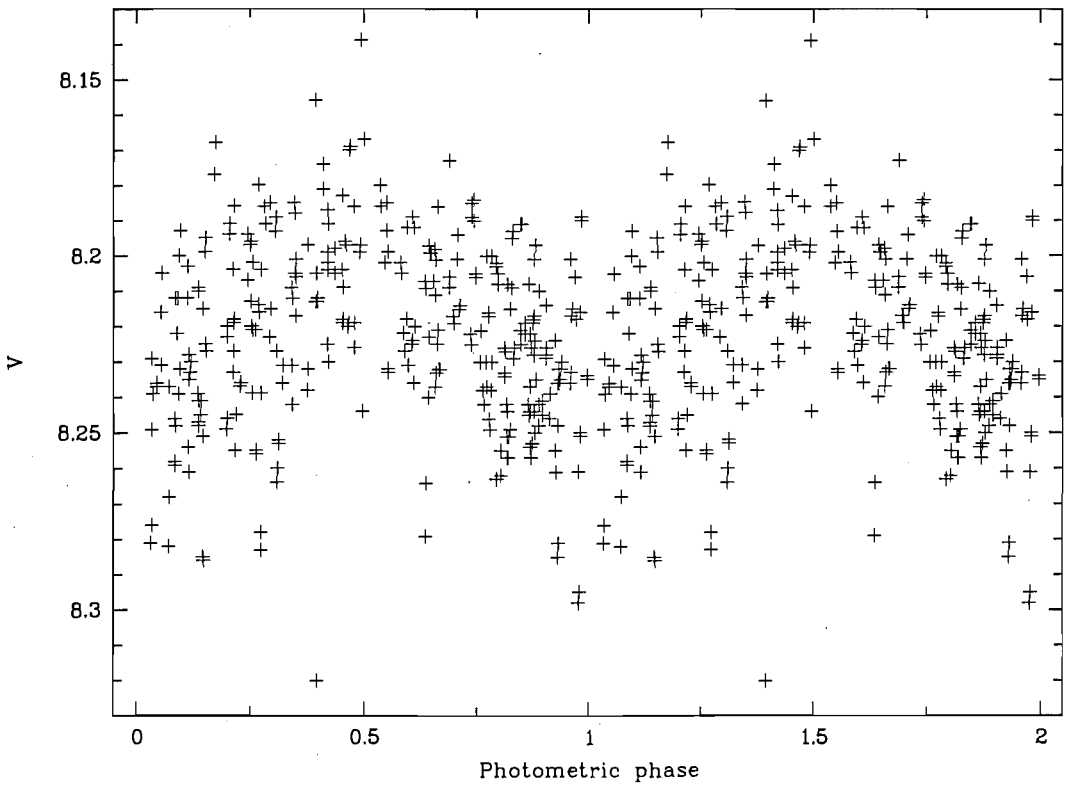

Figure 2.5: Spot wave of HD 222259, phased according to a period of 2·8482 days and an epoch of minimum of JD2448931·14836.

2.5 Some general results

Three stars, discussed in the following three chapters, were selected for detailed analysis in this thesis. They are CS Ceti (HD 6628), selected because of its high level of activity and because it was found to be a single-lined spectroscopic binary with a good orbital solution; BB Sculptoris (HD 9770), selected because it was found to contain an eclipsing binary system; and GT Mus which has been the subject of continuing observations at MJUO for nearly two decades. Of the other stars, interesting preliminary results were obtained for two which should be further analysed in detail. The preliminary results are summarized in the following two sections.

2.5.1 HD 147633

HD 147633 (SAO 226738) is a known triple system[16] in which the separation of the AB×C system is not less than 10·2″. The AB binary system was observed at MJUO and it is listed by Hirshfeld & Sinnott (vol. 1) as having a period of 311·2 years with inclination $i = 180°$,

[16]Hirshfeld A., and Sinnott R. W., 1985, *Sky Catalogue 2000·0*, Cambridge University Press and Sky Publishing Corporation, Vol. 2.

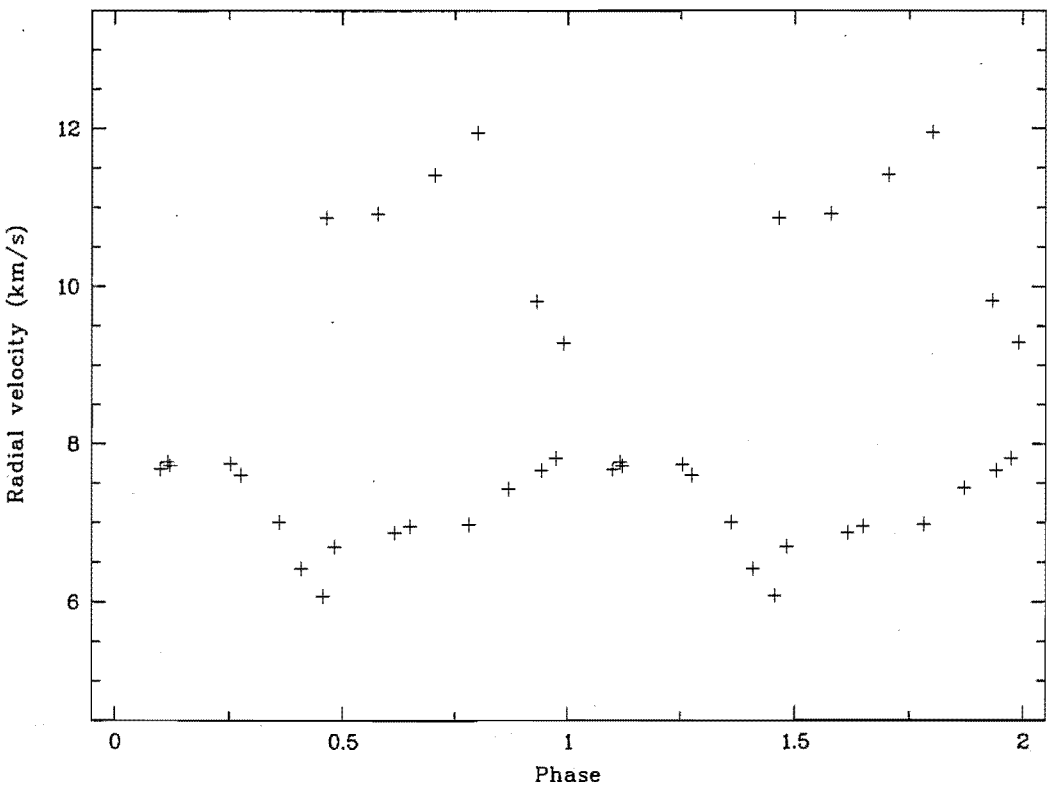

Figure 2.6: Radial velocities of HD 222259, phased according to a period of 2·84 days and the epoch of minimum of the spot wave of Figure 2.5.

angular semi-major axis a =1·66″ and parallax $\pi = 91$ pc, giving $a = 150$ AU. HD 147633 is listed in the candidate list in the second edition of the catalogue of chromospherically active binaries by Strassmeier *et al.*[17] Medium-resolution spectra obtained at MJUO (Figure 2.2) confirmed that it has moderate H and K emission.

High-resolution Hα spectra (Figure 2.1) showed that the HD 147633AB system contained a double-lined spectroscopic binary with a radial-velocity difference between the two stars of up to ~80 km/s. Clearly that cannot be the radial velocity of the known AB system, and one of the stars in that system must itself be a shorter-period binary and probably, therefore, contains the active star. Examination of the profiles and strengths of the Hα and metal lines suggests that the new binary comprises an F-type and a K-type star. The presence of both spectra at roughly similar line strengths implies that the two stars are not several magnitudes apart in brightness as would be the case if both were on the main sequence or if the K star were a class III giant; instead the K star may be a subgiant at the stage of evolving off the main sequence towards the ascending giant branch. Both spectra are rotationally broadened. The 6708 Å Li I absorption line is also present (Figure 2.3); further spectra will need to be obtained in order to determine whether it is

[17]Strassmeier, Hall, Fekel and Scheck, *op cit*, Table 7

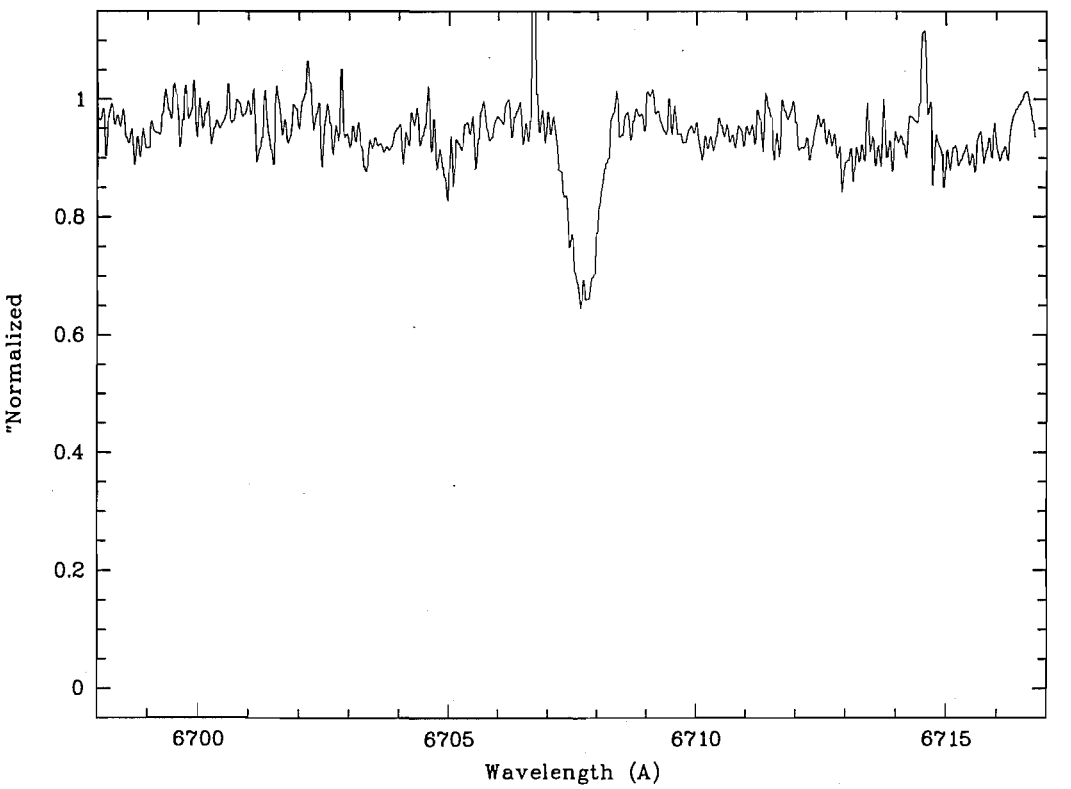

Figure 2.7: Lithium λ6708 spectrum of HD 222259, obtained at MJUO on JD2449860·10283.

present in light of both stars or only one. An orbital solution from the high-resolution spectra which have been obtained, together with analysis of the photometric data which have been obtained should facilitate the determination of the physical parameters of the two stars.

2.5.2 HD 222259

The binary system HD 222259 has recently been observed and results have been published[18] which indicate that its secondary is chromospherically active. Although the separation of the two components is $\sim 8''$, it was not always possible to resolve them at MJUO or, on other occasions, to detect more than one star. It is probable that some of the spectra which have been obtained are dominated by the light of the primary and presumed inactive star HD 222259A.

Medium resolution spectra obtained in this project (e.g. Figure 2.4) display moderate H and K emission. HD 222259 is the only system studied in this project for which a coherent spot wave, shown in Figure 2.5, was observed to persist (although the possibility that some effects due to binary ellipticity are also present cannot at this stage be excluded)

[18]Soderblom D. R., King J. R. and Henry T. J., 1998, *AJ*, **116**, 396

throughout the whole of the observation period, from JD2448931 to JD2450717. The ephemeris of the spot wave is

$$\mathrm{HJD} = 2448931{\cdot}14836 + (2{\cdot}8482 \pm 0{\cdot}0001) \times E$$

with the minimum at phase zero. Figure 2.6 shows the radial velocities obtained from the high-resolution spectra of HD 222259 phased according to a period of 2·84 days with the same epoch as the spot wave. The interpretation of the pattern found must await further analysis and treatment by the Orbsol program — the S/N of the spectra of this system is the worst of all of the stars in the project, rarely being better than 20:1, and all of the velocities will have to be checked carefully for reliability. It should still, however, be possible to determine a period and possibly also the mass function of the system from the radial velocities, as well as information about the surface structure of the star from the photometry. The λ6708 Li I line is strongly present in absorption. The spectrum shown in Figure 2.7 was obtained at a time when both of the stars of the HD 222259 system were resolved and most of the light captured was that of the primary star HD 222259A, but some light of the secondary is also present.

Chapter 3

CS Ceti

The star CS Ceti[1] is also identified as HD 6628, SAO 166806, CPD −23 130, EUVE J0106 −228, IRAS 01043−2307, RE J10106−225 and HIP 5227. The spectral type and luminosity class are listed as G5 IV in the SAO Catalogue and as G5 V in the Michigan Spectral Catalogue.[2] Eggen[3] implied that CS Cet was, on the basis of its colours, distance and space velocity "assumed to be a halo giant". From the Hipparcos data, Schrijver[4] identified CS Cet as a variable single star with an amplitude in m_V of 0·10 mag. and a period of 4·50 days, and a light curve has been fitted[5] to the data.

McGale *et al*[6] suggested that CS Cet might be an RS CVn system, on the basis of a distance of 33 pc calculated from its assumed G5 V spectral type and its EUV emission calculated from ROSAT count rates. The Hipparcos parallax,[7] however, is $\pi = 0{\cdot}00756'' \pm 0{\cdot}00108''$, entailing a distance of 132 ± 22 pc and suggesting that the object is brighter than a G-type dwarf. CS Cet is listed in the Catalogue of Faint Extreme Ultraviolet Sources[8] as one of the sources detected by both the EUVE and ROSAT missions, with EUVE 0·046 counts/s (luminosity $L_{\mathrm{EUV}} \approx 6{\cdot}3 \times 10^{22}$ W), and ROSAT fluxes as listed in Table 3.1. IRAS fluxes, magnitudes and colours[9] are listed in Table 3.2. Medium-resolution spectra of the CaII H and K lines obtained at MJUO (Figure 3.1) confirmed that CS Cet is strongly active.

---

[1] *IBVS* No. 4659

[2] Houk N., 1982, *Michigan Spectral Catalogue*, vol. 3, Univ. Michigan, Ann Arbor

[3] Eggen O. J., 1976, *ApJS*, **30**, 351

[4] Schrijver H., 1997, *The Hipparcos and Tycho Catalogues* Vol. 5, ESA Publications Division, Noordwijk

[5] Schrijver H,, *op cit*, vol. 10, and Grenon M., 1997, *The Hipparcos and Tycho Catalogues* vol. 12, ESA Publications Division, Noordwijk

[6] McGale P. A., Pye J. P., Barber C. R., and Page C. G., 1995, *MNRAS*, **275**, 1232

[7] Schrijver H., *op cit*, vol. 5

[8] Lambton M., Lieu R., Schmidt J. H. M. M., Bowyer S., Voges W., Lewis J. and Wa X., 1997, *ApJS*, **108**, 545

[9] calculated using the conversion formulae of Hickman M. A., Sloan G. C. and Canterna R, 1995, *AJ*, **110**, 2910

WFC filter (Å)	Flux (counts/s)	
S1	60 – 140	0·078
S2	110 – 200	0·039
XRT flux (counts/s)		3·52

Table 3.1: ROSAT EUV count rates for CS Cet, obtained from the NASA *HEASARC* database.

Band (μm)	IRAS flux	Magnitude
12	0·34	4·8
25	0·25	3·6
60	0·40	1·2
IR colours		Indices
[12]−[25]		1·2
[25]−[60]		2·4

Table 3.2: IRAS fluxes of CS Cet in the 12, 25 and 60 μm bands, together with magnitudes and colour indices calculated therefrom.

3.1 MJUO $UBVRI$ photometry and spot-modulation

The photometry obtained at MJUO is summarized in Table 3.3. It is expected that the primary of CS Cet, being a strongly active star, will have a light curve that is significantly modulated by photospheric spots. That this is so is confirmed by the standard deviation and range of values of V in Table 3.3, where the brightest recorded value of V is less than two standard deviations brighter than the mean value, implying that the standard deviation is enlarged by real variability in the data superimposed on the random error. Fourier analysis of the V light curve produced no prominent power spectrum peaks, in particular none corresponding to the 4·50 days period found in the Hipparcos photometry.[10]

When analysing the spectral type and physical characteristics of the active star, it will be necessary to estimate the magnitude and colours of the unspotted star. Since spots dim a star in V, the minimum value of V as given in Table 3.3 will be adopted as the best estimate of the magnitude of the CS Cet system with the primary in an unspotted state. Since spots redden a star's colour indices, but the dimmest observed values of V are possibly unreliable, values of the colours one standard deviation bluer than their mean values will be adopted as the best estimate of the colours of the system with the primary in an unspotted state, although probably an estimate which errs towards excessively red values. The adopted values are listed in Table 3.4.

[10]Schrijver H, *op cit*, vol. 10, and Grenon, *op cit*

Bandpass or Colour	Mean (mag)	St. Dev. (mag)	Minimum (mag)	Maximum (mag)	No. of Observations
V	7·794	0·071	7·711	8·379	169
$U-B$	0·286	0·096	−0·697	0·583	169
$B-V$	0·884	0·058	0·517	1·470	169
$V-R$	0·734	0·066	0·413	1·501	169
$V-I$	1·283	0·065	0·689	1·644	169

Table 3.3: MJUO $UBV(RI)_J$ photometry of CS Cet. The $(V-R)$ and $(V-I)$ colours have been converted to Johnson colours using the 8th and 20th transformation equations of Table 4 of Taylor B. J., 1986, *ApJS*, **60**, 577.

Bandpass or Colour	Adopted value with unspotted primary
V	7·711
$U-B$	0·190
$B-V$	0·826
$V-R$	0·668
$V-I$	1·218

Table 3.4: Adopted values of UBVRI for CS Cet with unspotted primary

3.2 High-resolution spectroscopy

Apart from one spectrum each in the Li 6708 Å region in order 34 of the spectrograph (orders 33 to 36 recorded), the He D_3 line region in order 39 (orders 37 to 41 recorded), and a region from 4900 Å to 5500 Å in orders 42 to 47, which is rich in metal lines, the spectra were all obtained in the Hα region in order 35 (orders 34 to 37 recorded). The S/N ratio of the spectra that were analysed ranged from $\sim$ 5 to $\sim$ 45, with most being $\sim$ 25.

3.2.1 Orbital parameters

Radial velocities were measured on a line by line basis using the spectral lines listed in Tables 2.4, 2.5 and 2.6. Additionally, one velocity was obtained from the emission features in a medium-resolution spectrum of the Ca II H and K lines. The mean velocities obtained from the individual spectra are listed in Table 3.5.

The best-fit orbital parameters, as yielded by the *Orbsol* program, are listed in Table 3.6. Figure 3.2 shows the radial velocities of Table 3.5, phased with the 27·332 days period where zero phase is the epoch of periastron passage. The velocity curve is plainly that of a single-lined spectroscopic binary. No doubling of metal lines is observed in any of the spectra, indicating that the secondary is some magnitudes dimmer than the primary.

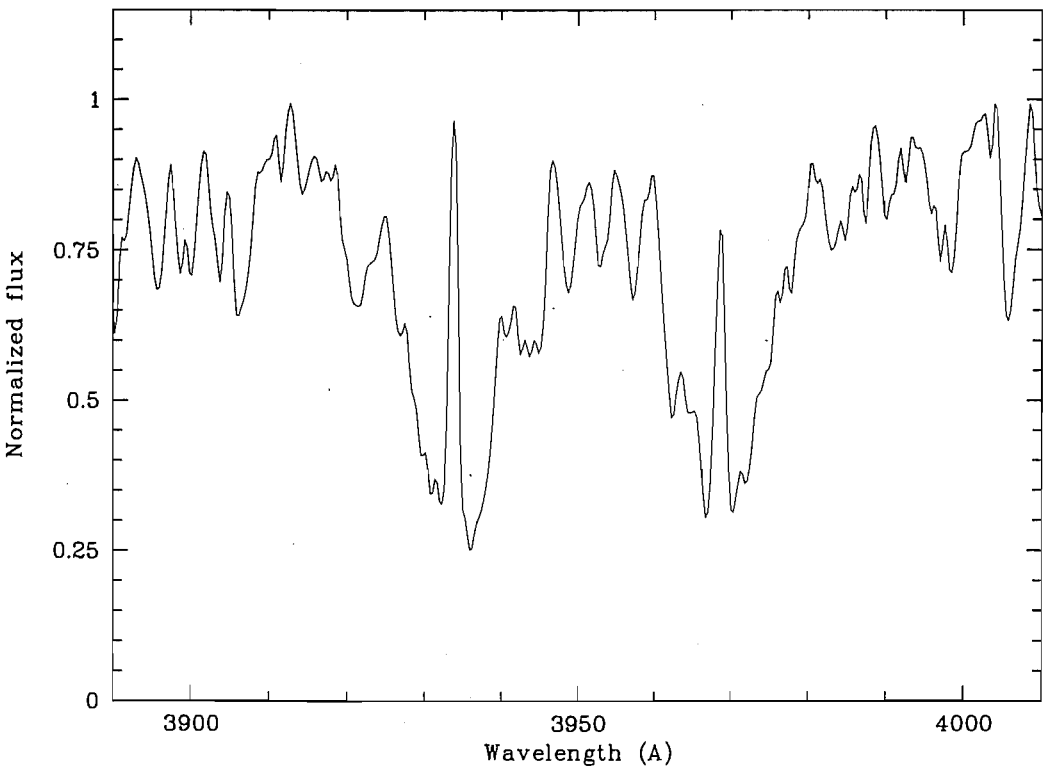

Figure 3.1: Medium-resolution spectrum of the H and K lines of CS Cet, obtained at MJUO, 1995 December 30.

3.2.2 Derived stellar and orbital parameters

Medium resolution spectra (e.g. Figure 3.1) of the Ca II H and K lines show strong emission features the radial velocities of which are those of the metal line spectrum of the primary star at red wavelengths (Table 3.5 and Figure 3.2). Hα-region spectra obtained at different phases of the orbital period (Figure 3.3) show strong emission in Hα. The Ca II H and K emission and the Hα emission indicate that the CS Cet primary has a very active chromosphere.

One Hα spectrum, obtained 1995 July 17 (HJD 2449916·128 in Table 3.5) and shown in Figures 3.3 (phase 0·084) and 3.4, exhibits a complex Hα feature consisting of an emission peak largely filling a blueward absorption feature and partially obscuring a second, redward, absorption feature. The approximate radial velocity of the blueward absorption feature is similar to that of the metal lines, indicating that it belongs to the photospheric spectrum of the primary, while the minimum flux ($\sim$0·8 of the continuum) of the redward absorption feature is consistent with its being the whole red half of the Hα absorption line of a putative late F or early G dwarf companion star.

To estimate the spectral class of the companion star and its radial velocity, Kurucz model atmosphere Hα line profiles[11] over the effective temperature range of 5500–8500 K

[11]Kurucz R. L., 1994, Kurucz CD-ROM No. 19, *Solar Abundance Model Atmospheres for 0,1,2,4,8*

H.J.D.	Orbital phase	Mean vel. (km/s)	St. Dev. (km/s)	Source spectrum
2449859·217	0·002	−0·63	0·54	Hα
2449204·201	0·037	−11·06	0·55	Hα
2449860·248	0·040	−11·27	0·95	Li
2449641·992	0·054	−11·59	0·51	D
2449916·128	0·084	−17·81	0·21	Hα
2450081·911	0·150	−20·51	3·04	H&K
2449290·029	0·177	−11·17	1·29	Hα
2450111·941	0·249	+1·62	2·03	Hα
2449539·073	0·289	+2·36	0·36	Hα
2449622·118	0·327	+8·43	0·91	Hα
2450308·074	0·425	+17·79	1·03	Hα
2450011·892	0·588	+36·65	0·59	Hα
2450012·978	0·628	+38·89	0·07	Hα
2449579·201	0·757	+47·71	0·97	Hα
2450263·143	0·781	+46·26	2·25	Green
2450294·238	0·919	+29·39	1·04	Hα
2450075·989	0·933	+22·88	1·38	Hα
2450295·137	0·951	+16·52	1·78	Hα
2449639·924	0·979	+7·87	0·54	Hα
2449941·097	1·000	+1·82	0·10	Hα

Table 3.5: Orbital radial velocities of CS Cet. The velocities are phased according to the period and date of periastron passage listed in Table 3.6. References in the "source spectrum" column are to échelle spectra in the Hα wavelength region ("Hα"), the region of the λ6708 Li line ("Li"), the D-lines region ("D"), and the λ4900–λ5500 region ("Green"), and to a medium-resolution spectrum in the H- and K-lines region ("H&K").

Parameter	Value
P (days)	27·332±0·008
γ (km/s)	18·38±0·59
K (km/s)	31·99±0·80
e	0·293±0·026
ω (°)	116·1±4·0
T (JD)	2449203·200±0·359
$a \sin i$ (Gm)	11·49±0·30
Mass function ($M_\odot$)	0·078±0·012

Table 3.6: Orbital parameters of CS Cet.

km/s, Smithsonian Astrophysical Observatory

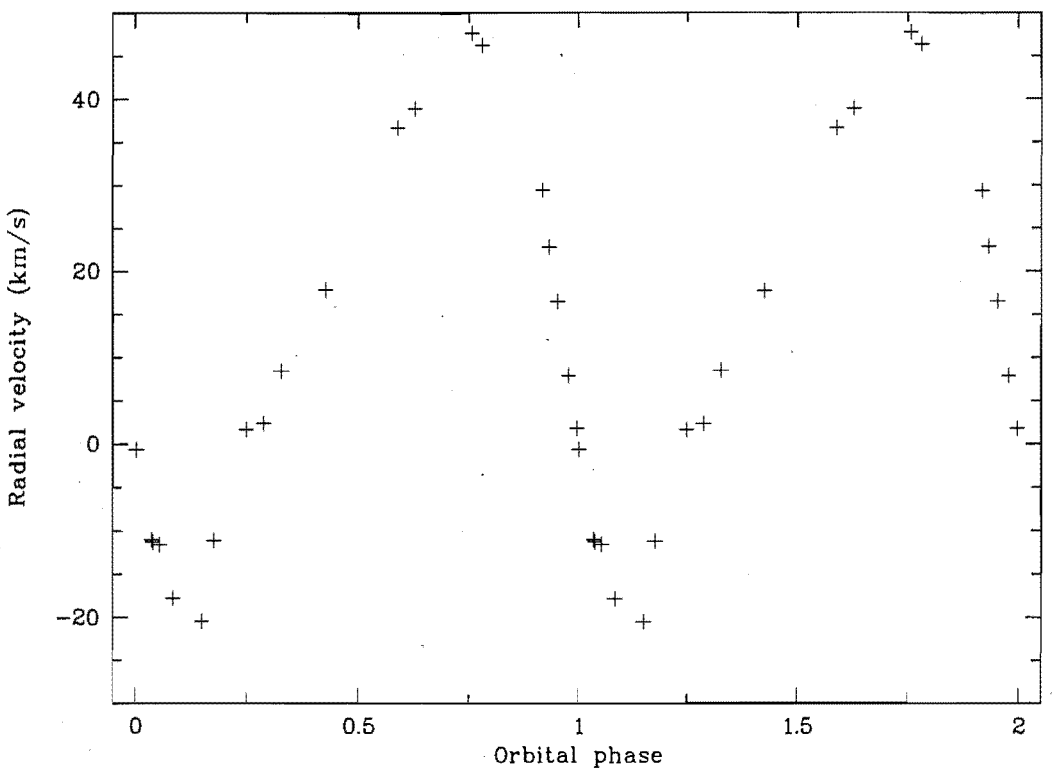

Figure 3.2: Radial velocities of CS Cet, phased according to the period and time of periastron passage set out in Table 3.6.

and $\log g$ =4·5 (c.g.s.) were scaled to fit the redward half-line of Figure 4 and the best fit was found with a line representing $T_{\rm eff}$ = 6250 K scaled to give a core flux of 0·773 of the continuum (the fitting was performed with a VMS/Fortran77 program written for the purpose by the author and listed in Appendix C). The radial velocity of the metal-line spectrum relative to the centre-of-mass of the solar system is −17·81±0·21 km/s and that of the fitted Kurucz model line is +60 ± 1 km/s which, with the computed system γ = +18·38±0·59 km/s, gives an amplitude ratio and therefore mass ratio of 1·14±0·05. With canonical values for $T_{\rm eff}$ from Gray,[12] and the assumption of luminosity class V from the $\log g$ value, the line fit suggests that the companion star is a main-sequence dwarf of spectral type approximately F6, having a mass of $\sim$1·3 $M_\odot$ and an absolute visual magnitude $M_V \approx 3{\cdot}8$.

The Hipparcos parallax[13] is π =0·00756″±0·00108″ (distance 132 ± 22 pc), implying a distance modulus of 5·607±0·290 mag. From the companion's magnitude and the mass ratio calculated above, and using the adopted value for V listed in Table 3.4, it follows that the active star in its unspotted state has an absolute visual magnitude of $M_V \approx 2{\cdot}4$ and mass $M \approx 1{\cdot}45\,M_\odot$. Application of the linear relations for $\log(M/M_\odot)$, $\log(R/R_\odot)$

[12] Gray, 1992, *op cit*, Table B1
[13] Schrijver H., *op cit*, vol. 5

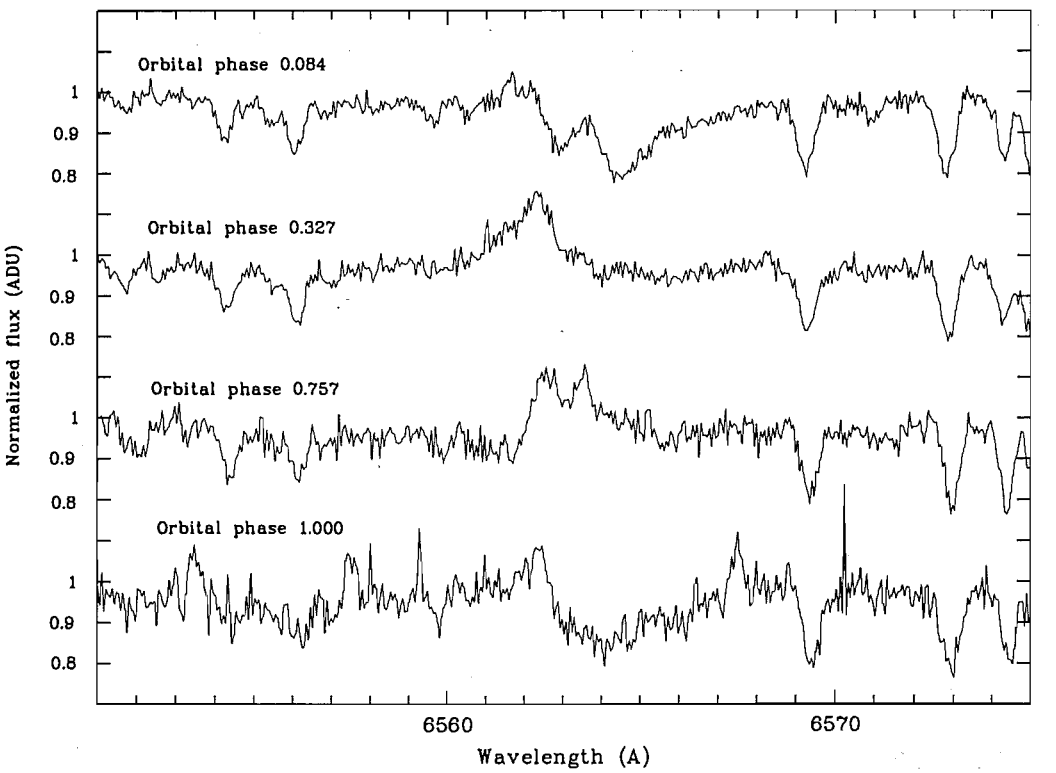

Figure 3.3: High-resolution Hα spectra of CS Cet. The individual spectra are marked with their phases according to the period and time of periastron passage set out in Table 3.6.

Bandpass or Colour	Interpolated value for companion star	Resulting value for active star	Barnes-Evans radius ($R/R_\odot$)
V	9·4	8·0	
$B-V$	0·49	0·94	4·6
$V-R$	0·44	0·72	5·0

Table 3.7: Calculated magnitudes and colours of the individual stars of CS Cet, and the radius of the active star calculated using the Barnes-Evans relation.

and $\log(L/L_\odot)$ in the case of luminosity class IV stars[14] to these values yields a radius of the active star of

$$R \approx 3{\cdot}8\, R_\odot \text{ or } \sim 2{\cdot}6\,\text{Gm}.$$

Interpolation in Table B1 of Gray[15] for colours for the companion and then subtraction of those colours from the adopted values for the combined light yielded the values for the two stars as listed in Table 3.7. The V value given for the active star corresponds to

[14]Schmidt-Kaler, *op cit*, at page 308
[15]Gray, 1992, *op cit*, Table B1

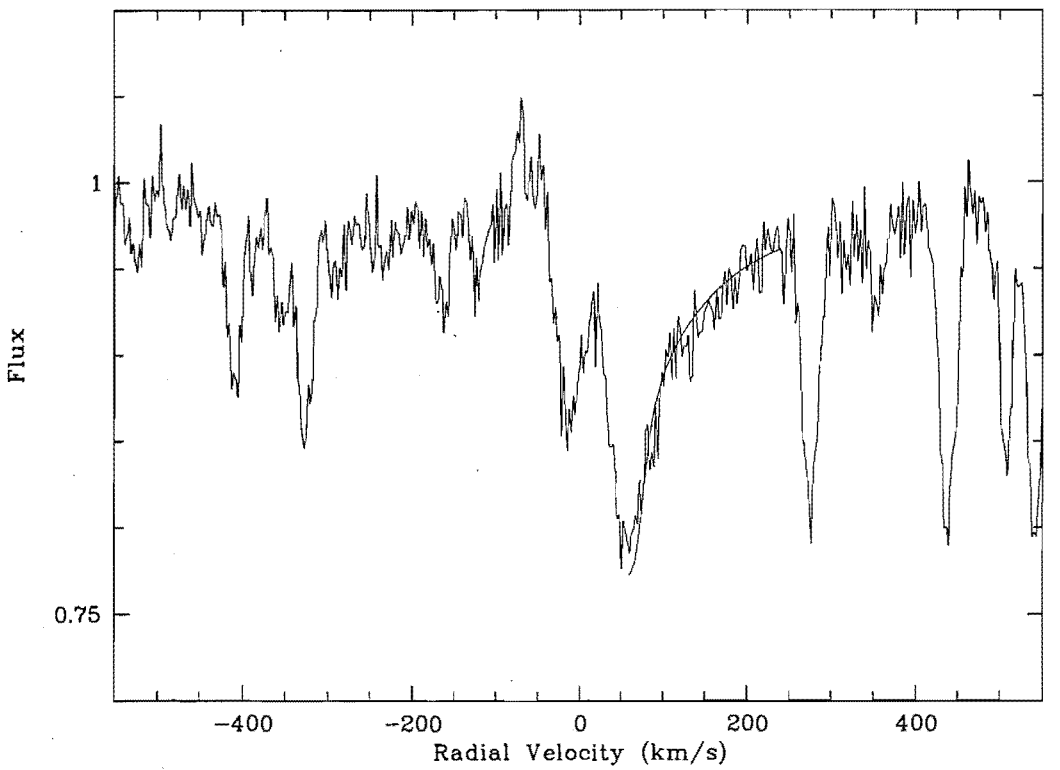

Figure 3.4: Hα spectrum obtained 1995 July 17, showing a 6250 K Kurucz model Hα line profile (smooth curve) fitted to the secondary's Hα absorption profile. The radial velocity scale is zeroed on the Hα absorption line of the primary star.

an absolute magnitude of M_V =2·4. The Barnes-Evans relation,[16], with the Hipparcos parallax, was then used to provide a second estimate of the radius of the active star. The radii derived by this method are ~30% greater than those previously calculated, which is not unreasonable given (a) the large uncertainties involved in several steps of the calculations and (b) the fact that the colours adopted for the active star are probably too red, introducing a systematic error which would tend to inflate the size of the star.. Taking all of the calculations into account, a reasonable value for the radius of the active star is

$$R = 4{\cdot}4 \pm 0{\cdot}6\, R_{\odot}.$$

The calculated $(B-V)$ colour of the active star (Table 3.4) is 0·94. Limiting values can be be estimated for the uncertainty in the colour: the colour index of the active subgiant must be redder than the combined colour index, 0·826, and the $(B-V)_0$ value of a luminosity class III–IV star (as implied by the calculated M_V value) is unlikely to be

[16]Barnes T. G., Evans D. S. and Parsons S. B, 1976, *MNRAS*, **174**, 503, and Barnes T. G., Evans D. S. and Moffett T. J., 1978, *MNRAS*, **183**, 285

redder than 1·09, the reddest value reported by Fitzgerald[17] for such stars. Hence,

$$(B-V)_{\rm P} = 0{\cdot}94^{+015}_{-011}.$$

The $(B-V)_0$-$T_{\rm eff}$ relation of Flower[18] gives

$$T_{\rm eff} = 4980^{+235}_{-280}\ {\rm K}$$

for which the tabulation of spectral types against colour index in Fitzgerald[19] yields a spectral type for the active star of G5-K1 III-IV.

Combination of the computed mass function (Table 3.6) with the mean of the masses calculated above yields a value for the angle of inclination of

$$i = 42{\cdot}^{\circ} \pm 4^{\circ}$$

and thence, with the computed value for $a \sin i$, a value for the semi-major axis of the orbit of the active star:

$$a = 17{\cdot} \pm 2{\cdot}\ {\rm Gm}$$

which is 3·9±1·1 times the calculated radius of the star.

3.2.3 Rotation of the active star

The Hipparcos measurements of parallax and proper motion[20] yield new values for the space motion of the system:

$$\begin{aligned} U &= +47{\cdot}6 \pm 7{\cdot}4\ {\rm km/s} \\ V &= -27{\cdot}7 \pm 4{\cdot}1\ {\rm km/s\ and} \\ W &= -23{\cdot}6 \pm 1{\cdot}0\ {\rm km/s}, \end{aligned}$$

implying that this is not a young system and its components might be expected to have achieved synchronous rotation. However, as discussed in Section 1.3.2, asynchronous rotation is found in a significant minority of active binary systems.

Rotational broadening of the metal lines of the high-resolution spectra of CS Cet was measured by the method described in Section 2.3.2, in the case of CS Cet using a spectrum of the G6/8 IV star δ Pavonis (HR 7665) and a limb-darkening coefficient of ϵ =0·78 obtained from Figure 17.6 of Gray,[21] using the $(B-V)$ and $T_{\rm eff}$ calculated above.

The best fit of width was found with a rotational-broadening function corresponding to

$$v \sin i = 13{\cdot}0\ {\rm km/s}$$

with a standard error of 0·48 km/s. As discussed in Section 1.3.4, since this is an asynchronously rotating system, it is not safe to assume that the axis of rotation of the active

[17] Fitzgerald M. P., 1970, *Astron. Astrophys.*, 4, 234
[18] Flower P. J., 1996, *ApJ*, **469**, 355
[19] *op cit*
[20] Schrijver H., *op cit*, vol. 5
[21] Gray, 1992, *op cit*

star is perpendicular to its orbital plane. If it is, the value for the orbital angle of inclination calculated above implies an equatorial velocity of rotation of

$$v = 19{\cdot}4 \pm 0{\cdot}49 \text{ km/s}.$$

With the calculated radius of the active star, these values imply a maximum limit on the rotation period for the active star of

$$P = 11{\cdot}5 \pm 1{\cdot}3 \text{ d}.$$

It is noted that this period is less than half of the computed orbital period and significantly different from the Hipparcos photometric period of 4·50 days.[22]

No peak corresponding to the rotation period was found in the power spectrum of the light curve. Assuming that the variation in the V photometry is due to spot modulation, this suggests that photospheric spots on the active star may be both numerous and short-lived. Typically, the photometric measurements were obtained at intervals ranging from two days to three weeks, at a frequency insufficient for detection of phenomena having a lifetime shorter than about 60 days in the best cases. Clearly the photometric variations had very much shorter periods than that.

CS Cet appears most likely to belong to a class of active stars which are not active *because* they are in short-period binary systems, but rather because the active star has been spun up by some other mechanism or has retained its primeval angular momentum. If the suggestion of Wood *et al*,[23] that RS CVn stars have extended coronae produced by their magnetic interaction which produce excess EUV emission relative to other binary systems (see Section 1.5.2 above), is true, then a system such as CS Cet which is not active because of its binarity might be expected to show a lower coronal EUV flux than RS CVn stars. The ROSAT WFC S1 (60–140 Å) count rate of 0·078 counts/s (see Table 3.1 above) is, however, by far the highest in the stars selected for this project, and it appears that either there *is* some magnetic interaction between the stars, or that the theory of Wood *et al* does not completely account for high-energy EUV emission.

One possible explanation is that the active subgiant in CS Cet is essentially an FK Comae-type star which is fortuitously in a binary system. In this system, however, the small mass ratio (Section 3.2.2) entails that the stars of the coalesced binary system would have been individually less massive than the present companion star, and thus they should not have evolved to the stage of post-main-sequence expansion and coalescence while the companion star remained on the main sequence.

An alternative explanation possibly lies in the model of Pinsonneault *et al*,[24] discussed in Section 1.3.3, wherein the deepening of convection as a star evolves off the main sequence results in the dredging-up of material of high angular momentum from a stellar core which has retained its primevally high rate of rotation, and the consequent spinning-up of the envelope of the star. This will be considered below in the context of the abundance of lithium.

[22] Schrijver H., *op cit*, vol. 5, and Grenon, *op cit*

[23] *op cit*

[24] *op cit*

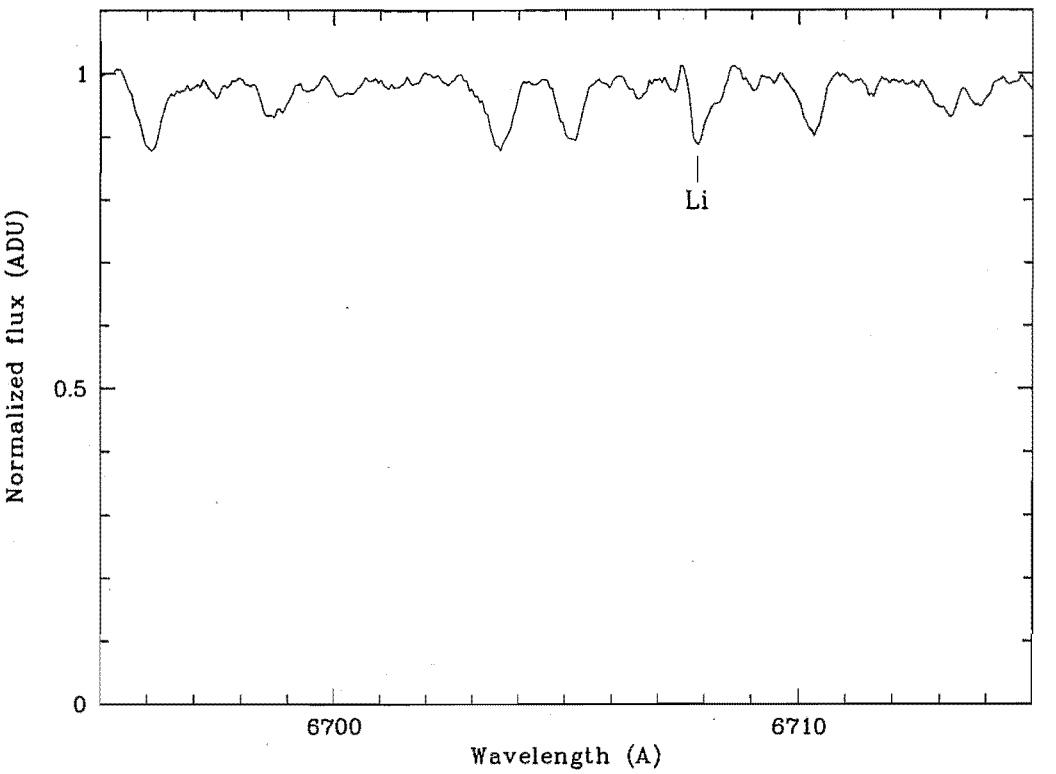

Figure 3.5: Spectrum of the λ6708 Li I line, obtained 1995 May 22.

3.2.4 Lithium abundance

One spectrum of the λ6708 Li I resonance doublet was obtained. Figure 3.5 shows a lithium line blended on its redward side with a telluric H_2O line. By fitting a gaussian to the non-blended part of the profile, the equivalent width of the line was determined to be 74 ± 5 mÅ. With the $T_{\rm eff}$ value calculated above (Section 3.2.2), the abundance of lithium was determined by two-dimensional cubic spline interpolation in the $T_{\rm eff}$ = 4250–5250 K columns of the curve of growth Table 2 of Soderblom *et al*[25] to be

$$\log N(\mathrm{Li}) = 1{\cdot}59^{+028}_{-036}$$

where $\log N(\mathrm{H}) = 12$. The data in Soderblom *et al*[26] were computed for main-sequence dwarfs, but the lithium abundance is much more sensitive to effective temperature than to surface gravity (Brown *et al*,[27] Pallavicini *et al*[28]) and uncertainties due to the latter are insignificant compared with those due to the former.

[25]Soderblom D. R., Jones B. F., Balachandran S., Stauffer J. R., Duncan D. K., Fedele S. B., and Hudon J. D., 1993, *AJ*, **106**, 1059

[26]*ibid*

[27]Brown J., Sneden C., Lambert D. L., and Dutchover E., 1989, *ApJS*, **71**, 293

[28]Pallavicini, Cerruti-Sola and Duncan, *op cit*

Iben[29] predicted $\log N(\mathrm{Li}) < 1{\cdot}5$ for giant stars, and Brown *et al*[30] analysed previous observations of 644 giants and found that only 8% had a lithium abundance $\log N(\mathrm{Li}) \geq 1{\cdot}2$. The range of values calculated for CS Cet lies above the Brown *et al* figure, suggesting that the active star has a real photospheric lithium excess, and the combination of lithium excess, fast asynchronous rotation and chromospheric activity favours the Simon & Drake[31] and Fekel & Balachandran[32] hypotheses (see Section 1.8) of a deep dredge-up in the early giant stage bringing ^{7}Li-rich material of high angular momentum from a fast-spinning stellar core to the outer envelope, the transfer of angular momentum spinning-up the stellar surface and creating a dynamo which drives the star's chromospheric activity.

3.2.5 Hα emission

To examine the emission in Hα, it was necessary to remove the photospheric spectra of both of the stars from the observations. The contribution of the companion star was removed by subtracting the same Kurucz model Hα profile that was used (Section 3.2.2) to classify the star. The absorption spectrum of the active star was removed by subtracting the rotationally broadened spectrum of δ Pav which was fitted to the active star's spectrum (Section 3.2.2). The program listed in Appendix D was used.

The resulting emission spectra have a single emission peak at the same wavelength as the Hα absorption line of the active star. The equivalent width of the peaks varied non-periodically throughout the period of observations between 0·798 Å and 1·331 Å, with a mean of 1·028 Å. Figure 3.6 shows a typical emission peak, obtained from the spectrum shown at orbital phase 0·327 in Figure 3.3.

The rotational broadening of the emission peak also varied considerably over the period of observation and, although the standard deviation of 12·3 km/s around the measured mean of 103·5 km/s must be accounted for partly by error arising from noise in the spectra, it is clear that there was real variation in the rotational velocity of the source material over the observation period which could be accounted for by variations in the distance outward from the centre of the active star of the source region. No periodicity was found in the variations.

Assuming that the material emitting in Hα is co-rotating with the star with the rotational period the upper limit of which was calculated above, the measured rotational velocities of the emitting material imply that it occupies a region $25{\cdot}5 \pm 2{\cdot}3\, R_\odot$ or, with the value calculated above for the radius of the active star, up to $5{\cdot}8 \pm 1{\cdot}1$ times the radius of the active star from the centre of the active star. The radii in this range are in accordance with the suggestion of Collier Cameron[33] that coronal loops extending beyond the Keplerian co-rotation radius of a rapidly rotating star may trap prominence-like condensations of excited material outside the co-rotation radius. As discussed in Section 1.9, observations of the star AB Dor[34] have yielded evidence for the existence of

[29] Iben I., 1967, *ApJ*, **147**, 624 and 650
[30] *op cit*
[31] *op cit*
[32] *op cit*
[33] Collier Cameron, 1988, *op cit*
[34] Collier Cameron and Robinson, *op cit*, and Collier Cameron and Woods, *op cit*

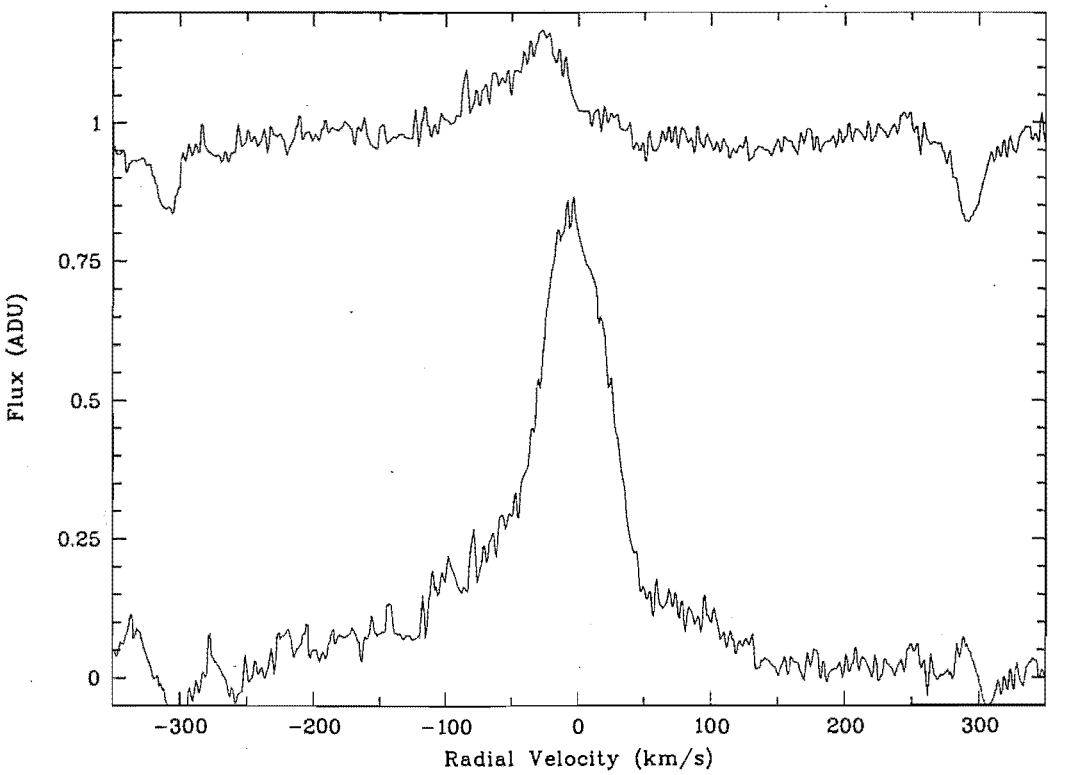

Figure 3.6: Upper plot: Hα spectrum of CS Cet, obtained 1994 September 26. Lower plot: residual Hα emission after subtraction of Kurucz model Hα line profile representing the companion star and a rotationally-broadened spectrum of HR 7665 representing the photospheric spectrum of the active star. The radial-velocity calibration of both plots is zero at the Hα laboratory wavelength.

such material emitting in Hα up to 4 stellar radii from the centre of the active star.

3.3 Conclusions

From high-resolution spectroscopy of CS Cet, an orbital radial-velocity curve has been obtained showing that CS Cet is a binary system with a period of 27·332±0·008 days and an orbital eccentricity of 0·293±0·026. Hα spectra show emission of a strength sufficient to more than fill the Hα absorption lines of both stars of the system.

Based on the fitting of a model Hα line to a single spectrum, it is concluded that the CS Cet system consists of a late F-type dwarf secondary and a chromospherically active G5-K1 III-IV primary having an absolute visual magnitude of $M_V \approx 2{\cdot}4$ and a mass $M \approx 1{\cdot}45\,M_\odot$. Based on this analysis, the rotation period of the active star has been calculated as not more than 11·5±1·3 days, a period less than half the orbital period of the system which suggests that the photosphere of the active star has been spun up by a transfer of angular momentum from a fast-spinning core. Assuming co-rotation, the

rotational velocities of the Hα emission show that the source of that emission is located in, and varies within, a range of distance of up to 5·8±1·1 times the radius of the active star from the centre of the star.

The m_V of the system varied over a range of 0·16 mag. but it was not measured with sufficient frequency to enable a period of variablity to be determined. Such periodicity as does exist certainly has a timescale less than 60 days.

If, in the future, digital templates are made for the Hα region that was mostly observed, it may be worthwhile to derive radial velocities from the échelle spectra by digital cross-correlation. The multiplex gain in using many lines simultaneously *might* enable the spectrum of the secondary star to be detected.

Chapter 4

BB Sculptoris

The well-known visual triple BB Sculptoris[1] is also listed as HD 9770, SAO 193189, Gliese 60 ABC, CPD−30° 181, RE J013501−295427, IRAS 01326−3010 and HIP 7372. The BB Scl system comprises two stars (A and B) in a well-defined 4·559-y orbit with semi-major axis 0·171″, and a third star (C), the AB×C system having an orbital period of 111·8 years and semi-major axis 1·419″.[2] The parallax was given as 0·052″±0·007″ by Jenkins[3] and a trigonometric distance of 18 ± 4 pc was reported by Woolley *et al.*[4] Distances of 18 pc[5] and 20 pc[6] have been obtained from the spectroscopic parallax. However, the parallax of the AB system since obtained by Hipparcos is π =0·04229″± 0·00147″.[7] The AB system fell into the category of resolved systems of which both components were observed simultaneously;[8] in the case of BB Scl, the measured parallax was that of the photocentre of the AB system.[9]

The spectral types and magnitudes of the individual components are necessarily difficult to determine because of the angular proximity of the three stars. The Michigan Spectral Catalogue[10] lists a spectral classification of K1 V for the whole system while Edwards[11] estimated the individual spectral types as K3V (A), K4V (B) and M2V (C) from Johnson V photometry. Hirshfield and Sinnott[12] list a V magnitude for the system of 7·1. Measurements of the V magnitude of the A+B system can be found in Edwards[13] who

[1] *IBVS* No. 4471

[2] Hirshfeld and Sinnott, *op cit*

[3] Jenkins, L. F., 1963, *Supplement to the General Catalogue of Trigonometric Stellar Parallaxes*, Yale University Observatory, Conn.

[4] Woolley, R., Epps, E. A., Penston, M. J., and Pocock, S. B., 1970, *Roy. Observ. Ann.*, No. 5

[5] Cutispoto G., Pallavicini R., Kürster M. and Rodonò M., 1995, *Astron. Astrophys.*, **297**, 764

[6] Cutispoto G., Kürster M., Messina S., Rodonò M. and Tagliaferri G., 1997, *Astron. Astrophys.*, **320**, 586

[7] Schrijver H., *op cit*, vol. 5

[8] Perryman, M. A. C., 1997, *The Hipparcos and Tycho Catalogues*, vol. 1, ESA Publications Division, Noordwijk

[9] Schrijver H., *op cit*, vol. 5

[10] Houk, *op cit*

[11] Edwards T. W., 1976, *AJ*, **81**, 245

[12] *op cit*

[13] *op cit*

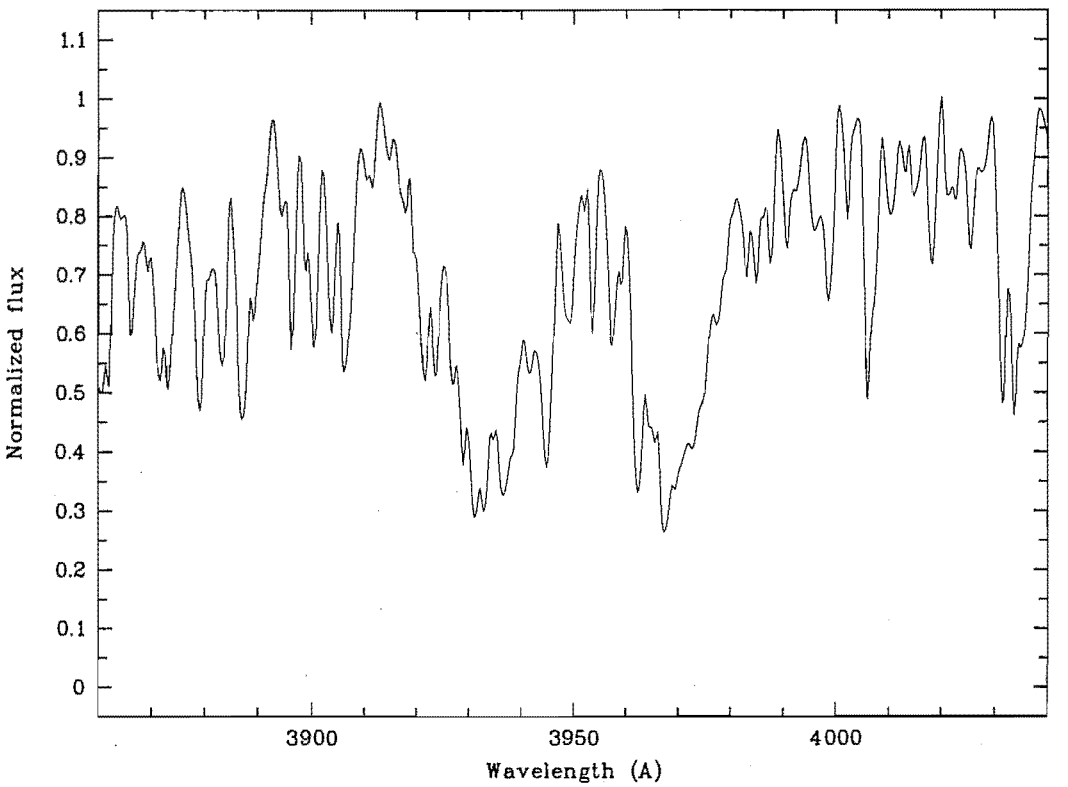

Figure 4.1: Ca II H and K lines spectrum of BB Scl, obtained at MJUO.

gives 7·09, Bessell[14] who found 7·11 and Cutispoto *et al*[15] who list 7·11. Also, the star was observed by Hipparcos. The *Hp* magnitude for A+B is 7·2533±0·0024.[16] Adopting a $(B-V)_C$ equal to the Tycho $B_T - V_T$ =0·909±0·011[17] and using Table 14.2 of van Leeuwen *et al*,[18] the corresponding V magnitude is 7·109 with an uncertainty "less than 0·01 mag".[19]

BB Scl was included in a list of suspected variable stars by Petit,[20] albeit without specification of magnitude range or variability type. Cutispoto *et al*[21] found an amplitude in V of about 0·07 mag. with a period of 6·29±0·24 d, but this has since been acknowledged[22] to be an alias of the true ∼0·48 d period.[23]

[14]Bessell M. S., 1990, *Astron. Astrophys. Supp.*, **83**, 357
[15]Cutispoto, Kürster, Messina, Rodonò and Tagliaferri, 1997, *op cit*
[16]Schrijver H., *op cit*, vol. 5
[17]*ibid*
[18]*op cit*
[19]*ibid*
[20]Petit, M., 1980, *IBVS* No. 1788
[21]Cutispoto, Pallavicini, Kürster and Rodonò, *op cit*
[22]Cutispoto, Kürster, Messina, Rodonò and Tagliaferri, 1997, *op cit*
[23]Section 4.2 below

Band (μm)	IRAS flux	Magnitude
12	0·5706	4·24
25	0·2611	3·53
60	0·3577	1·31
IR colours		Indices
[12]−[25]		0·711
[25]−[60]		2·22

Table 4.1: IRAS fluxes of BB Scl in the 12, 25 and 60 μm bands, together with magnitudes and colour indices calculated therefrom.

WFC filter	Passband (Å)	Flux (counts/s)	Log $L_{\rm EUV}$ (ergs/s)
S1	60 – 140	$43{\cdot}9\times10^{-3}$	28·76
S2	110 – 200	$55{\cdot}2\times10^{-3}$	28·94
EUV to optical flux ratio			1·53

Table 4.2: ROSAT WFC EUV fluxes and luminosities for BB Scl

4.1 Identification as a chromospherically active star

The BB Scl system was definitively identified with the ROSAT wide field camera source (2)RE013501−295430 by Mason *et al*,[24] based in part on spectra of 1 Å resolution obtained in 1991 and 1992 on the SAAO 1·9-m telescope, which show emission of approximate equivalent width 0·2 Å in the H and K lines. Moderate emission peaks are also observed in spectra obtained in the course of this program in 1996 with the MJUO MRS (Figure 4.1). The Michigan Spectral Catalogue[25] makes no mention of H and K emission, but that is presumably because of the lower resolution. The IRAS fluxes of BB Scl as given by Wolstencroft *et al*[26] and their conversion to magnitudes according to the formulae given by Hickman *et al*[27] are set out in Table 4.1, and the ROSAT wide field camera count rates as listed in the NASA HEASARC database are listed in Table 4.2 with EUV luminosities as given by Hodkin and Pye.[28]

Cutispoto *et al*[29] inferred that, in the absence of evidence of a close binary system, the surface activity was probably due to the rapid rotation of a young star. How-

[24]Mason, K. O., Hassall, B. J. M., Bromage, G. E., Buckley, D. A. H., Naylor, T., O'Donoghue, D., Watson, M. G., Bertram, D., Branduardi-Raymont, G., Charles, P. A., Cooke, B., Elliott, K. H., Hawkins, M. R. S., Hodgkin, S. T., Jewell, S. J., Jomaron, C. M., Sekiguchi, K., Kellett, B. J., Lawrence, A., McHardy, I., Mittaz, J. P. D., Pike, C. D., Ponman, T. J., Schmitt, J., Voges, W., Wargau, W, and Wonnacott, D., 1995, *MNRAS*, **274**, 1194

[25]Houk *op cit*

[26]Wolstencroft R. D., Savage A., Clowes R. G., MacGillivray H. T., Leggett S. K. and Kalafi M, 1986, *MNRAS*, **223**, 279

[27]*op cit*

[28]Hodgkin S. T. and Pye J. P., 1994, *MNRAS*, **267**, 840

[29]Cutispoto G., Pallavicini R., Kürster M. and Rodonò M., 1995, *Astron. Astrophys.*, **297**, 764

ever the galactic (U, V, W) velocity components which Eggen[30] calculated for BB Scl are $(+22{\cdot}2, -5{\cdot}3, -31{\cdot}6)$ km/s in Eggen's left-handed coördinate system, and such velocity components are typical of old disk stars.

The value given by Hodgkin and Pye for $\log L_{\rm EUV}$ in the WFC S1 passband equates to a luminosity of $5{\cdot}75 \times 10^{21}$ W in that wavelength range. Adopting the absolute magnitudes in V derived in Section 4.3 below for the separate A and B stars of BB Scl, and deriving bolometric corrections direct from absolute magnitudes by cubic spline interpolation in Allen[31] §99 (using a bolometric correction for star B appropriate to a star of $M_V = 7{\cdot}69$ as estimated in Section 4.3 below), gives a total bolometric magnitude for components A and B of BB Scl of

$$M_{\rm bol}(\text{BB Scl}) = 4{\cdot}96$$

corresponding to a bolometric luminosity of

$$L_{\rm bol}(\text{BB Scl}) = 3{\cdot}15 \times 10^{26} \text{ W}$$

and, therefore a ratio

$$\frac{L_{\rm EUV}}{L_{\rm bol}} = 1{\cdot}82 \times 10^{-5}$$

for the EUV in the S1 passband. The low ratio implies that the excess EUV flux associated with chromospheric activity[32] has its origin in the secondary component of BB Scl, the primary component contributing ~79% of the light in the optical band but, especially if it is, as Eggen's velocities suggest, an old disk star, little in the EUV.

4.2 The light curves

Single-channel photoelectric photometry in the $UBV(RI)_{\rm C}$ system of the unresolved AB×C system was obtained in 1992 and 1993 using the SAAO 0·5-m telescope and from 1993 to 1996 using the two 0·6-m MJUO telescopes. V data obtained in 1994 July (an observation fortuitously caught the system in primary eclipse) revealed that one of the components of the AB visual binary system is itself an eclipsing binary for which the ephemeris of primary eclipse is

$$\text{HJD} = 2448930{\cdot}6448 + (0{\cdot}476525 \pm 0{\cdot}000013) \times E.$$

The phased light curve (Figure 4.2) shows that the primary eclipse has a depth about 0·22 mag. whereas that of the secondary eclipse is about 0·18 mag., indicating that they are indeed two different eclipses and the above ephemeris is to be preferred to one in which the period is half as long and the secondary eclipse is not visible. It also appears that the orbit is close to circular, since the eclipses are of comparable duration and the phase of central secondary eclipse is 0·50.

Table 4.3 lists the orbital and photometric periods of all of the pairs of K-type dwarfs listed in the second catalogue of chromospherically active binary stars of Strassmeier *et*

[30]Eggen O. J., 1962, *Roy. Obs. Bull.* No. 51

[31]Allen, *op cit*

[32]Armado and Byrne, *op cit*, and Wood *et al, op cit*

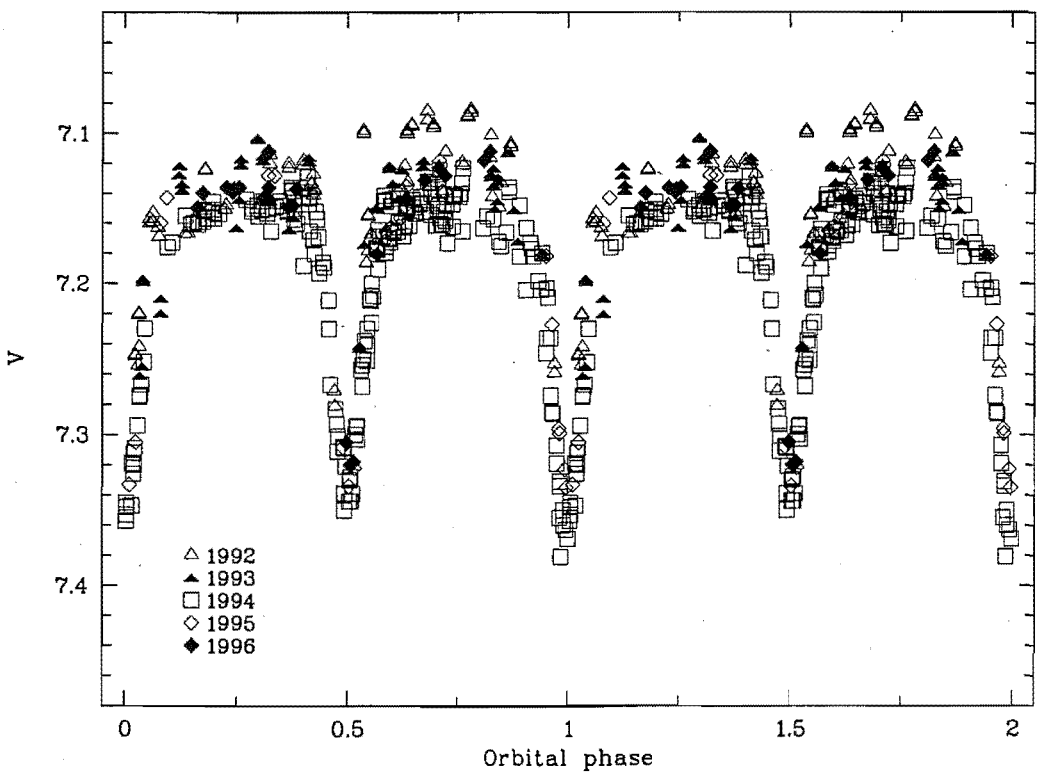

Figure 4.2: Phased V light curve from SAAO and MJUO photometry of BB Scl

Name	Components	Orb. period (d)	Phot. period (d)
V808 Tau	K3V+K3V	11·929	6·82
BD+64 487	K2V+K2V	44·38	
OU Gem	K3V+K5V	6·992	7·36
DH Leo	K0V+K7V	1·070	1·067
LR Hya	K0V+K0V	6·866	3·145
HD 165590C	K7:V+K7V	25·762	
BY Dra	K4V+K7·5V	5·975	3·827
HR 7578	K2–3V+K2–3V	46·817	16·5
BD−00 4234	K3Ve+K7Ve	3·757	

Table 4.3: Orbital and photometric periods of known active K-dwarf binaries listed in the second catalogue of active binaries by Strassmeier *et al.* In the case of DH Leo, the components and orbital period listed are those of the close binary in the triple system.

al.[33] Except for DH Leo, they all have periods of several days. In DH Leo, as in BB Scl, the system of interest is a close binary in a triple system, and the orbital period is 1·070 days. The close binary in DH Leo is listed as having Hα emission above the continuum.

[33]Strassmeier, Hall, Fekel and Scheck, *op cit*

4.2.1 Variability due to spots and tidal distortion

The out-of-eclipse magnitudes show considerable scatter over the four years of observation. The combined magnitude of the system ABC was as bright as 7·10 in 1992, but about 7·14 in 1994. Such variations are typical in active-chromosphere binary stars because of the variation in spot numbers on timescales of years. Most of the data came from 1994 observations at MJUO, and the scatter for that year is clearly less than that for all the photometric data considered together (see Figure 4.2).

The phased $(B-V)$ light curve (Figure 4.3) constructed from observations made at SAAO in 1992 (the highest quality colour photometry available) shows a considerable scatter out of eclipse – again suggesting the presence of substantial and variable cooler surface regions on one or both of the eclipsing stars.

If one or a pair of active stars with extensive surface spots is present in this close binary system with a half-day period, one might hope to find photometric evidence of a rotation period also of the order of half a day. One might also hope to find some confirmation of the observation by Hall[34] that very fast-rotating active stars tend to show rigid-body rather than differential rotation (see Section 1.6.2). The observations show a greater brightness between phases 0·6 and 0·9 than between phases 0·1 and 0·4 which might be due to the presence of spots non-uniformly distributed in longitude. The considerable scatter in the 0·6 to 0·9 interval would then be attributed to variation in spot numbers over the long time of the observations, and possibly also to the drift in orbital phase of the rotationally modulated spot wave. There is less scatter in the 0·1 to 0·4 interval in which the brightness shows a single peak at about phase 0·3.

4.3 Physical parameters of the stars

The flatness of the light curves out of eclipse and the fact that the eclipses occur at even intervals of ~0·5 of phase and are of similar duration, indicate a well-detached system in a circular orbit or at least one with negligible eccentricity. The slightly different depths of the two eclipses imply a small difference in mean surface flux density, or equivalently effective temperature.

The combined light of the BB Scl system becomes bluer during both eclipses. This is a small (0·02–0·05 mag) but definite effect which can be seen most clearly in the $(U-B)$, $(B-V)$, $(V-R)$ and $(V-I)$ light curves of Cutispoto *et al*[35] and in the $(V-I)$ light curve of Tagliaferri *et al.*[36] The increased blueness of the combined light from the AB system during both primary and secondary eclipses indicates that the light from the star not involved in the eclipsing system is bluer than the light from either of the eclipsing stars, and therefore that the third light comes from star A, star B being the eclipsing binary. The contribution of the dim M2 V star HD 9770 C can be ignored since, at $V \approx 11{\cdot}5$ mag., it contributes only ~1·5% of the combined light of the system.

The available spectral classifications of the A and B components indicate that these

[34] Hall, 1991, *op cit*

[35] Cutispoto, Kürster, Messina, Rodonò and Tagliaferri, *op cit*

[36] Tagliaferri G., Covino S., Cutispoto G., and Pallavicini R., 1999, *Astron. Astrophys.*, **345**, 514

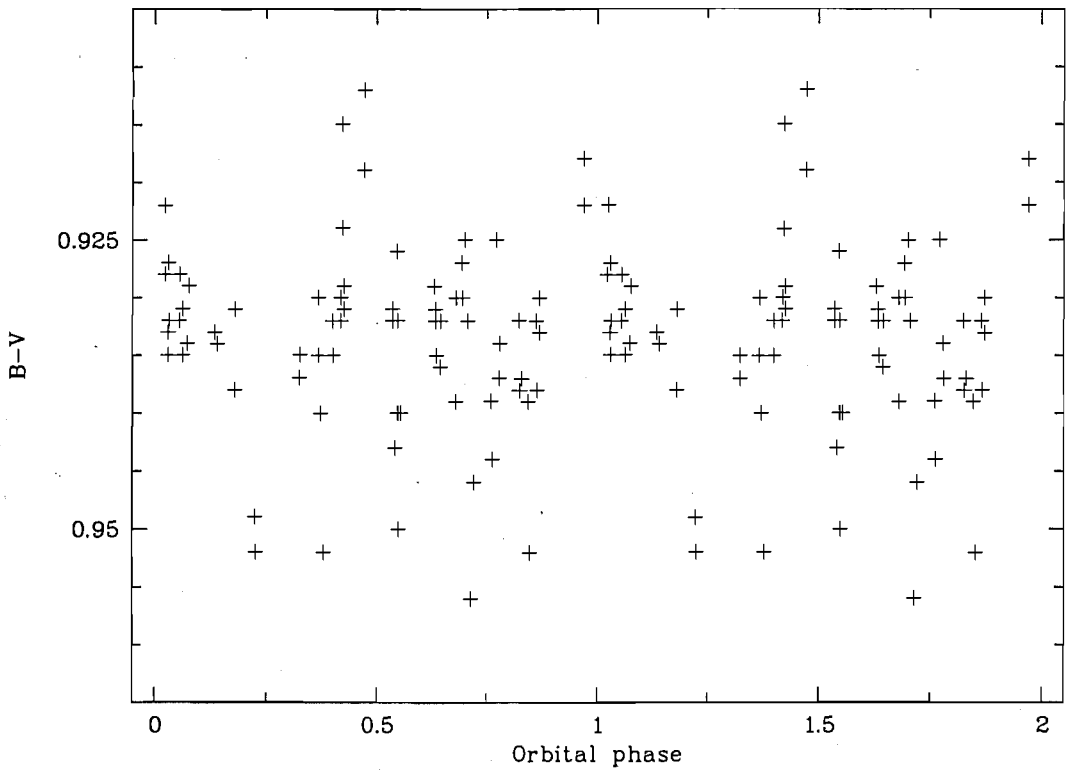

Figure 4.3: Phased $(B-V)$ light curve from SAAO photometry of BB Scl obtained during 1992

components consist of main-sequence stars. Calculated from the measured Hipparcos parallax, π =0·04229″±0·00147″ (which implies a distance modulus of 1·869 mag) and magnitudes, $Hp_{\rm A}$ =7·511 and $Hp_{\rm B}$ =8·941,[37] the absolute magnitude of star A (after conversion from Hipparcos to Johnson magnitudes) is M_V =5·50 and that of the component B is M_V =6·93. Thus M_V =7·69 for the two individual components of B, which for main sequence stars corresponds to spectral class K6 dwarfs having a colour index of $(B-V)_0$ ≈1·2, mass $M_{\rm A}$ ≈0·69 $M_\odot$, and $T_{\rm eff}$ ≈ 4590 K.[38] This implies a colour index of star A, given the Tycho colour index for the unresolved AB system of $(B-V)_{0,{\rm AB}}$ ≈0·909,[39] of $(B-V)_{0,{\rm A}}$ ≈0·84. Such a colour index is consistent with the star being of spectral type K1 as given by Houk,[40] with a visual magnitude ∼0·7 mag. brighter than expected for a zero-age main sequence star of that spectral type.[41]

[37] Schrijver H., 1997, *op cit*, vols 5 and 10
[38] Schmidt-Kaler *op cit*
[39] Schrijver H., 1997, *op cit*, vol. 5
[40] Houk *op cit*
[41] Canonical $(B-V)$ and M_V values taken from Gray, 1992, *op cit*, Table B1

4.3.1 Wilson-Devinney analysis

Note: This sub-section 4.3.1 reports work which was not the work of the author of this thesis, but which is included for the sake of completeness and because it was used as a basis for further reasoning about the nature of the BB Scl system. The author provided estimates of probable spectral type, brightness, colour and effective temperature which were derived as discussed in the preceding section to Dr J. D. Pritchard who had modified a version of the Wilson-Devinney (hereinafter "WD") program,[42] and he executed the program and derived the results reported in this subsection. In the absence of radial-velocity curves giving a precise mass ratio, no mass difference was inferred from the slight difference in effective temperature indicated by the light curves, and initially equal values were assumed for the masses of the two stars. The work reported in the remainder of this section 4.3.1 is that of Dr Pritchard and not of the present author.

The modifications to the WD code added the option to model the stellar surface fluxes with Kurucz stellar atmosphere models[43] in addition to the built-in blackbody and Carbon & Gingerich[44] model approximations.

With the mass ratio (q) set to unity, $T_{\rm eff,\,primary} = 4\,590\,{\rm K}$ and with the orbital period fixed at 0·476525 d, the semi-major axis was adjusted to obtain components of mass $M = 0{\cdot}69\,M_{\odot}$. The bolometric albedos and gravity darkening coefficients were set to appropriate values for convective envelopes (0·5 and 0·3 respectively) while limb-darkening coefficients were taken from tables created from Kurucz[45] solar metallicity models.

The parameters solved for were the orbital inclination, the effective temperature of the secondary component, the surface potentials of both components, the phase offset and the monochromatic luminosities of the primary component, and the third light contributions for each of the five $UBV(RI)_{\rm C}$ light curves. The five light curves were analysed simultaneously using the Method of Multiple Subsets[46] in order to circumvent the strong correlation between third light and the inclination. It was necessary to analyse all the available data together, despite the significant scatter from year to year caused, presumably, by spot activity on one or the other, or perhaps both, of the components of the binary system. No one year by itself had sufficient data obtained over a short enough period of time to make a meaningful analysis possible.

The preliminary analysis suggested that B_2 is slightly cooler than B_1. Therefore based on the resultant colours for the A, B_1 and B_2 components, the individual spectral types of the three components were re-estimated to be K1/2V, K3/4V and K4/5V respectively. (Reassuringly, these preliminary colours differ insignificantly from the colours derived from the finally adopted solution.) This suggests a mass ratio for the eclipsing system of $q = 0{\cdot}966$ and an effective temperature for B_1 of $T_{\rm eff,\,primary} = 4\,660\,{\rm K}$. With these new estimates the semi-major axis was re-adjusted to obtain the appropriate masses and then

[42] Wilson, R. E., 1979, *ApJ*, **234**, 1054, and 1994, *PASP*, **106**, 921

[43] Kurucz, R. L., 1993, *New Atmospheres for Modeling Binaries and Disks* in *Light Curve Modeling of Eclipsing Binary Stars*, ed. Milone E. F., Springer-Verlag, Berlin

[44] Carbon D. and Gingerich O, 1969, in *Theory and Observation of Normal Stellar Atmospheres* ed. Gingerich O., MIT Press

[45] Kurucz, 1993, *op cit*

[46] Wilson, *op cit*

Parameter	Value	Uncertainty
Model parameters		
Period	0·476525 d	0·000013 d
Inclination (i)	86·°	4·°
Mass ratio (q)	0·966	adopted
Semimajor axis (a)	2·856 $R_\odot$	adopted
Effective temperatures, $T_{\rm eff,1}$	4590 K	adopted
$T_{\rm eff,2}$	4485 K	20 K
Surface potentials, Ω_1	4·9	0·3
Ω_2	5·2	0·5
Derived properties		
Masses, M_1	0·71 $M_\odot$	adopted
M_2	0·68 $M_\odot$	adopted
Radii, R_1	0·72 $R_\odot$	0·2 $R_\odot$
R_2	0·74 $R_\odot$	0·2 $R_\odot$
R_2/R_1	1·03	0·05

Table 4.4: Parameters of the adopted light curve solution. Uncertainties are conservative estimates based on consideration of the standard errors reported by the WD code and the stability of the suggested corrections over many ($\sim$ 100) iterations.

further iterations were performed. At this stage the adjusted parameters were also broken into a third subset containing the two surface potentials.

Several thousand iterations of adjusting each parameter subset in turn were performed. As a consequence of the low degree of correlation between the adjusted parameters in each subset the iterations migrated only very slowly even as the overall weighted-sum of the squares of the residuals fell slowly but constantly. Throughout these iterations the suggested parameter corrections were typically comparable to, or somewhat smaller than, their standard errors, as reported by the WD code. The solution adopted as representative is that for which all the suggested parameter corrections became smaller than their respective standard errors by a factor of ten for consecutive iterations. This solution has a very slightly cooler and smaller secondary star, though only by $\sim$2% in T and $\sim$7% in R. Table 4.4 lists the physical parameters of the adopted model while Table 4.5 lists the corresponding photometry.

The achieved precision of the synthetic light curve fits to the observations, measured as the r.m.s. of the residuals between the observations and models, was only of the order of 3–5%. This is due mainly to the inherent scatter from epoch to epoch, presumably caused by changing spot patterns on the surfaces of the active stars in the system. Also, due to this scatter and assuming that one or other or both components of B is indeed the active system, the parameters reported here in some sense represent the "mean, equivalent non-active stars". To deduce the true properties of the components of the eclipsing binary would require the modelling of light curves obtained over a short time period relative to the time scale on which the pattern of activity changes. Furthermore there remain large

	Component			
Bandpass	A	B_1	B_2	B_1+B_2
U	9·03	10·5	11·0	10·0
B	8·53	9·8	10·2	9·2
V	7·64	8·8	9·1	8·2
R	7·12	8·2	8·5	7·6
I	6·64	7·7	7·9	7·0
Standard system indices				
$U-B$	0·50	0·7	0·8	0·7
$B-V$	0·89	1·0	1·1	1·0
$V-R$	0·52	0·6	0·6	0·6
$V-I$	1·00	1·1	1·2	1·2

Table 4.5: Photometric properties of stars A, B_1 and B_2 from the light curve solution. The contribution to third light from star C is neglected. The magnitudes are calculated from the fluxes reported by the WD code at orbital phase 0·25. The uncertainties in the photometry for Star-A and the combined photometry for Star-B_1+B_2 are probably not more than 0·01 mag. For the individual Star B_1 and Star B_2 photometry the uncertainties are somewhat greater due to the uncertainties in the radii derived from the light curve solutions, and results are consequently given to only one significant figure. Nonetheless they are probably not greater than perhaps 0·2–0·3 mag.

uncertainties in some of the derived properties of the binary system and its components, nonetheless some useful insight has been gained.

Notwithstanding the relatively low precision of the curve fits, the effective temperature of the secondary component relative to the adopted effective temperature of the primary is well defined, with an uncertainty of just 0·4%. This is due to the strong temperature-dependence of relative flux with respect to wavelength over the near-ultraviolet – near-infrared regime at these cool stellar temperatures. Changing the effective temperature of the secondary by as little as 100 K (i.e. 2% of its value) produces a markedly worse fit to the observed light curves, especially in U. For much the same reasons, the light contribution from star A, i.e. third light (neglecting star C), is also well defined with an uncertainty of not more than 5%. The ratio of the radii (i.e. R_2/R_1) by contrast is not well defined, the uncertainty deriving chiefly from the large scatter at orbital phases corresponding to ingress into and egress from eclipses. However R_1 and R_2 are anti-correlated so that the total stellar surface area is rather better defined with an uncertainty of ~6%.

As mentioned above, visual photometry has been obtained by a number of workers. Table 4.6 tabulates that of Edwards,[47] Bessell,[48] Schrijver[49] and Grenon,[50] and Cutispoto *et al*[51] as well as the results derived here based on the MJUO photometry and light curve

[47] *op cit*
[48] *op cit*
[49] Schrijver H., 1997, *op cit* vol. 5
[50] *op cit*
[51] Cutispoto, Kürster, Messina, Rodonò and Tagliaferri G, *op cit*

Magnitude Index	Edwards	Bessell	Schrijver vol. 5 Hipp.	Schrijver vol. 10 Tycho	Cutispoto *et al* (1997)	MJUO
V_{A+B}	7·09	7·11	7·11	7·240	7·11	7·13
V_A	7·72		7·37			7·64
V_B	7·99		8·80			8·20
$(U-B)_{A+B}$					0·58	0·58
$(B-V)_{A+B}$		0·92		0·909	0·92	0·93
$(V-R)_{A+B}$		0·545			0·54	0·55
$(R-I)_{A+B}$		0·525				0·52
$(V-I)_{A+B}$		1·070		0·95	1·07	1·06

Table 4.6: Visual photometry from Edwards, *op cit*, Bessell, *op cit*, Schrijver H., *op cit*, vol. 5, Grenon, *op cit*, Cutispoto, Kürster, Messina, Rodonò and Tagliaferri, *op cit*, and this work. Edwards makes no mention of the uncertainties in his measures. From comments made by Bessell, uncertainties within 0·02 mag for his measures can be assumed. For the Hipparcos measures the uncertainty in V_{A+B} and V_A is probably dominated by the uncertainty in the transformation from Hp to V which is still "less than 0·01 mag" while for V_B the uncertainty is dominated by the uncertainty in Hp of 0·217 mag. The uncertainties in the Tycho measurements are 0·009, 0·011 and 0·01 for V_T, $(B_T - V_T)$ and $(V_T - I_T)$ respectively. Cutispoto *et al* write that the typical accuracy of their absolute photometry "is of the order of 0·01 mag", except in the case of $(U-B)$ where it is "somewhat larger". The uncertainties in the MJUO photometry are discussed in detail in Section 4.3 but can probably safely be assumed to be not worse than 0·05 mag.

analysis.[52] As can be seen, there is good agreement with respect to the photometry for the combined A+B system. There is also reasonable agreement between Edwards and the Mt. John results for the V magnitudes of the individual components (V_A and V_B). However these are in quite significant disagreement with the Hipparcos measurements.

One might quite reasonably expect that the high resolution space-based results of Hipparcos should be preferred over the poorer seeing ground-based results which, at least in the case of the MJUO observations, did not resolve the C component from the A+B system let alone the individual A and B components themselves. However a few simple calculations are enough to cast uncertainty over the accuracy of the Hipparcos measures of V_A and V_B. The V light curve in Figure 4.2 clearly indicates depths of approximately 0·22 and 0·18 mag for primary and secondary eclipses respectively. The Hp light curve measured by Hipparcos[53] similarly shows two eclipses with depths of at least 0·18 mag, although phase coverage during minima is quite sparse. A beautiful V light curve by Tagliaferri *et al*[54] shows two eclipses of more or less equal depths of 0·16 mag, although the primary eclipse is probably made a little shallower than usual by a brightening of

[52] Section 4.3
[53] Grenon, *op cit*
[54] *op cit*

the system that starts at an orbital phase of approximately 0·7 and quite possibly lasts throughout primary minimum and through to an orbital phase of perhaps 0·1.

It is assumed that two eclipses of at least 0·16 mag in depth in V or (more or less equivalently) in Hp are required. In the case where an eclipsing binary has two mimima of equal depths, the maximum depths possible occur when the two eclipses are total, i.e. two components with exactly equal surface flux densities and radii in an orbit seen precisely edge on (inclination equals 90°). If the Hipparcos Hp magnitudes for the system (Hp_{A+B} =7·2533±0·0024) and the individual components (Hp_A =7·511±0·058 and Hp_B =8·941±0·217) are adopted, and half of the light of component B is apportioned to each of two components (B_1 and B_2) with exactly equal surface flux densities and radii (i.e. $Hp_{B_1} = Hp_{B_2}$ =9·694±0·217 mag), then the total system brightness during a total eclipse is $Hp_{A+B_{1/2}}$ =7·3745±0·0024 mag. Comparing this with the total system brightness out of eclipse implies the maximum depth for two eclipses of equal depth is only 0·1212±0·0291 mag, which is inconsistent with the requirement that the depths be at least 0·16 mag.

If the condition of both eclipsing components having equal surface flux densities is relaxed, then one eclipse will become deeper while the other becomes shallower. If either (or both) the conditions of equal radii and a 90° inclination are relaxed, both eclipses become shallower. In the case of BB Scl there do indeed appear to be slightly unequal surface flux densities for the two eclipsing components (since the eclipses are probably of different depths) and hence (assuming main sequence stars of the same age),[55] the two components will almost certainly have unequal radii and, in that case, it is even more difficult to reconcile the Hipparcos individual magnitudes for components A and B with the light curves. Therefore, on the basis of the overwhelming evidence of the light curves (SAAO and MJUO, the Hipparcos one and that of Tagliaferri *et al*[56]) it is concluded that the Hipparcos individual magnitudes for components A and B must be in error and that those derived from the light curve analysis as listed in Table 4.6 are to be preferred.

4.3.2 The A star of BB Scl

The published orbital parameters of the AB visual binary system,[57] combined with the Hipparcos parallax of 0·04229″, yield a total mass for the system of M_{AB} =3·18±0·36 $M_\odot$. The total mass of an AB system consisting of a stars of the masses given in Table 4.4, M_1 ≈0·71 $M_\odot$ and M_2 ≈0·68 $M_\odot$, and a K1 star somewhat evolved off the zero-age main sequence at M ≈0·76 $M_\odot$ is only ∼2·15 $M_\odot$.

In the absence of a large colour excess, any attempt to account for the missing mass by assuming a large interstellar extinction is rejected, and there are no supporting grounds for assuming the large errors in the Hipparcos parallax or published orbital parameters which might account for it. Instead, it is suggested that the missing mass is to be found in star A; that it is also a binary system, but not eclipsing.

For consistency with the Hipparcos colour index and the Michigan Spectral Catalogue

[55] See Section 4.3

[56] *op cit*

[57] Hirshfeld and Sinnott, *op cit*

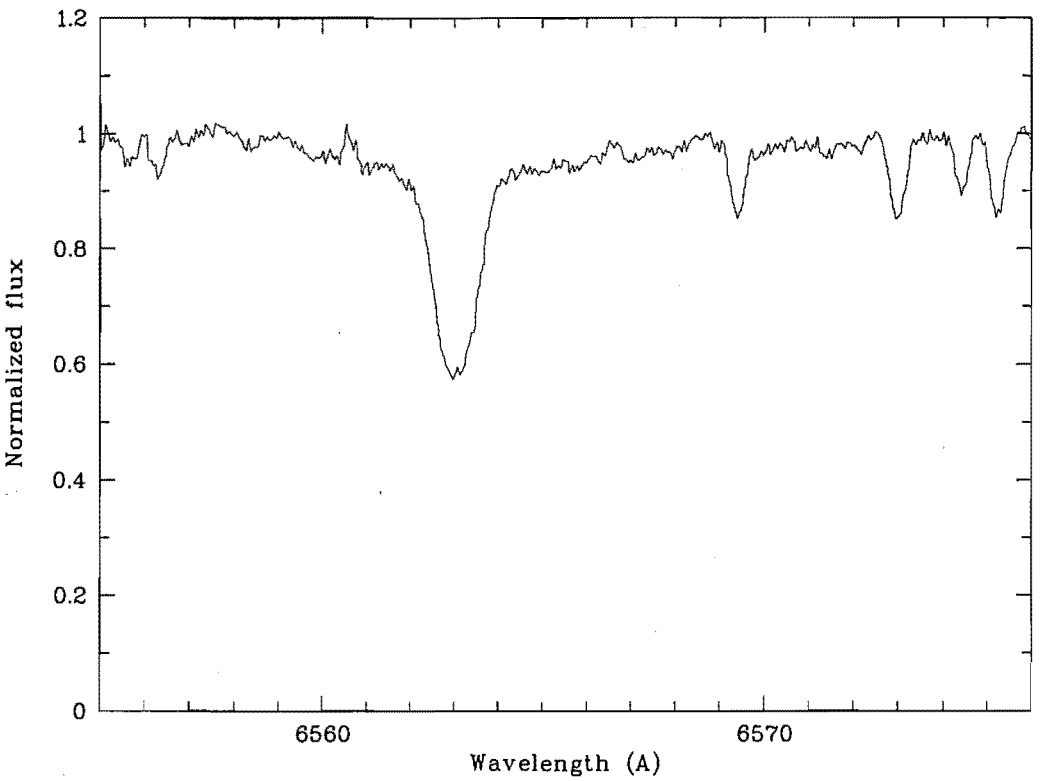

Figure 4.4: A typical Hα spectrum of BB Scl, obtained 1995 July 16.

classification,[58] it is suggested that the A_1 primary star is a K1 star on the main sequence, V =6·1 and M ≈0·76 $M_\odot$, while the A_2 secondary is a K3/4 main sequence star of V =6·8 and M ≈0·72 $M_\odot$. The total mass of such a system would be ∼1·48 $M_\odot$, giving a total mass of the AB double-binary system of ∼2·87 $M_\odot$ which is within the range of masses consistent with the Hipparcos parallax and the published orbital parameters for the AB system. The low ratio of EUV to bolometric flux calculated above (Section 4.1) implies that the A star or system is not itself chromospherically active, and therefore (assuming synchronous rotation) probably not a short-period binary.

4.4 High-resolution spectroscopy

Spectra centred on the Hα line were obtained from 1993 October to 1996 August, and additional spectra in the region of the lithium 6708 Å resonance doublet were obtained during 1994.

[58] Houk *op cit*

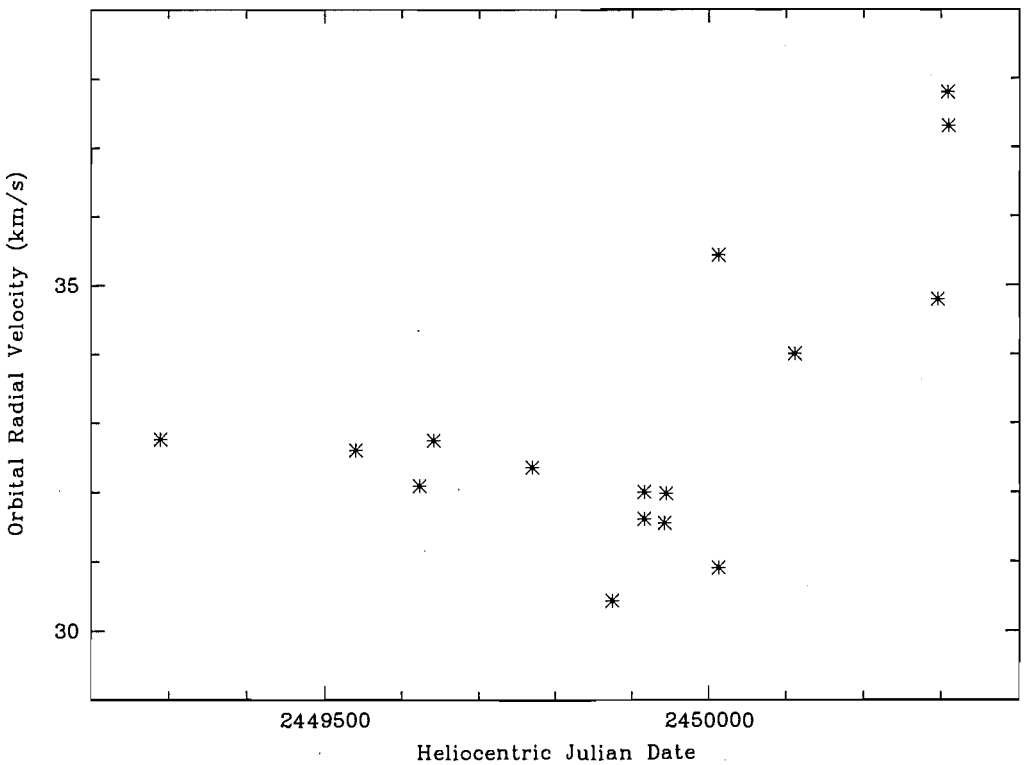

Figure 4.5: Radial velocities of BB Scl as computed from high-resolution spectra

4.4.1 The metal-line spectrum

The high-resolution spectra contain mainly Fe I lines which, as can be seen in the cases of the λ6569, λ6574 and λ6575 lines in Figure 4.4, are weak. V I lines in the λ6200 region, and the few Ca I, Ni I and Ti I lines included in the spectra are also weak. The same metal lines in comparison spectra of ϵ Eri (HR 1084, K2 V, $v \sin i < 17$ km/s)[59] obtained using the same instruments, typically have a core depth about 0·1 of the continuum flux greater than the lines of the BB Scl system. The metal lines do not show any significant broadening. Measured FWHMs vary by ±0·075 Å relative to the same lines in the spectrum of ϵ Eri.

Only one metal-line spectrum appears to be present and this can be accounted for by the dominance of the light of the A_1 type-K1 star, while the continuum flux from the eclipsing B stars, together with the smearing-out effect of rotational broadening on the lines in the spectra of the B stars[60] is responsible for the weakness of the A_1 star's and the two B stars' metal lines.

[59] Hoffleit, D., and Jaschek, C., 1982, *The Bright Star Catalogue*, Yale University Observatory, Conn., 4th Revised Ed.

[60] See Section 4.4.4

4.4.2 Radial velocities

The WD analysis did not directly yield information on the orbital velocities of the stars, but the amplitude of variation K may be calculated on the assumption of a circular orbit and using the data in Table 4.4:

$$\begin{aligned} K &= \frac{2\pi a \sin i}{P} \\ &= 37{\cdot}6 \pm 0{\cdot}1 \text{ km/s}. \end{aligned}$$

Radial velocities were computed on a line-by-line basis using the lines listed in Tables 2.4, 2.5 and 2.6 where of sufficiently good S/N. If the metal lines are those of the bright, non-eclipsing star A_1, one would not expect to see high-frequency variations corresponding to the orbital motion of the eclipsing binary B stars, but rather the orbital period of the presumed A system superimposed on the 4·559-y period of the AB system and the 111·8-y period of the AB×C system.

The measured velocities, plotted in Figure 4.5, do not show any short-period variation, and their total range is much smaller than the amplitude calculated above for the variations in the orbital velocity of the eclipsing B stars. By extrapolation from Dommanget and Nys,[61] a maximum in the relative radial velocities of the A and B systems should have been evident in early 1996 ($\sim JD2450150$). The measured velocities do show a maximum very approximately at that time, though few échelle spectra with good S/N were obtained and the scatter is large. Radial-velocity variation due to the orbital motion of the A system alone may have been lost in the noise, or may be small because of a small angle of inclination of the orbital plane of the system.

4.4.3 Hα line

The Hα absorption line (Figure 4.4) shows a FWHM of 1·11±0·13 Å which is suggestive of a K-type star, but the flux in the line centre is consistently 0·56±0·02 of the adjacent continuum, suggesting that the observed feature may be an Hα absorption line from the stars A which is considerably filled in by the continuous spectra from the stars B. The FWHM and core depth were unvarying within the limits specified over the whole of the observation period.

Photometry using wide and narrow band Hα filters similarly shows Hα flux varying only by 0·04 mag. over the whole of the observation period, with no periodicity and, in particular, no correlation with the orbital phase of the eclipsing system.

In order to remove the third light of the K-type star or stars A which apparently dominated the spectra, a spectrum of ϵ Eri, scaled to match the core depth of the λ6569 Fe I line in the BB Scl Hα spectra, was subtracted from the BB Scl spectra. The results of this process for a selection of orbital phase values are shown in Figure 4.6.

All of the spectra were obtained during eclipses or else after primary and before secondary eclipse: no spectra were obtained after secondary and before primary eclipse. It

[61] Dommanget, J., and Nys, O., 1982, *Second Catalogue d'Éphémérides*, Roy. Obs. Belgium Comm., Ser. B, No. 124

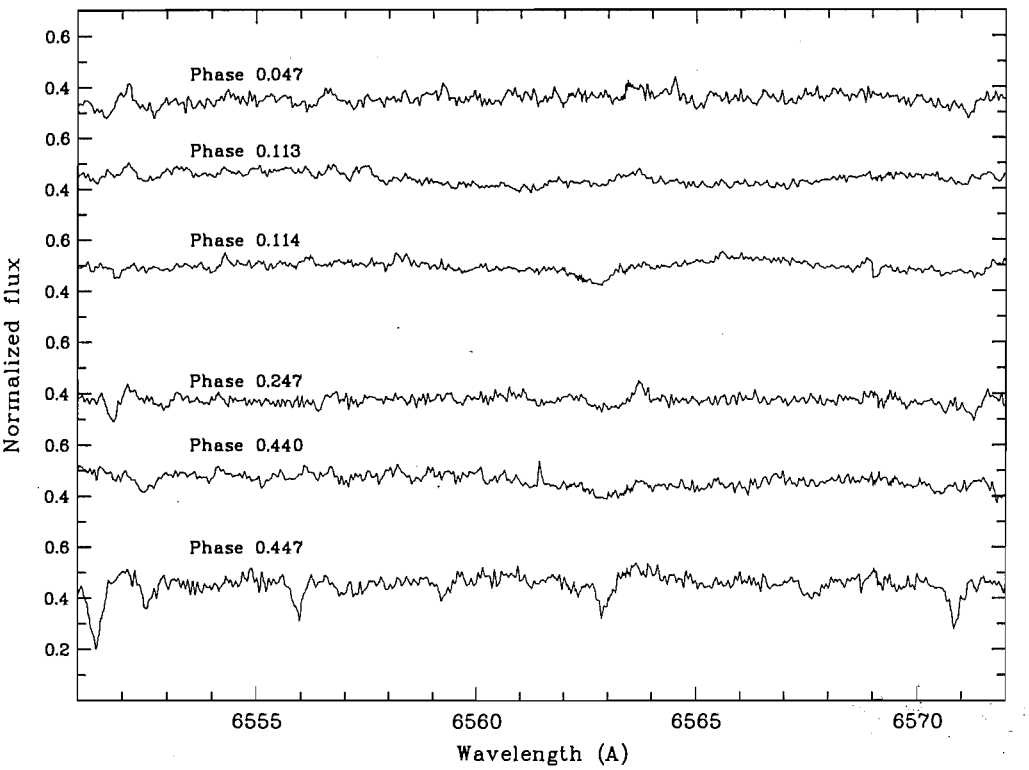

Figure 4.6: Hα spectra of BB Scl after subtraction of the scaled spectrum of HR 1084, arranged according to orbital phase of the eclipsing binary system. No barycentric or stellar radial velocity corrections have been applied.

is clear, however, that spectra obtained out of eclipse show an almost completely filled-in Hα line. In the spectra obtained from orbital phase 0·113 to orbital phase 0·440, as the primary star is approaching and the secondary star receding, the spectra exhibit a very weak absorption feature to the blue side of a barely-discernible broad emission feature, while the primary eclipse shows an apparently exactly filled-in line, and the secondary eclipse possibly shows weak absorption masked by a telluric line. Given the motions of the two stars, it appears that the primary is responsible for the absorption feature and the secondary for the emission feature. It is concluded that both of the eclipsing stars are active, the B_1 primary with chromospheric emission in Hα almost strong enough to completely fill in its own Hα absorption, while the B_2 secondary is more active, with chromospheric emission in Hα sufficiently strong to show a small net emission in its own spectrum and to completely fill in the combination of its own absorption and the weakened absorption of the B_1 primary during primary eclipse.

4.4.4 Rotational broadening

If, as is expected having regard to their putative age, the two eclipsing stars are rotating synchronously with their orbital motion, and they have the radii confirmed by the Wilson-

Devinney analysis, they should exhibit a rotational $v \sin i$ of $\sim$ 75 km/s. The consequential large rotational broadening, of the order of 3 Å, combined with noise in the spectra, has almost completely smeared out the metal lines in the spectra of the active stars, though some traces of the λ6573 Ca I line and/or λ6575 Fe I line may be seen when not masked by telluric absorption.

4.4.5 Lithium lines

The relevant high-resolution spectra showed no trace of the lithium λ6708 resonance doublet. If as the stars of BB Scl are main sequence stars of less than solar mass, as indicated by the physical analysis above, then the mechanism proposed by de la Reza *et al*[62] and discussed in section 1.8 would not be expected to operate. The absence of excess lithium is at least consistent with the physical analysis herein!

4.5 Conclusion

The light curve in V shows that one of the components of the AB visual binary system in BB Scl is an eclipsing binary system with an orbital period of 0·476525±0·000013 days. The colour index changes during eclipses imply that the B component of BB Scl is the eclipsing system.

From the light curve analysis, there is a well-defined difference of 105 ± 20 K between the effective temperatures of the two eclipsing stars. While their relative radii are not defined with high precision, the total surface area of the two eclipsing stars is better determined and, with the colour photometry, is consistent with the system consisting of a pair of K3 to K5 dwarfs. Échelle spectra of the Hα line indicate that both stars of the eclipsing binary system are active, the secondary being more strongly active, at least in Hα, than the primary. The light curve in V shows short-period variability characteristic of fast-rotating spotted stars, and we conclude that the eclipsing binary system is a BY Dra-type system consisting of two K-type dwarfs and having the shortest orbital period of any known system of that type. The inclination of the system obtained from the light curve analysis is $i = 86° \pm 4°$.

On the basis of the measured magnitudes and colour index, the published orbital parameters and the Hipparcos parallax, it is concluded that the A component of BB Scl is probably also a binary system, consisting of K1 and K3 V stars, possibly with a small angle of inclination. The whole BB Scl system thus comprises five stars, two of them in the active BY Dra system B, two in the non-active system A, and the (presumed) single star C of type M2 V.

[62] *op cit*

Chapter 5

GT Muscae

The RS CVn-type single-lined spectroscopic binary, HD 101379, forms, with the eclipsing binary HD 101380, the bright (V ~5·1) quadruple system GT Muscae (HR 4492). The HD 101380 system was classified as a single A0/1 V star in the Michigan Spectral Catalogue,[1] and as an A0+A2 V eclipsing binary in a 2·755-days orbit by Collier.[2]

Houk and Cowley[3] classified HD 101379 as G5/8 III. Collier assigned a spectral type of K4 III to the active star on the grounds of the colour index ($B-V$ =1·5±0·1) of the light remaining after subtraction of the light of the HD 101380 system according to canonical colour values obtained from Johnson.[4] Murdoch *et al*[5] showed that the colour excess could not be explained by the reddening of a G5/8 star by photospheric spots, the observed reddening requiring a 'polar' spot as much as 1000 K cooler than the photosphere covering the entire surface of the star, but calculated that the colour excess could alternatively be explained by the reddening of a G5/8 star by a combination of interstellar reddening of A_V =0·15 mag. and 0·45 mag. of reddening by circumstellar material.

GT Mus has been identified[6] with the IRAS source IRAS 1137 −6507. The system was listed by Mitrou *et al*[7] as one for which there was no acceptable EUVE detection in the Lex/B (50–180 Å) and Al/Ti/C (160–240 Å) bands but it is listed by Dempsey *et al*[8] as a ROSAT PSPC (position-sensitive proportional counter) 0·1–2·4 keV x-ray source with a count rate of 2·85±0·18 counts/s and calculated x-ray luminosity L_x =39·43×10^{23} W. That is the fourth-highest x-ray luminosity in the Dempsey *et al* list, after the stars BM CVn (L_x =69·55×10^{23} W), TW Lep (L_x =61·33×10^{23} W) and 1E1213·9+3809 (L_x <48·21×10^{23} W). The ratio of x-ray to bolometric luminosity listed in the NASA

[1]Houk N. and Cowley A. P., 1975, *Univ. Michigan Catalog of Two-dimensional Spectral Types for the HD Stars*, vol. 1, Univ. Michigan, Ann Arbour

[2]Collier A., 1982, Ph.D. Thesis, Univ. Canterbury

[3]*op cit*

[4]Johnson H. L., 1966, *Ann. Rev. Astron. Astrophys.*, **4**, 193

[5]Murdoch K. A., Hearnshaw J. B., Kilmartin P. M., Gilmore A. C., 1995, *MNRAS*, **276**, 836

[6]Odenwald S. F., 1986, *ApJ*, **307**, 711

[7]Mitrou C. K., Mathioudakis M., Doyle J. G. and Antonopoulou E., 1997, *Astron. Astrophys.*, **317**, 776

[8]Dempsey R. C., Linsky J. L., Fleming T. A. and Schmitt J. H. M. M., 1993, *ApJSS*, **86**, 599

HEASARC database,

$$\frac{L_{\rm x}}{L_{\rm bol}} = 1{\cdot}29 \times 10^{-4},$$

is an order of magnitude less than the typical ratio for a chromospherically active star, confirming that it is only one of the A and B systems of GT Mus that is active, the inactive system contributing the excess non-x-ray flux that reduces the ratio to its observed value.

Gurzadyan & Cholakyan[9] identified GT Muscae as a system which adheres to an inverse relation between stellar separation and the strength of emission in the Mg II λ2800 ultraviolet doublet, and suggested that it belonged to a class of close ($a \leq 2{\cdot}7\,R_{\odot}$) binaries having a common chromosphere ("roundchrom") surrounding both stars such that the source of chromospheric emissions may be a highly excited region between the stars.

An orbital solution for the single-lined binary system HD 101379, derived from radial velocities, was provided by Murdoch *et al.*[10] Their orbital ephemeris with T_0 at the time of periastron passage was

$$\text{HJD} = (2444929 \pm 6) + (61{\cdot}448 \pm 0{\cdot}007) \times E.$$

In the course of the present program, 45 high-resolution spectra in the Hα region as well as spectra in the λ6708 Li region and in the region of the Fraunhofer D-lines were obtained from 1994 to 1996. The published data of Collier Cameron[11] and Murdoch *et al*,[12] have been used in this analysis as well as the photometry subsequently obtained in the continuing observation program at MJUO. The GT Mus system is not resolved into its component stars in the MJUO photometric and spectroscopic observations, which all include the light from both HD 101379 and HD 101380. A spectrum of the Ca II H and K lines of the GT Mus system as a whole (Figure 5.1) shows moderate emission peaks in the cores of the lines.

5.0.1 Hipparcos data

GT Muscae is one of the systems in respect of which photometric data are given both for the system as a whole in Volume 5, and separately for the components HD 101379 and HD 101380 in Volume 10, of the Hipparcos data catalogues.[13] The magnitude given in Volume 5 for the whole system is Hp =5·01; the magnitudes given in Volume 10 are Hp =5·519 and Hp =6·608 for the components even though all magnitudes were obtained with the same image disector tube. The latter add to a combined magnitude of Hp =5·180; the discrepancy of 0·17 mag. is not explained. Additionally, the transformation of the Hp magnitudes to standard Johnson V magnitudes depends on the spectral type of the stars.[14] In the case of GT Mus, the spectral type of the active star which is responsible for most of the flux in $BVRI$, is a critical unknown which has to be determined,[15] and it would

[9] *op cit*

[10] *op cit*

[11] Collier Cameron A., 1987, *S. Afr. Astron. Obs. Circ.*, **11**, 57

[12] *op cit*

[13] Schrijver H., *op cit*, vols 5 and 10

[14] van Leeuwen F., Lindegren L. and Mignard F., 1997, *The Hipparcos and Tycho Catalogues*, vol. 3, ESA Publications Division, Noordwijk

[15] see Murdoch *et al, op cit*

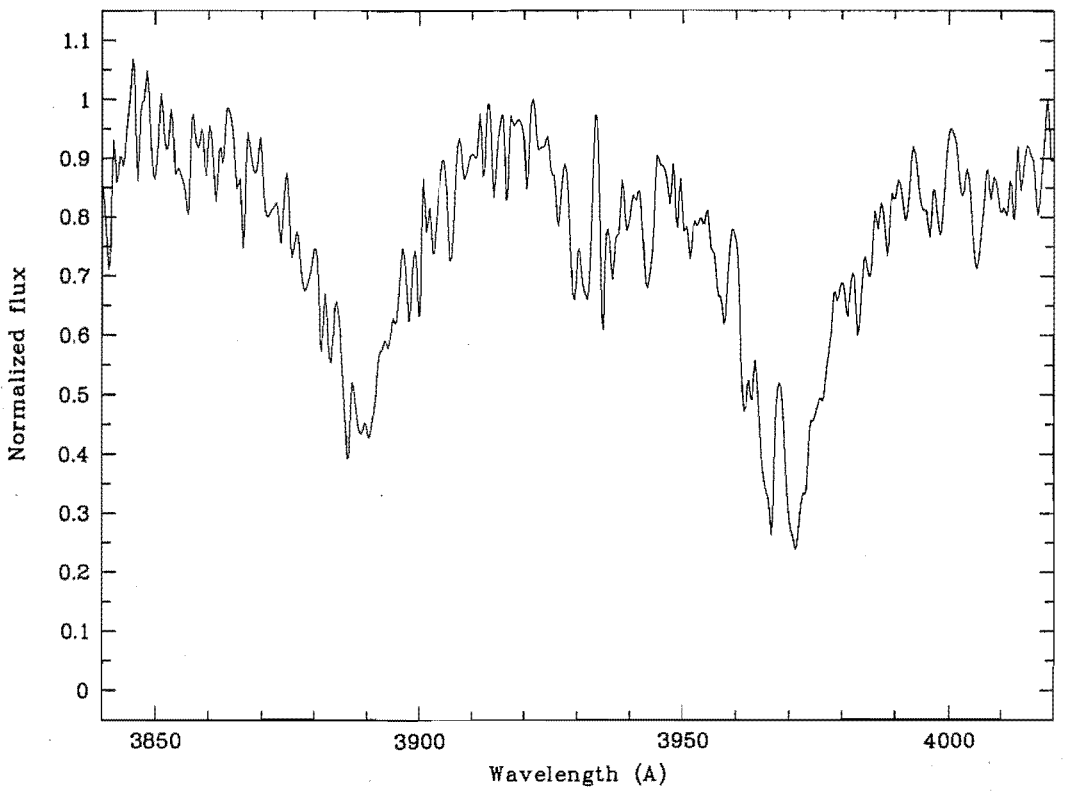

Figure 5.1: Spectrum of the CaII H and K lines of the GT Mus system, obtained at MJUO.

be unsafe to rely on photometric data which presume a spectral type. For those reasons, the present analysis uses the Hipparcos parallax, but not the photometric data given in Volumes 5 and 10.

The Hipparcos measurement of parallax[16] is π =0·00581″ ± 0·00064″, corresponding to a distance of 172 ± 17 pc. In Murdoch *et al*[17] the system exhibited a brightness peak of V =4·95 mag. between JD2448400 and JD2448500 and the system has not been brighter than that in subsequent observations. The Hipparcos parallax implies a distance modulus of 6·179±0·227 mag. and therefore an absolute magnitude of $M_V = -1{\cdot}18 \pm 0{\cdot}25$ for the whole GT Mus system when the active star was, presumably, in its least-spotted observed state.

5.1 The eclipsing binary system HD 101380

The longer time base of the photometry has facilitated a yet more precise determination of the ephemeris of this system. The B band was chosen for analysis rather than the

[16]Schrijver H., *op cit*, vol. 5
[17]*op cit*

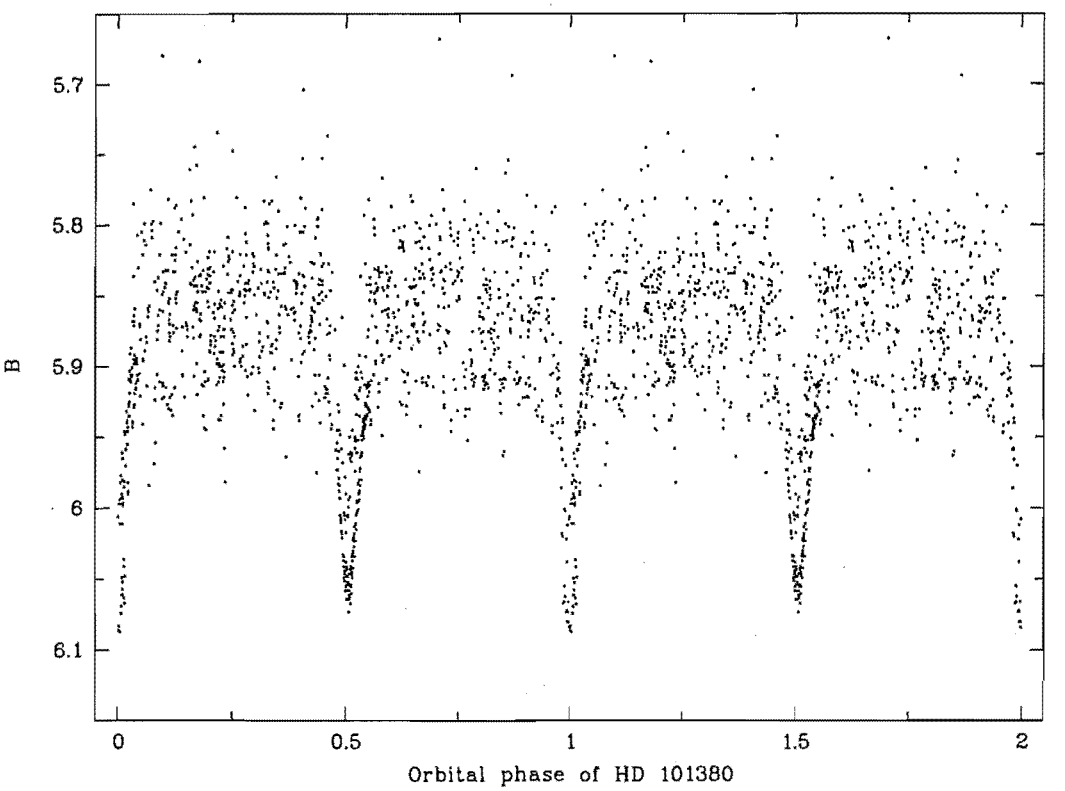

Figure 5.2: B photometry of GT Mus phased according to the ephemeris of the HD 101380 eclipsing binary system. The large out-of-eclipse scatter is due to the active HD 101379 system, not the eclipsing binary HD 101380.

V band because the latter is dominated by the light of the red giant in HD 101379. On adding the more recent data to the data of Collier Cameron[18] and Murdoch *et al*[19] and plotting magnitude as a function of phase according to the period of Murdoch *et al*,[20] it was found that the eclipses, in particular the secondary eclipses for which more data were obtained, were poorly resolved. The period was adjusted until the rms deviation from Gaussians fitted to the eclipses was least, and then the epoch was adjusted to place the primary eclipse at zero phase (Figure 5.2). The ephemeris so determined was

$$HJD = (2444362{\cdot}716 \pm 0{\cdot}003) + (2{\cdot}754591 \pm 0{\cdot}000003) \times E.$$

The quoted uncertainty represents the range over which adjustment of the period resulted in no change to the rms deviation from the fitted Gaussians to 6 decimal places. The variable flux contributed by the HD 101379 system blurs the eclipse curves and causes scatter within the eclipses as well as in the out-of-eclipse light curve.

[18] Collier Cameron, 1987, *op cit*
[19] *op cit*
[20] *ibid*

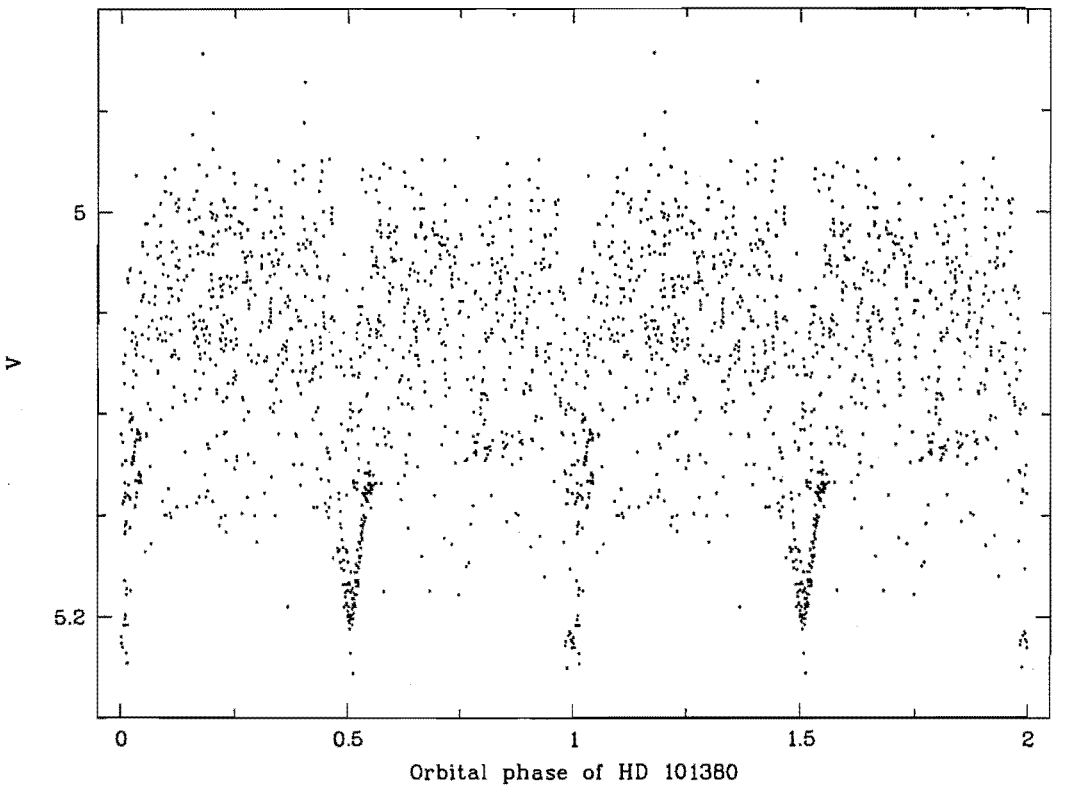

Figure 5.3: V photometry of GT Mus phased according to the ephemeris of the HD 101380 eclipsing binary system. The large out-of-eclipse scatter is due to the active HD 101379 system, not the eclipsing binary HD 101380.

5.1.1 Colours

A true determination of the colour excess, if any, of HD 101379 must depend on the subtraction of the true light of the HD 101380 system from the combined light of GT Mus. Accepting the spectral type of A0 V for the primary star of HD 101380, Collier[21] and Murdoch *et al*[22] assigned a spectral type of A0 V to the secondary also and subtracted passband fluxes calculated from canonical colours for that spectral type. With the improved parallax from Hipparcos, it has now been possible to assign an approximate absolute visual magnitude to the HD 101380 system, and thence obtain corresponding colour indices, representing the mean colour of the system, from published tables. It was assumed that the published luminosity classification (Class V) was correct. The Hipparcos parallax and an adopted visual magnitude V =6·40[23] yield an absolute visual magnitude of M_V =0·22 for the two stars, and the colours corresponding to a mean magnitude of

[21] *op cit*
[22] *op cit*
[23] See Murdoch *et al, op cit* and Section 5.2.4 for reasoning.

Unreddened colour	Index for the combined light of HD 101380
$(U-B)$	0·036
$(B-V)$	0·032
$(V-R_{\rm J})$	0·051
$(V-I_{\rm J})$	0·128

Table 5.1: Calculated colours of the combined light of the HD 101380 system.

0·97 for the two stars were obtained by interpolation in the table in §99 of Allen[24] for the $(U-B)$ colour, in Gray's Table B1 for the $(B-V)$ and $(V-R_J)$ colours, and in Table 3 of Taylor[25]for the $(V-I_C)$ colour. The $(V-I_C)$ colour was converted to the Johnson system by means of the 11th conversion formula in Table 4 of Taylor. The colours so obtained are set out in Table 5.1.

Before removal of the light of HD 101380 from the observed light of GT Mus, the $(V-R_C)$ and $(V-I_C)$ colours of the latter were transformed to the Johnson system using the 8th and 20th transformation equations of Table 4 of Taylor.[26] Then, instead of approximation of the eclipses of HD 101380 with Gaussians, as in Murdoch *et al*,[27] all the data obtained within phases 0·00–0·05, 0·45–0·55 and 0·95–1·00 on the ephemeris of Figure 5.2 were removed from the set to exclude any errors in modelling the eclipses. Finally, assuming the light of HD 101380 to be constant in all passbands out of eclipse, the light of HD 101380 was subtracted separately from each observation of the combined light of the GT Mus system in each passband according to the equation

$$\text{mag(HD 101379)} = \text{mag(GT Mus)} - 2{\cdot}5\log\left(1 - 10^{0{\cdot}4[\text{mag(GT Mus)}-\text{mag(HD 101380)}]}\right)$$

and the colour indices were recomputed. The resulting colours of HD 101379 alone are plotted in Figure 5.4 and were used for all of the following photometric analysis of that system.

5.1.2 Magnitudes and colours of the individual stars

Although not required for the analysis of the active HD 101379 system, the opportunity was taken to calculate the unreddened $(B-V)$ and $(V-R_J)$ colours of the individual stars of HD 101380.

For this purpose, the light curve in B (Figure 5.2) was used because its eclipses are the most well-defined. The long time-span of the light curves implies that the eclipses of the HD 101380 system have occurred while the light from the HD 101379 system had a large number of different, presumably random, values within its range of variation, so that a common mean value of the latter can be assumed at all phases of the eclipsing light

[24] *op cit*
[25] *op cit*
[26] *ibid*
[27] *op cit*

curve. From Figure 5.2, that mean magnitude of the GT Mus system is B =5·85, and the primary and secondary eclipse magnitudes in the centre of each eclipse are, respectively,

$$B_{\rm P} = 6{\cdot}075 \text{ mag.}$$

and

$$B_{\rm S} = 6{\cdot}055 \text{ mag.}$$

From the analysis in Section 5.1.1, a value of 6·43 was obtained for the magnitude in B of the combined light of HD 101380. The mean B flux of the HD 101379 and HD 101380 systems, $L_{B,\rm HD101379}$ and $L_{B,\rm HD101380}$ respectively, were calculated to be

$$\begin{aligned} L_{B,\rm HD101380} &= 10^{-0{\cdot}4\times 6{\cdot}43} \\ &= 2{\cdot}6792 \times 10^{-3} \text{ flux units} \end{aligned}$$

and

$$\begin{aligned} (\text{Flux of GT Mus}) &= (\text{Flux of HD 101379}) + (\text{Flux of HD 101380}) \\ L_{B,\rm HD101379} &= 10^{-0{\cdot}4\times 5{\cdot}85} - 2{\cdot}6792 \times 10^{-3} \\ &= 1{\cdot}8917 \times 10^{-3} \text{ flux units} \end{aligned}$$

where the arbitrary unit of flux is the flux in B of a zero B-magnitude star, as received at the top of the earth's atmosphere.

Similarly, from the quantities $B_{\rm P}$, $B_{\rm S}$ and $L_{B,\rm HD101379}$, the fluxes of the HD 101380 system in primary and secondary eclipse were calculated respectively as —

$$\begin{aligned} L_{\rm P} &= 1{\cdot}8236 \times 10^{-3} \text{ and} \\ L_{\rm S} &= 1{\cdot}8927 \times 10^{-3}. \end{aligned}$$

The geometry of eclipsing binary systems gives the following approximate relations, which ignore limb-darkening effects

$$\begin{aligned} L_{B,\rm HD101380} &= F_{\rm P}S_{\rm P} + F_{\rm S}S_{\rm S} \\ L_{\rm P} &= F_{\rm P}S_{\rm P} + F_{\rm S}S_{\rm S} - F_{\rm P}S_0 \\ L_{\rm S} &= F_{\rm P}S_{\rm P} + F_{\rm S}S_{\rm S} - F_{\rm S}S_0 \\ L_{B,\rm HD101380} - L_{\rm P} &= F_{\rm P}S_0 \\ L_{B,\rm HD101380} - L_{\rm S} &= F_{\rm S}S_0 \\ \left(\frac{L_{B,\rm HD101380} - L_{\rm P}}{L_{B,\rm HD101380} - L_{\rm S}}\right) &= \left(\frac{F_{\rm P}}{F_{\rm S}}\right) \end{aligned}$$

where $F_{\rm P}$ and $F_{\rm S}$ are the surface fluxes in B per unit surface area of the primary and secondary stars respectively, $S_{\rm P}$ and $S_{\rm P}$ are the visible surface areas of the primary and secondary stars respectively, and S_0 is the maximum surface area of each star which is occulted during eclipse. Substituting the calculated values for the fluxes gave the result

$$\frac{F_{\rm P}}{F_{\rm S}} = 1{\cdot}0878.$$

Stellar parameter	Primary star of HD 101380	Secondary star of HD 101380
$(B-V)_0$	0·02	0·05
$(V-R_J)_0$	0·04	0·06
$(V-I_J)_0$	0·11	0·15
M_V	0·87	1·19
m_V	7·05	7·37
Sp.	A0·6 V	A1·7 V

Table 5.2: Calculated colours of the individual stars of the HD 101380 system, and the approximate visual magnitudes and spectral types corresponding to the $(B-V)_0$ colours.

The Barnes-Evans formulae[28] relate a visual surface parameter, $\mathcal{F}_V$ to the $(B-V)_0$, $(V-R_J)_0$ and $(R-I_J)_0$ colour indices. The parameter $\mathcal{F}_V$ is in fact, the quantity $(-0{\cdot}25\log F_V + \text{const.})$, so that, using the Barnes-Evans formulae for the individual colour indices which are appropriate for A-type, luminosity class V stars, it is possible to define a quantity

$$\begin{aligned} -0{\cdot}25\log\left(\frac{F_\mathrm{P}}{F_\mathrm{S}}\right) &= \mathcal{F}_V(\text{primary}) - \mathcal{F}_V(\text{secondary}) \\ &= -0{\cdot}333\Delta(B-V)_0, \\ &= -0{\cdot}429\Delta(V-R_J)_0, \\ &= -0{\cdot}783\Delta(R_J-I_J)_0 \end{aligned}$$

where $\Delta(\text{colour index})$ is the difference between the colour indices of the primary and secondary stars. Substituting the calculated value for the flux ratio resulted in the values

$$\begin{aligned} \Delta(B-V)_0 &= 0{\cdot}027 \\ \Delta(V-R_J)_0 &= 0{\cdot}021 \\ \Delta(R_J-I_J)_0 &= 0{\cdot}012, \end{aligned}$$

which, when applied to the colours listed in Table 5.1, yielded the colours for the individual stars listed in Table 5.2. Corresponding visual magnitudes and spectral types were obtained by interpolation from the $(B-V)_0$ colours in Table B1 of Gray,[29] and those are also listed in Table 5.2.

5.2 Photometry of HD 101379

In Figure 5.4, the data set of Murdoch *et al*[30] is extended by the addition of more recent observations. In its brightest state the GT Mus system has been observed at V =4·95

[28] Barnes, Evans & Moffett, *op cit*, and Barnes, Evans & Parsons, *op cit*

[29] *op cit*

[30] *ibid*

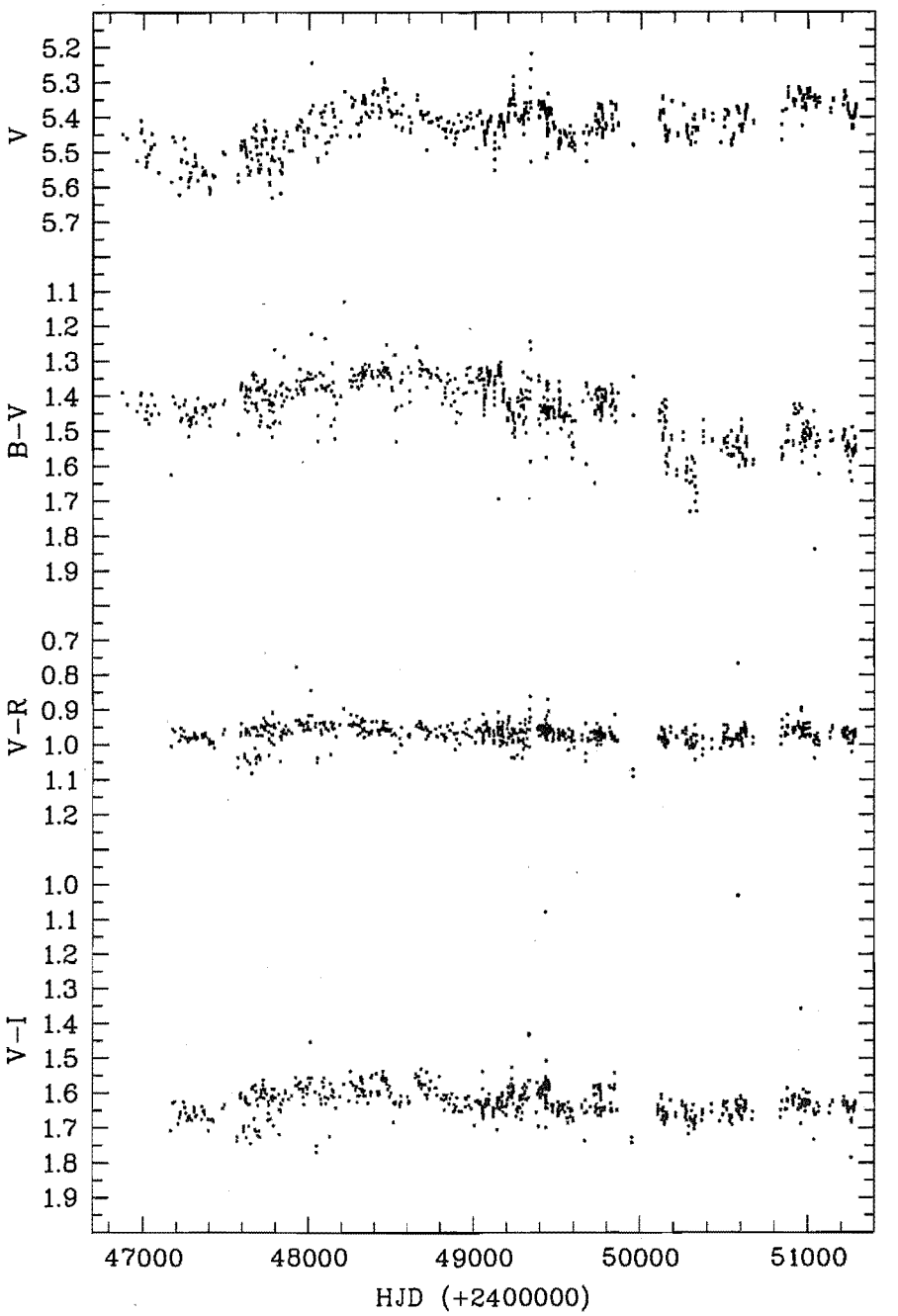

Figure 5.4: Colour photometry of GT Mus after removal of the light of the HD 101380 eclipsing binary system. $(U-B)$ photometry is not included because U data have been obtained only during scattered intervals. The $(V-R)$ and $(V-I)$ colours have been transformed to the Johnson system.

which, with the adopted magnitude of HD 101380 of V =6·40, implies a magnitude for HD 101379 alone of V =5·2. With the Hipparcos distance modulus of 6·179, this entails an absolute magnitude not dimmer than $M_V = -1{\cdot}0$ for the HD 101379 system. Since the secondary of HD 101379 is not seen in the spectrum, it is almost certainly a dwarf star. Hence the absolute magnitude refers to the primary in the HD 101379 system, and the value of $M_V = -1{\cdot}0$ supports the conclusion of Collier[31] that the primary is a giant which "has reached an evolutionary stage close to the tip of the ascending giant branch."

5.2.1 Long-period variability

The light curve in V in Figure 5.4 shows continuous variation over a range of 0·1 to 0·2 magnitudes and on a time scale several times longer than the orbital period of the HD 101379 system. The initial part of the curve, up to about JD 2447700, appears to contain a fluctuation of about 700 days in length, followed by a poorly-defined dip and longer recovery in brightness occupying 600–700 days to about JD 2448400, and another fluctuation of 900–1000 days. Further, less well-defined fluctuations of the order of several hundred days have followed since then. There has been a progressive mean increase in brightness in V of ∼0·2 magnitudes over the entire term of the data set.

Murdoch *et al*[32] suggested that the general mean brightening might be caused by the decrease in size of a polar spot or, alternatively, by the reduction in size of spots at lower latitudes. They also saw evidence of the onset of a compact group of spots in the decrease in brightness after JD 2447500, and suggested that there might have followed a time of stable minima and increasing maxima (presumably the epoch of progressive brightening to about JD 2448400) suggesting the migration of the spots towards the equator out of a situation of partial circumpolarity. It is not at all clear, however, that there was such a time of stable minima in the extended data set and, while migration in latitude is expected (Chapter 1), the light curve does not clearly offer positive evidence for it. The general loss of definition of the variations after about JD 2450000 may be due to longitudinal smearing of the spots as suggested by Murdoch *et al*, possibly involving the effects of differential rotation on a spot group which was migrating in latitude, or to the formation of less compact spot groups. The fact that fluctuations in brightness did continue indicates that spots continued to come into and pass out of existence and that the effects are not solely due to the same spot or spots that were responsible for the earlier fluctuations.

5.2.2 Spot waves

The V band of HD 101379, as shown in Figure 5.4, exhibits a persistent short-period variability of the order of 0·2 magnitudes. Murdoch *et al*[33] however, found no periods similar to the orbital period of the active star persisting throughout the time of the observations. Following the subtraction of the light of the HD 101380 system by the method adopted in this project, the complete data set, including both the data of Collier

[31] *op cit*
[32] *op cit*
[33] *ibid*

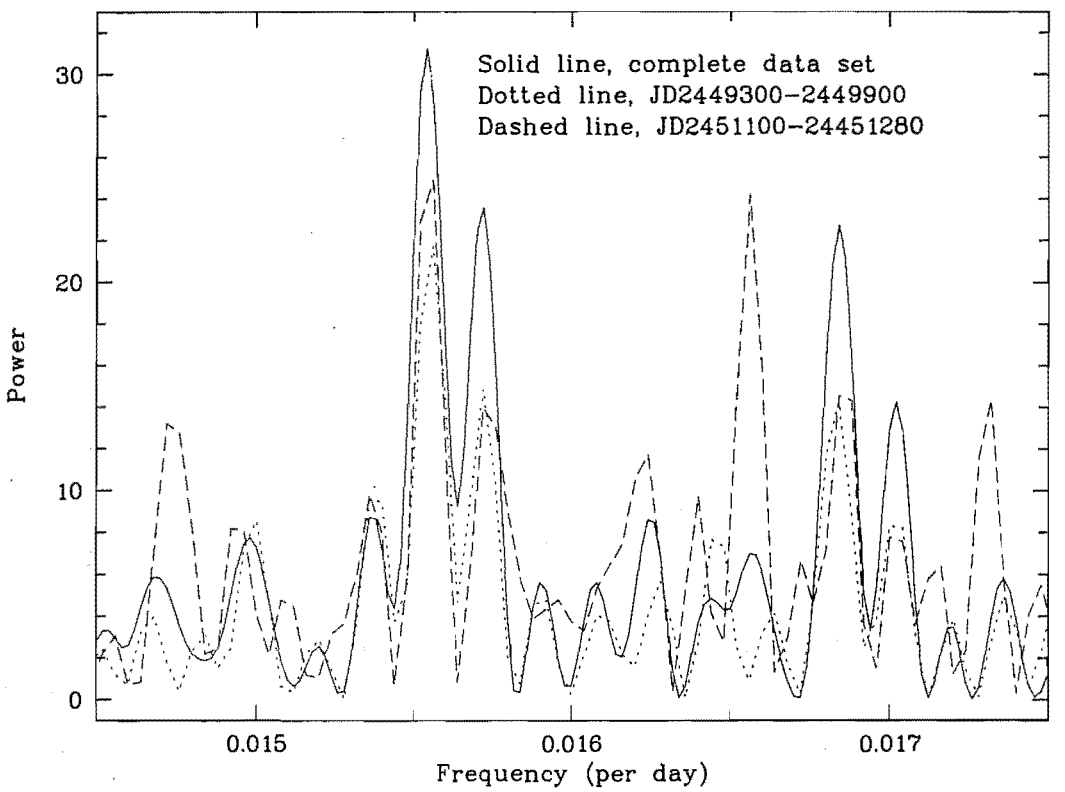

Figure 5.5: Power spectra of HD 101379 V data for the complete data set and for two well-observed $\sim$ 600 day intervals following the intervals plotted in Figure 5 of Murdoch *et al, op cit.*

Interval (JD2400000 +)	Primary period (d)	No. of observations
49300–49900	64·31	544
49900–50500	64·47	30
50500–51100	62·97	55
51100–51280	64·35	447

Table 5.3: Spot-wave periods of HD 101379 in time intervals since JD2449300.

Cameron[34] and the data obtained at MJUO since the analysis by Murdoch *et al*, was Fourier transformed[35] and the resulting power spectrum (Figure 5.5, solid line) shows a strong peak at 64·35 days (0·0155 cycles/day).

Murdoch *et al* did find variations having periods slightly longer than the orbital period when the data obtained over shorter time intervals of ~600 days were examined. The

[34] Collier Cameron, 1987, *op cit*

[35] See Section 2.2

data obtained since then have now been divided for comparison into similar time intervals and the results are tabulated in Table 5.3. There were insufficient data points in two of the intervals for detailed examination of the power spectrum and, although they did yield broad, low power (8·15 and 7·71) spectrum "peaks", they are not included in Figure 5.5. The two well-observed intervals showed principal power spectrum peaks at 64·31 and 64·35 days, similar to that of the complete data set at 64·35 days, and significantly longer than the 61·448-d orbital period.

5.2.3 Spot temperatures and extent

The method of Vogt[36] was used to determine the temperature difference between the most-spotted and least-spotted parts of the stellar photosphere, and the fraction of the photosphere which was covered by spots. Vogt defined a geometrical quantity, G, representing the fractional area of the spot in terms of the stellar disc, and showed that, in the case of a single star or binary where the companion contributes negligible flux to the system and where the star possesses spots which are at some phase of the stellar rotation wholly in view and, at another phase, wholly out of view so that only the immaculate photosphere is observed, then

$$\Delta m_\lambda = -2{\cdot}5 \log \left\{ 1 + G \left[\frac{F'(\lambda)}{F(\lambda)} - 1 \right] \right\} \tag{5.1}$$

where Δm_λ is the magnitude difference at wavelength λ between phases of maximum and minimum spot visibility, and $F'(\lambda)$ and $F(\lambda)$ are the specific intensities at wavelength λ of the spotted and unspotted photospheres respectively at disc centre. Equation 5.1 can be solved for G,

$$G = \frac{10^{-\Delta m_\lambda \times 0{\cdot}4} - 1}{F'(\lambda)/F(\lambda) - 1}$$

and, making the assumption that G is "reasonably independent" of wavelength i.e., in terms of the V and R bandpasses,

$$\begin{aligned} G(\lambda 5500) &= G(\lambda 7000) \\ \left[\frac{10^{-\Delta m_V \times 0{\cdot}4} - 1}{(F'_V/F_V) - 1} \right] &= \left[\frac{10^{-\Delta m_R \times 0{\cdot}4} - 1}{(F'_R/F_R) - 1} \right] \\ \left[\frac{(F'_R/F_R) - 1}{(F'_V/F_V) - 1} \right] &= \left[\frac{10^{-\Delta m_R \times 0{\cdot}4} - 1}{10^{-\Delta m_V \times 0{\cdot}4} - 1} \right]. \end{aligned} \tag{5.2}$$

The right hand side of Equation 5.2 contains the observed data. To determine G, Vogt used the Barnes-Evans relation[37] which relates the visual surface brightness parameter,

$$\mathcal{F}_V = 4{\cdot}2207 - 0{\cdot}1V_0 - 0{\cdot}5 \log \phi \tag{5.3}$$

[36] *op cit*

[37] Barnes, Evans and Parsons, *op cit*, and Barnes, Evans and Moffett, *op cit*

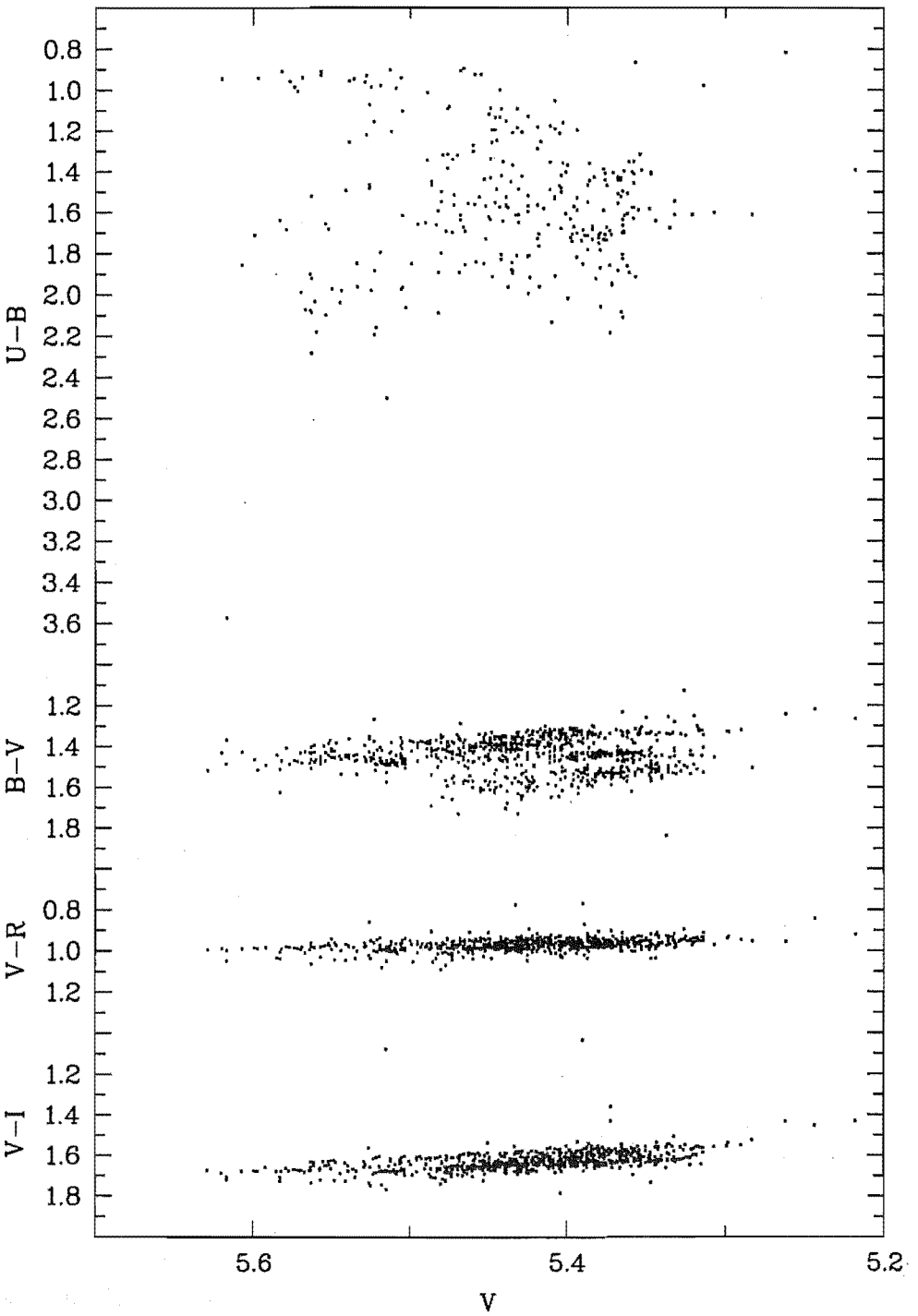

Figure 5.6: Colours vs V magnitude for the light of HD 101379 only.

where V_0 is the unreddened V magnitude and ϕ is the stellar angular diameter, to the unreddened $(V - R_J)$ colour index. For any given star,

$$V_0 = -2{\cdot}5 \log F_V + \text{constant}$$

where the constant, like ϕ, depends on the distance of the star. Substitution into Equation 5.3 gives

$$\mathcal{F}_V = 4{\cdot}2207 - 0{\cdot}1(-2{\cdot}5 \log F_V + \text{constant}) - 0{\cdot}5 \log \phi$$

whence

$$\log F_V = 4\mathcal{F}_V + \text{constant}$$

(the constant now embodying all the distance-dependent terms) and

$$\frac{F'_V}{F_V} = 10^{4(\mathcal{F}'_V - \mathcal{F}_V)}$$

where $\mathcal{F}'_V$ is the relation for the spotted star. For stars having $(V - R) > 0{\cdot}7$, the Barnes-Evans calibration of $\mathcal{F}_V$ against $(V - R)$ gives

$$\begin{aligned} \mathcal{F}_V &= 3{\cdot}841 - 0{\cdot}321(V - R)_0 \\ \mathcal{F}'_V - \mathcal{F}_V &= 0{\cdot}321[(V - R)_{\text{star}} - (V - R)_{\text{spot}}] \end{aligned}$$

where $(V - R)_{\text{star}}$ is the $(V - R)$ colour index for the unspotted photosphere. Defining $D = (V - R)_{\text{star}} - (V - R)_{\text{spot}}$,

$$\left(\frac{F'_V}{F_V}\right) = 10^{4(0{\cdot}321D)}$$

and similarly, for the surface brightness ratio at the R band,

$$\left(\frac{F'_R}{F_R}\right) = 10^{4(0{\cdot}321 - 0{\cdot}1)D}.$$

Substituting in Equation 5.2 gives

$$\frac{10^{0{\cdot}884D} - 1}{10^{1{\cdot}284D} - 1} = \frac{10^{-\Delta m_R \times 0{\cdot}4} - 1}{10^{-\Delta m_V \times 0{\cdot}4} - 1}.$$

which can be solved iteratively for D from which the temperature difference between the spotted and unspotted star can be found by looking up a suitable calibration. Substitution also gives

$$G = \frac{10^{-\Delta m_V \times 0{\cdot}4} - 1}{10^{1{\cdot}284D} - 1},$$

the fractional spotted area of the star.

The active star of GT Mus does not satisfy the condition that the spot or spots must be concentrated on one face of the star at some phase of its rotation so that, at another phase, a completely unspotted photosphere is observed. As a result, the solution for D will

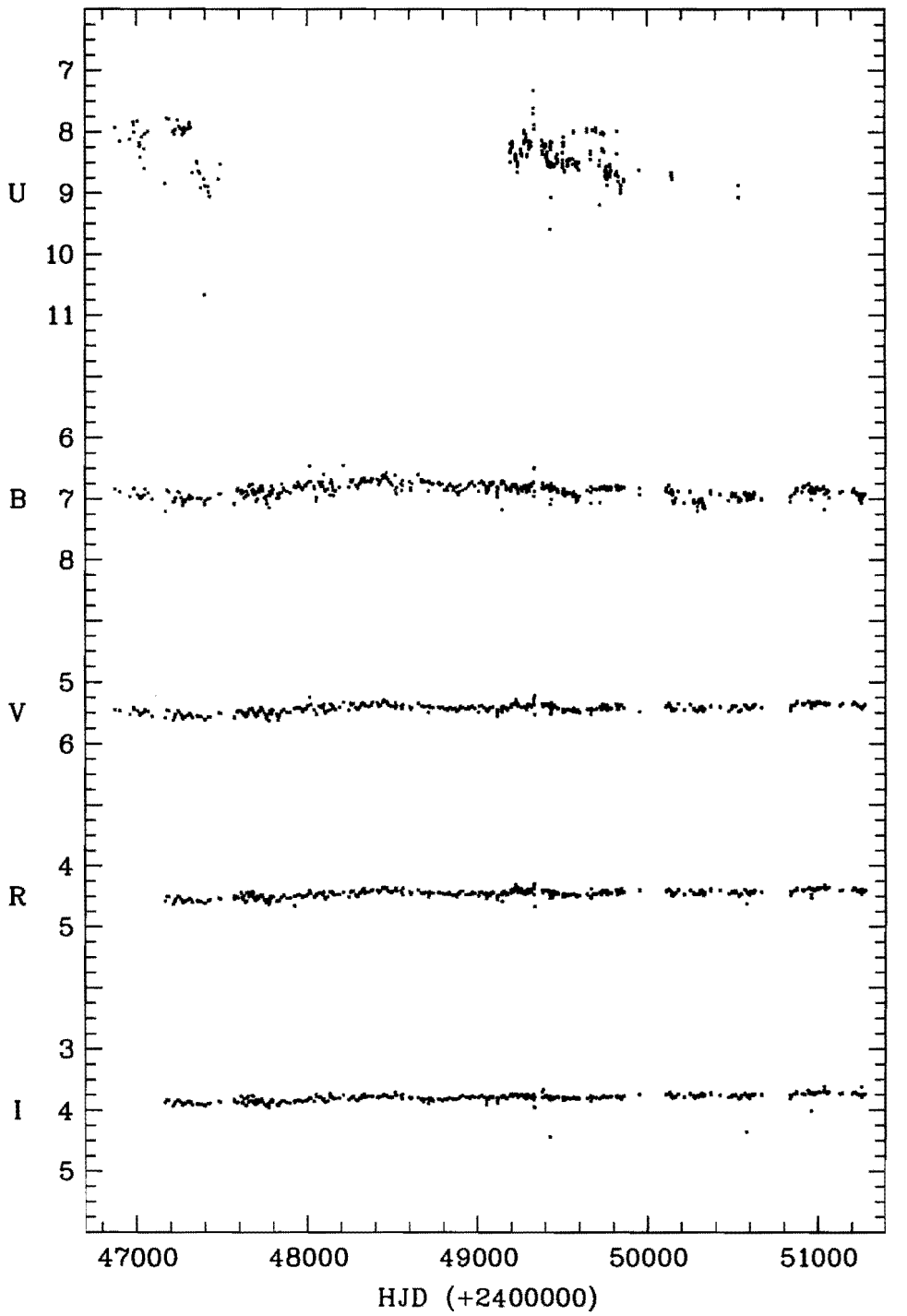

Figure 5.7: $UBV(RI)_{\rm J}$ light curves for HD 101379 only.

Interval (JD2400000 +)	Δm_V ±0·005	Δm_R ±0·005	D ±0·08	$\Delta T_{\rm eff}$ ±100 (K)	G ±0·001
51204–51280	0·071	0·052	−0·16	500	0·17
49025–49209	0·046	0·033	−0·11	400	0·15
47880–48188	0·049	0·038	−0·10	850	0·07
47569–47736	0·072	0·051	−0·10	350	0·24

Table 5.4: Amplitudes of variation V and R, amplitude (D) of variation in $(V-R)$ derived therefrom using the method of Vogt, corresponding variation in $T_{\rm eff}$ assuming that the bluest value of $(V-R)$ corresponds to $T_{\rm eff}$ = 4950 K, obtained using the calibration of Gray, and the fractional change in spot coverage of the star derived therefrom using the method of Vogt.

give only the temperature difference between the spot(s) and the *least* spotted face of the star, necessarily less than the temperature difference between the spot and the unspotted photosphere, and the solution for G will underestimate the fraction of the photosphere that is covered by spots. The true temperature difference between spot and immaculate photosphere will be greater than the difference found by Vogt's method. The method also assumes an unreddened $(V-R)$. The light of HD 101379 is reddened (see the discussion in Section 5.2.4) and there will be a systematic underestimate of the temperature variation as a result, but the reddening is least in $(V-R)$ and this error is expected to be small compared with measurement errors and their consequences.

The light curve variations in V of HD 101379 are small, and those in R smaller still, and light curves with well-defined amplitudes are not evident in much of time span of the photometry. However, some intervals were found when amplitudes could be obtained with an acceptably small degree of uncertainty, and the method of Vogt was applied to them. The results are listed in Table 5.4. The earliest set, from JD2447569 to JD2447736, covers an interval when the flux in V was increasing from the first long-term minimum shown in Figure 5.4 and yields the smallest range of variation in $T_{\rm eff}$. This is consistent with an extensive spot coverage resulting in relatively small change in colour and temperature as the star rotated and with the observed low flux in V. The second set, from JD2447880 to JD2448188, covers an interval when the flux in V was approaching its first maximum after the minimum represented by the first set, and it yields the largest variation in $T_{\rm eff}$. This is consistent with a more concentrated grouping of spots so that the variations in $T_{\rm eff}$ and colour became larger as the star rotated; the higher flux in V implies that the tighter grouping came about by way of an actual decrease in the fraction of the stellar surface covered by spots, and this was confirmed by the calculated value for G, the fractional spot coverage. The third set, from JD2449025 to JD24449209, covers an interval when the flux in V was approaching a second maximum, with a value intermediate between those in the first two intervals, and the variation in $T_{\rm eff}$ also has an intermediate value — implying that the reduction in the amplitude of the variations in V, colour and $T_{\rm eff}$ since the second set were due to an actual increase in the fractional spot coverage which reduced the contrast between the most- and least-spotted faces of the star, which is confirmed by the increase

in the coverage parameter G. The last set, from JD2451204 to JD2451280, covers the most recent observations in the data-set which can be seen in Figure 5.4 to undergo an obvious dimming followed by a recovery in one rotation of the star. The variation in $T_{\rm eff}$ in this case was larger than that of the preceding set, even though the flux in V was less. This indicates that in this interval there was both an increase in total spot coverage and a decrease in the spot coverage of one face of the star as the spots became more concentrated into one or more regions of longitude of the star, and this also is confirmed by the increase, albeit small, in the coverage parameter G.

5.2.4 Colour excess

Collier[38] argued, on the basis of colour indices, that the primary of the HD 101379 system must be of a spectral type as late as K4. The photometry obtained since then implies that the star cannot be a giant later in type than K0 III. The $(U-B)$ colour of the light of HD 101379 alone, as computed in the present project, has frequently been as blue as 0·9 (Figure 5.6), the value given by Allen,[39] §99, for a K0 giant. A few points close to 0·8 suggest that the star would be better classified as a late G giant.

It is, nevertheless, certain that the starlight is reddened. The $(U-B)$ data are scattered over a typical range of 0·4 magnitudes. One of the reasons given by Murdoch *et al*[40] for adopting a V magnitude of 6·4 rather than 6·3 for the HD 101380 system was the fact that "the measured 'outside-HD 101380-eclipse' U magnitude of GT Mus is occasionally fainter than U =6·3". At some times the extinction is such that the HD 101379 system contributes very little light in U to the combined light of GT Mus. The colours other than $(U-B)$ are also reddened relative to canonical values for a G5 to K0 giant. The $(B-V)$ and $(V-R)$ colours have only rarely been bluer than 1·3 and 0·9 respectively, the values given by Gray[41] for an unreddened K2/3 giant, and the $(V-I)$ colour, on the other hand, is usually redder than 1·5, a value given by Taylor[42] for a K3/5 giant. As Figure 5.6 most clearly shows, all of the colours have been occasionally observed at values bluer than those mentioned , implying that the values mentioned are reddened values: taking into account the fact that even the estimation of a spectral type not later than K0 III is based on light which has been reddened to some degree, and the probable reddening due to cool regions of the photosphere which are observed as spots, the photometry supports the Houk & Cowley[43] classification of G5/8 III. The combination of that relatively early spectral type and a magnitude not dimmer than $M_V = -1{\cdot}0$, together with the fluctuations of several hundred days observed in the light curve, suggests that the primary star has evolved beyond the peak of the ascending giant branch as suggested by Collier.[44] The analysis in Section 5.2.3, however, in particular the finding that at least some of the long-term changes in V correlate with changes in the spot coverage and in the difference in effective

[38] *op cit*
[39] *op cit*
[40] *ibid*
[41] Gray, 1992, *op cit*, Table B2
[42] *op cit*, Table 3
[43] *op cit*
[44] *op cit*

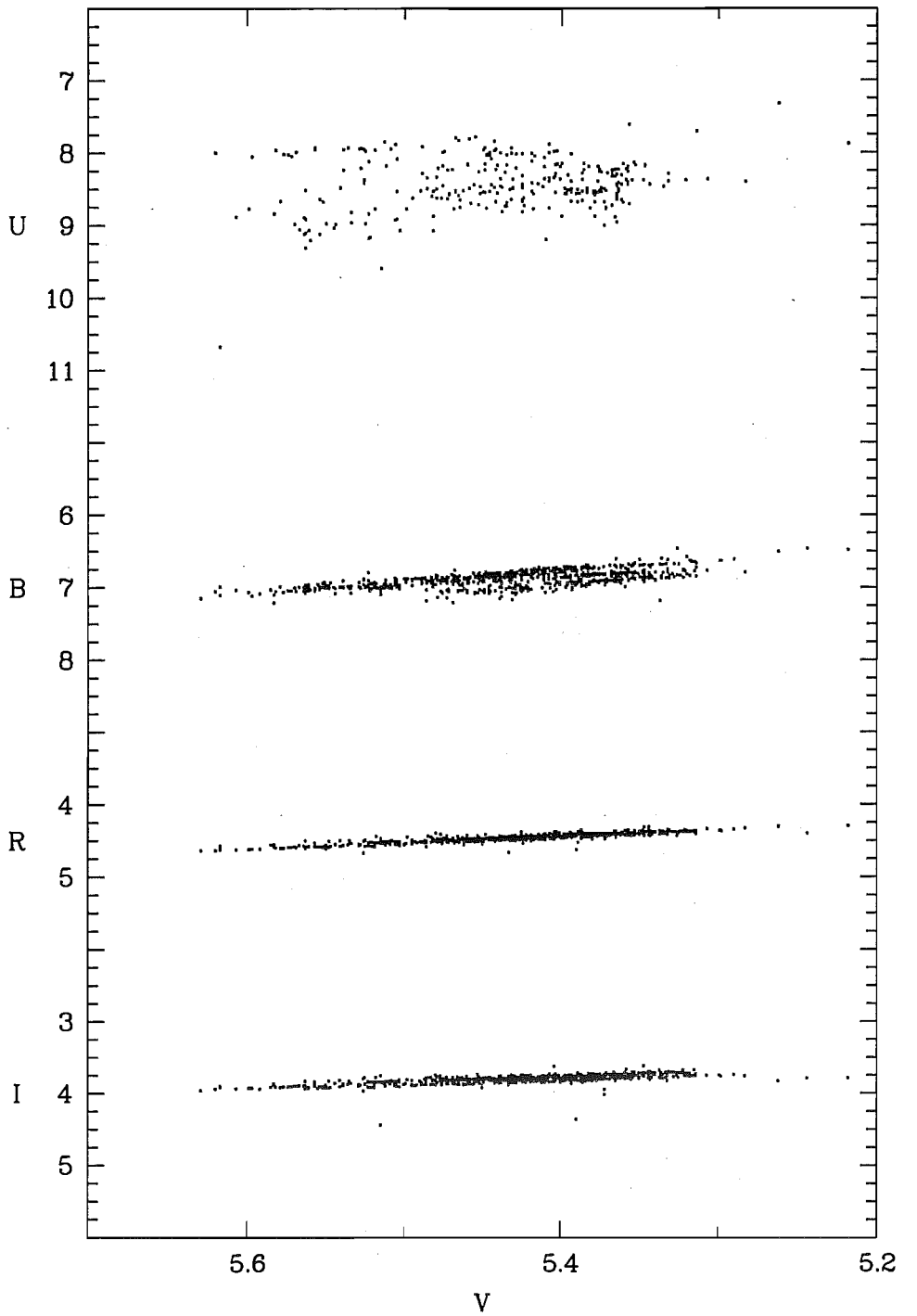

Figure 5.8: $UB(RI)_J$ vs V magnitudes for the light of HD 101379 only.

temperature between least- and most-spotted faces of the star, indicates that the long-term variability is explicable by changes in the spot coverage and density and does not require pulsation of an evolved star to be invoked as an additional cause of variability.

The reddening in $(B-V)$ since about JD 2448500 which can be seen in Figure 5.4 appears in Figure 5.6 as an almost-separated group of redder values of $(B-V)$ at given values of V. A similar but less obvious feature can also be seen in $(V-I)$ and possibly also in $(V-R)$, and was noted by Murdoch *et al*[45] who estimated its onset at JD 2448200 which is approximately the time that the long-term reddening evident in the $(B-V)$ plot in Figure 5.4 began. The same grouping appears in the plot of B against V in Figure 5.8, and less obviously on the scale used in the plot of I against V, from which it is concluded that the decreased mean flux in B and increased mean flux in I since about JD 2448200 are responsible for the increases in reddening. The trend at the end of the plot of $(B-V)$ in Figure 5.4 is not certain, but it appears possible that the reddening has continued to increase.

The three bluest points in the plots of $(V-I)$ in Figures 5.4 and 5.6 correspond with three unusually dim points in the I band (Figure 5.7). The same three observations also yielded dim points in the other bands, including U when it was observed in one case. The reality of those points is doubted.

5.3 High-resolution spectroscopy

GT Mus was the brightest object observed in the project, with markedly shorter integration times than all of the other objects, and it was rarely necessary to apply any filtering to the images to reduce cosmic ray strikes. With few exceptions, the reduction of the images has been restricted to the fitting of a dispersion solution using the standard MIDAS procedures and Th-Ar reference spectra, and the rebinning of the orders in 0·025 Å intervals, also using standard MIDAS procedures.

5.3.1 Rotation and radius of the active star

As shown by Murdoch *et al*,[46] the observed metal-line spectrum is that of the active giant in HD 101379. The FWHMs of the λ6200, λ6219 and λ6750 Fe I lines and the λ6768 Ni I line were measured in the best quality spectra, and the method described in Section 2.3.2 was used to measure their rotational broadening. Lines of the star HR 99 (α Phe), observed with the same instrument and settings including slit width, were used, and a limb-darkening coefficient of ϵ =0·78 was used, corresponding in Figure 17.6 of Gray[47] to the values of $(B-V)$ and $T_{\rm eff}$ for a K0 III star given in Gray's Table B2.

The best fit of FWHM was found with a rotational broadening of

$$v_{\rm rot} \sin i = 15 \cdot 96 \pm 0 \cdot 2 \,{\rm km/s}.$$

[45] *op cit*, Section 4.5
[46] *op cit*
[47] Gray, 1992, *op cit*

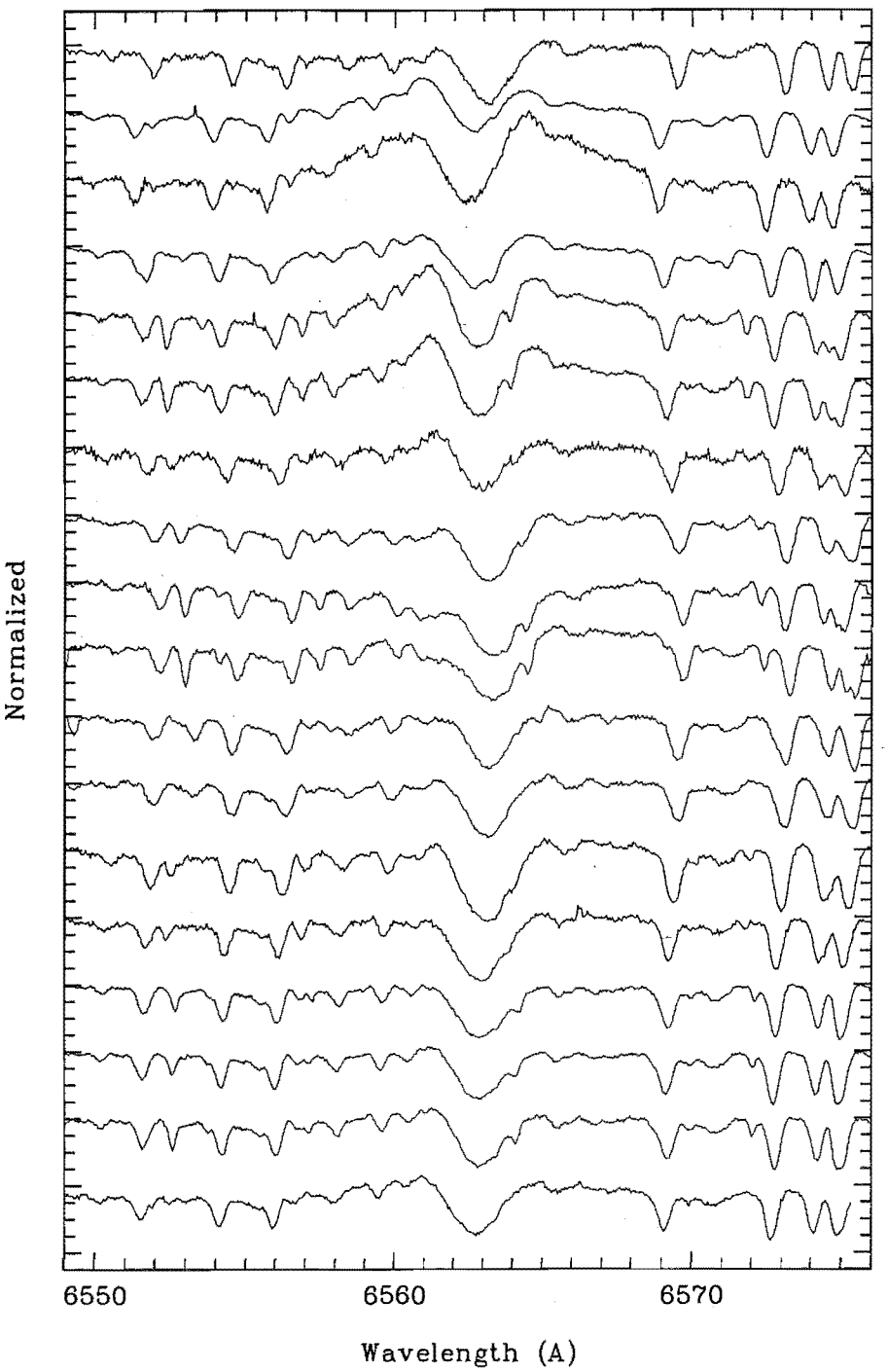

Figure 5.9: A selection of normalized Hα spectra of GT Mus, arranged in chronological order, top to bottom. Tick marks represent one tenth of the continuum flux.

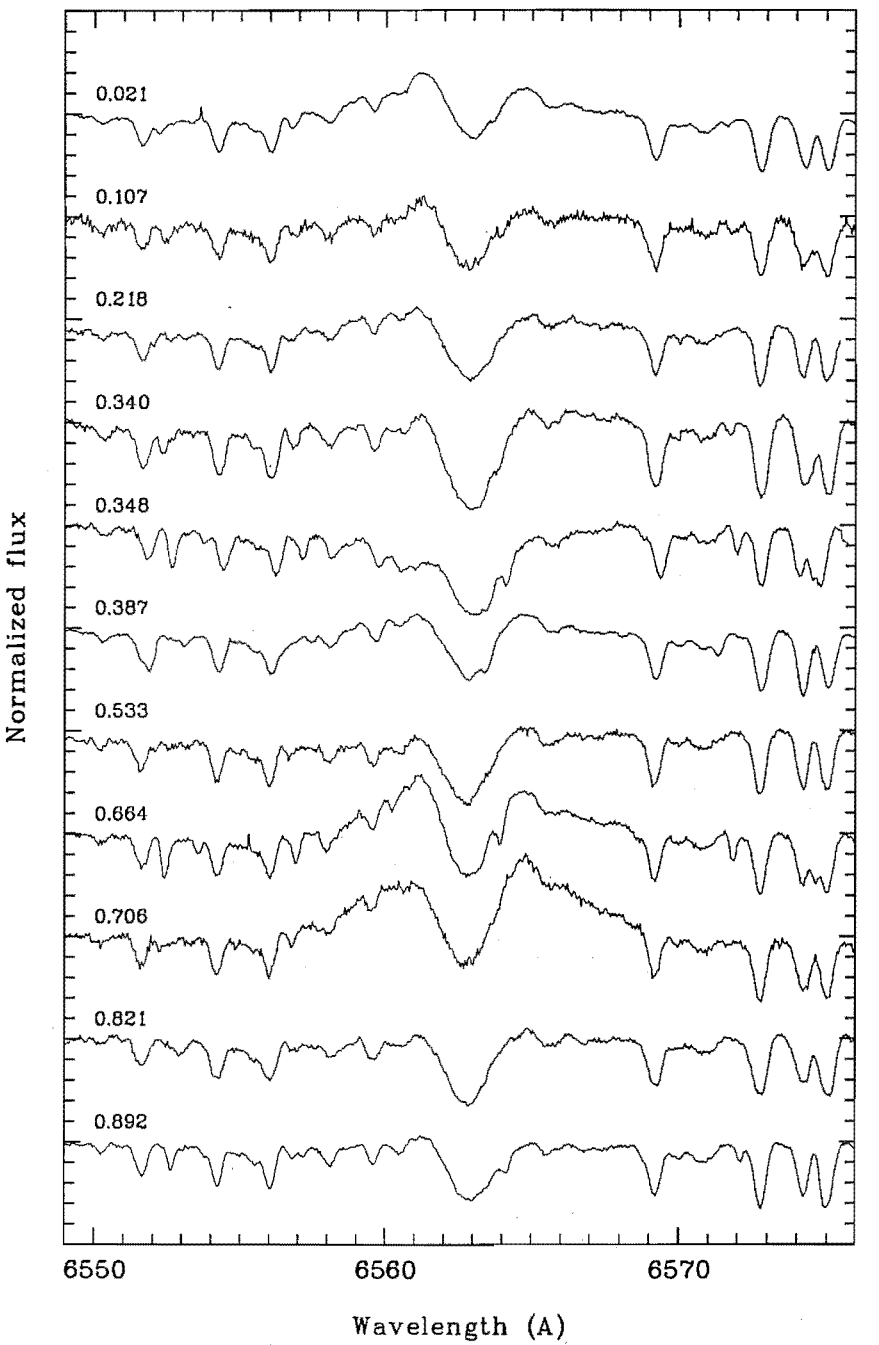

Figure 5.10: Normalized Hα spectra of GT Mus and their phase in the orbital period of HD 101379 as determined by Murdoch *et al, op cit.* The wavelengths have been corrected to place the metal lines at their laboratory rest wavelengths. Tick marks represent one tenth of the continuum flux. Spectra obtained on successive nights have been omitted.

Since the rotational broadening of HR 99 would be non-zero, if small, the measured rotational velocity is a lower limit and the actual velocity may exceed that amount by some hundreds of metres per second. The precision was limited by variation in the measurement of the FWHM of the lines of GT Muscae from spectrum to spectrum, and this variation is attributed to error in locating the proper level of the continuum as discussed in Section 3.2.3.

Assuming a rotational period similar to the orbital period found by Murdoch *et al*,[48] the measured rotational velocity implies a radius of

$$R \sin i = 19{\cdot}38 \pm 0{\cdot}03\, R_{\odot}$$

and, since the system is not eclipsing, the actual value of R must be greater than 19·4 $R_{\odot}$. That is at the upper limit of radii for class II giants of late G to K0 spectral type,[49] and gives further support to the suggestion (Section 5.2.4) that the primary of HD 101379 has evolved off the ascending giant branch and is becoming a bright giant.

5.3.2 The Hα absorption line

The eighteen spectra with the best S/N are shown in Figure 5.9. The Hα absorption line is shallow (core typically 0·3 of continuum flux below the immediately adjacent continuum); a variable emission does not fill the absorption line but is visible in the adjacent continuum. The absorption line is broader at its junction with the continuum than the wings of a normal Hα line (in this case that of HR 99) when rotationally broadened by convolution with a point-spread function corresponding to 16 km/s. A mechanism other than rotational broadening is responsible and, since the wings of the line are affected, it must be in the deep photosphere of the star.

The Hα absorption lines have a characteristically triangular rather than Gaussian shape, and this suggests the Doppler-shift distribution due to radial-tangential macroturbulence calculated by Gray,[51] superimposed on the elliptical distribution produced by rotational broadening. The interaction of such convective macroturbulence in the deep photosphere with the fast rotation of the active star could induce magnetic Alfvén waves[52] carrying energy to the active chromosphere.

5.3.3 Hα emission

The emission feature is at least as broad as 12 Å at the continuum as shown in a spectrum (phase 0·706 in Figure 5.10) obtained in 1994 August when the emission was most prominent. While some of the broadening will be due to chromospheric turbulence, bearing in mind that the source of the emission may extend several stellar radii beyond the photosphere,[53] it is probable that it is mostly attributable to stellar rotation.

[48] *op cit*

[49] See Schmidt-Kaler, *op cit*, Allen,[50] §100, and Gray, 1992, *op cit*, Table B2

[51] See Figure 18.4 of Gray, 1992, *op cit*

[52] See, for example, Mullan, *op cit*, and Bopp and Fekel, *op cit*

[53] For example in coronal loops as proposed by Collier Cameron, 1988, *op cit*, and in 1996, *Proc. IAU Symp. 176, Stellar Surface Structure*, eds Strassmeier K. G. and Linsky J. L.,Kluwer, Dordrecht, p. 449.

In addition to the broadening, the emission is usually Doppler-shifted relative to the Hα absorption line. In the spectra obtained from phases 0·892 to 0·218 in Figure 5.10, the emission is shifted blueward relative to the absorption line, and in the spectra obtain in phases 0·348 to 0·706 it is shifted redwards. This is evidence for an asymmetrical emission region around the star with the strongest source of emission (possibly a coronal loop or loops) being concentrated to one side of the star, or for an emission region in magnetic field lines in the space between the active star and its companion, the emitting region rotating relative to the companion with the active star and so showing a Doppler shift which is directly due to the orbital motion rather than to stellar rotation. In a system with synchronous or near-synchronous rotation, both hypotheses, and a combination of them, are consistent with the observed Doppler shifts.

5.4 Conclusion

From the eclipsing light curves of GT Muscae it is deduced that the eclipsing system HD 101380 consists of two A0/2-type dwarfs, one being 0·32 mag. in V dimmer than the other, in an orbit of 2·754591±0·000003 days. Analysis of the light of GT Muscae after subtracting the calculated fluxes of the A stars shows that the light of the active star is reddened in a manner consistent with absorption in the near ultraviolet and re-emission in the infrared by local, possibly circumstellar, dust grains having an optical depth at times as great as ~3. The V magnitude and colours during intervals of minimum reddening, together with the stellar radius calculated from the presumed synchronized rotation period and measured rotational broadening of metal lines, imply that the star responsible for the single-lined spectrum of HD 101379 is a G5/8 bright giant.

Modelling of spot coverage and temperature relative to the least-spotted face presented by the star indicates that variations in the light curve of the star of the order of several hundred days can be explained by variations in both the amount of the surface of the star which is covered by spots and the degree of concentration of the spots in confined regions of the stellar photosphere. The spot patterns decay on a time scale of less than 10 orbital periods of the HD 101379 system. The presence of differential rotation having a period which increases with increasing latitude is implied by power spectra of the spot modulations giving periods varying over a range several days longer than the orbital period and presumed synchronized rotation period of the active star.

The HD 101379 system emits strongly in Hα with an asymmetrical Doppler shift which implies that the emission is stronger on one side of the star or that a principal emission region is situated in magnetic field lines in the space between the active star and its companion and rotates relative to the companion with the active star. Since the rotation period is at least similar to the orbital period, it is not possible to distinguish between the two possibilities.

See discussion in Section 1.9

Chapter 6

Observations outside the main program

Astronomers in other institutions occasionally ask the Mount John University Observatory to assist them by observing southern stars. While completing this project, high-resolution spectra of two active-chromosphere stars were also obtained for other observers. The work that was done is presented in this chapter.

6.1 Observations of CF Tucanae

The eclipsing binary system CF Tuc (HD 5303, SAO 255716, 2EUVE J0053 −74.6, 2RE 0053 −743851, IRAS 00515 −7455) comprises an active K4 subgiant in a 2·797672 d orbit with a G0 dwarf.[1] Since its identification as an RS CVn-type system by Hearnshaw and Oliver,[2] CF Tucanae has been further identified as a moderately active microwave source,[3] a flaring[4] x-ray source,[5] and a flaring[6] extreme ultraviolet source.[7] Donati[8] reported detection of a Zeeman signature indicating the presence of strong magnetic fields in the atmosphere of the active star. Gurzadyan & Cholakyan[9] found that CF Tucanae obeyed an inverse linear relation found to exist for binaries with a separation less than $2{\cdot}7\,R_{\odot}$ between the strength of emission in the Mg II λ2800 ultraviolet doublet and the separation of the stars, and suggested that it was a system having a "roundchrom", a common chromosphere surrounding both stars such that emissions have their source in highly excited material between the stars.

[1] Budding E., 1985, *IBVS* No. 2779; Budding E. and McLaughlin E., 1987, *Ap&SS*, **133**, 45

[2] Hearnshaw J. B. and Oliver J. P., *IBVS* 1342

[3] Slee *et al, op cit*

[4] Kürster M. and Schmitt J. H. M. M., 1996, *Astron. Astrophys.*, **34**, 211

[5] Drake S.A., Simon T. and Linsky J. L., 1992, *ApJS*, **82**, 311, and Kürster M., 1996, in *Proc. IAU Symp. 176, Stellar Surface Structure*, eds Strassmeier K. G. and Linsky J. L., Kluwer, Dordrecht, p. 477

[6] Kürster M., 1994, in *Proceedings of the Eighth Cambridge Workshop, Cool Stars, Stellar Systems, and the Sun*, ed. Caillaut J. P., *PASPC*, **64**, p. 658

[7] Pounds *et al, op cit*

[8] Donati J.-F., 1996, in *Proc. IAU Symp. 176, Stellar Surface Structure*, eds Strassmeier K. G. and Linsky J. L., Kluwer, Dordrecht, p. 58

[9] *op cit*

Budding *et al*[10] interpreted the broadband photometry obtained over a number of years as evidence for a single large star spot of angular radius 15·3° to 17·1° centred at 45° latitude and drifting down in longitude at a rate of ~50° per year[11] so that, at the time of the spectroscopic observations, its longitude would have been 139° if the drift continued to be uniform.

CF Tucanae is also one of the active stars which have been mapped using Doppler imaging techniques. Kürster & Dennerl[12] and Kürster[13] have published maps using the ephemeris of Budding,[14] showing an almost unspotted hemisphere at phase 0·0 (facing the dwarf companion), an extensive low-latitude spot centred at phase 0·8, a polar spot, and scattered smaller spots. Kürster[15] found that periodic x-ray emission from the system showed a strong maximum near phase 0·8 which implies, *if* the active star is the x-ray source, a spatial correlation of the photospheric and coronal active regions.

6.1.1 Hα spectroscopy and interpretation

The work towards which the present author contributed is reported in Budding *et al.*[16] The main concern of the paper was the investigation of correlations between microwave signal enhancement and broad-band photometric flux diminution due to photospheric spots. This involved determining the longitudinal drift of the active star's photospheric spots and, it being assumed that the chromospherically active regions were at the same longitudes as the spots, the task was to obtain high-resolution spectra of the Hα line at suitable phases of the binary orbit.

Three spectra were obtained, on 1996 July 29, 30 and 31, and the regions about the Hα line are shown in Figure 6.2. The spectra in Figure 6.2 have been further filtered using the MIDAS "filter/smooth" procedure to remove cosmic ray strikes not eliminated by the median filtering during reduction. The three spectra show—

1. In the spectrum obtained at orbital phase 0·0332, an Hα absorption line at close to zero radial velocity relative to the solar system (no correction was made for the underlying radial velocity of the CF Tucanae system). The line is partially filled by the emission of the active star and the filling is approximately symmetrical, implying that the region of the star responsible for the emission is not concentrated on a limb of the star, for otherwise it would be Doppler-shifted by the stellar rotation.

2. In the spectrum obtained at orbital phase 0·726, a red-shifted absorption line partially filled by emission.

3. In the spectrum obtained at orbital phase 0·336, a blue-shifted absorption line largely filled by a weaker emission feature.

[10]Budding E., Jones K. L., Slee O. B. and Watson L., 1999, *MNRAS*, **305**, 966

[11]Budding E. and Zeilik M, 1995, *ApJ*, **319**, 827

[12]Kürster M. and Dennerl K., 1993, in *Physics of Solar and Stellar Coronae*, eds Linsky J. L. and Serio F., Kluwer, Dordrecht, p. 443

[13]Kürster, 1996, *op cit*

[14]*op cit*

[15]Kürster, 1996, *op cit*

[16]Budding E., Jones K. L., Slee O. B. and Watson L., *op cit*

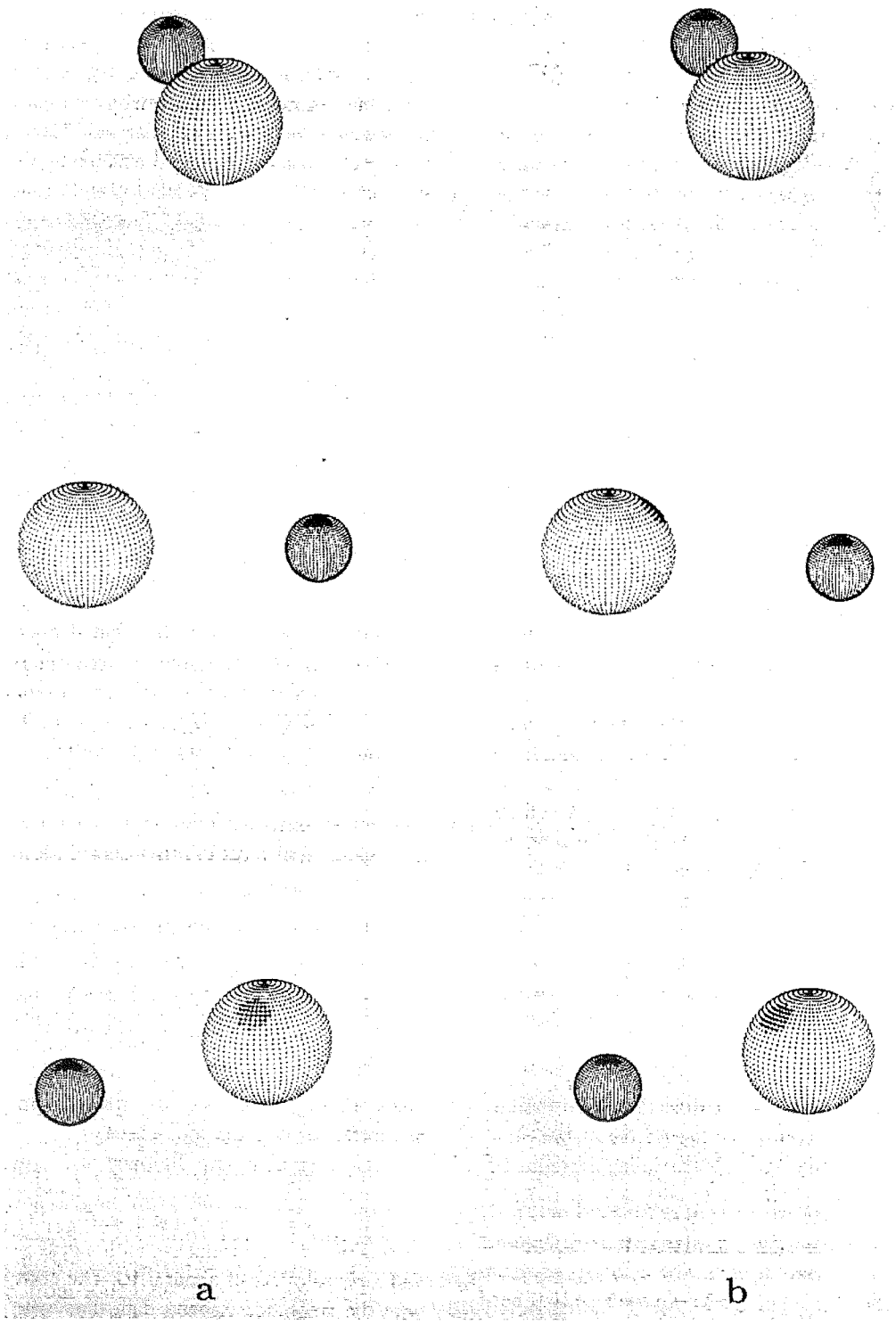

Figure 6.1: BINARY-MAKER representations of CF Tuc at phases corresponding respectively to the spectra in Figure 6.2, (a) with the active region located according to the original ephemeris and (b) with the active region set back in longitude to 160°.

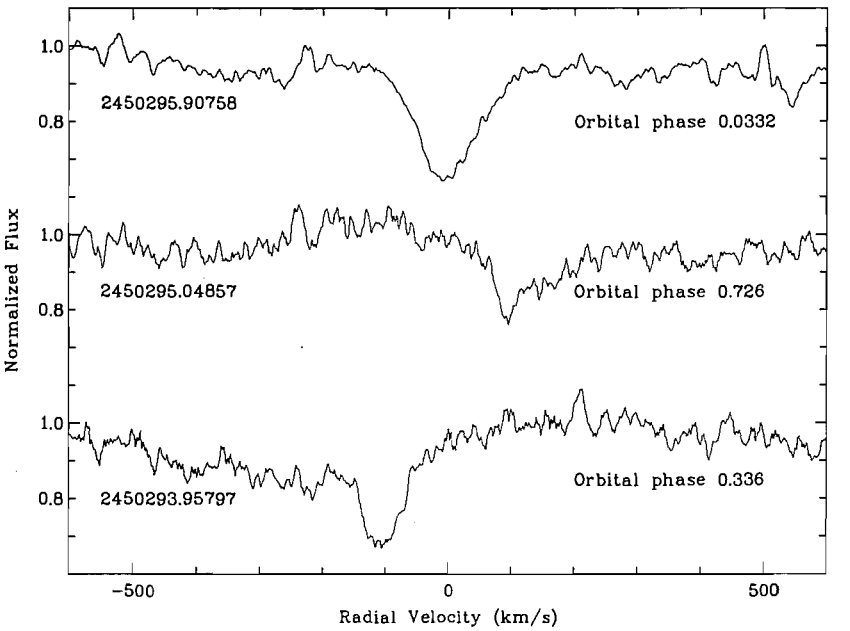

Figure 6.2: Hα spectra of CF Tucanae and their phase in the orbital ephemeris of Budding E., 1985, *IBVS* No. 2779. Radial velocities are those of the Hα absorption line relative to the centre of mass of the solar system.

The Budding ephemeris[17] explains the Doppler-shifting of the Hα absorption line in the high-resolution spectra: if the underlying system radial velocity is such as to make the radial velocity of the active star close to zero at phase 0·0332, its orbital radial velocity will be directed towards the observer at phase 0·336 and away from the observer at phase 0·726. BINARY-MAKER representations of the spot (Figure 6.1, set a) place the the spot out of the line of sight, around the limb of the star, at phase 0·0332, fully in sight, close to face-on, at phase 0·336, and out of sight again, around the receding limb of the star, at phase 0·726. Better congruence between the position of the spot and the apparent strength of the emission is obtained if the longitude of the spot is increased to 160° (Figure 6.1, set b) so that the spot is still invisible at phase 0·0332 and visible at phase 0·336, but also visible at phase 0·726. It is less clear that a single spot of the described angular extent could be longitudinally correlated with the source of the emission which partially fills the Hα absorption line at all of the observed phases, but the angle of inclination of the CF Tucanae system is 71·6°[18] and a tilt of the axis of rotation of the active star of 22·4° towards the observer could bring a chromospheric source aligned with the spot into the line of sight if it is well extended beyond the photosphere of the star as in, for example, the theory of Gurzadyan & Cholakyan.[19]

[17]Budding, *op cit*
[18]Budding and Zeilik, *op cit*
[19]*op cit*

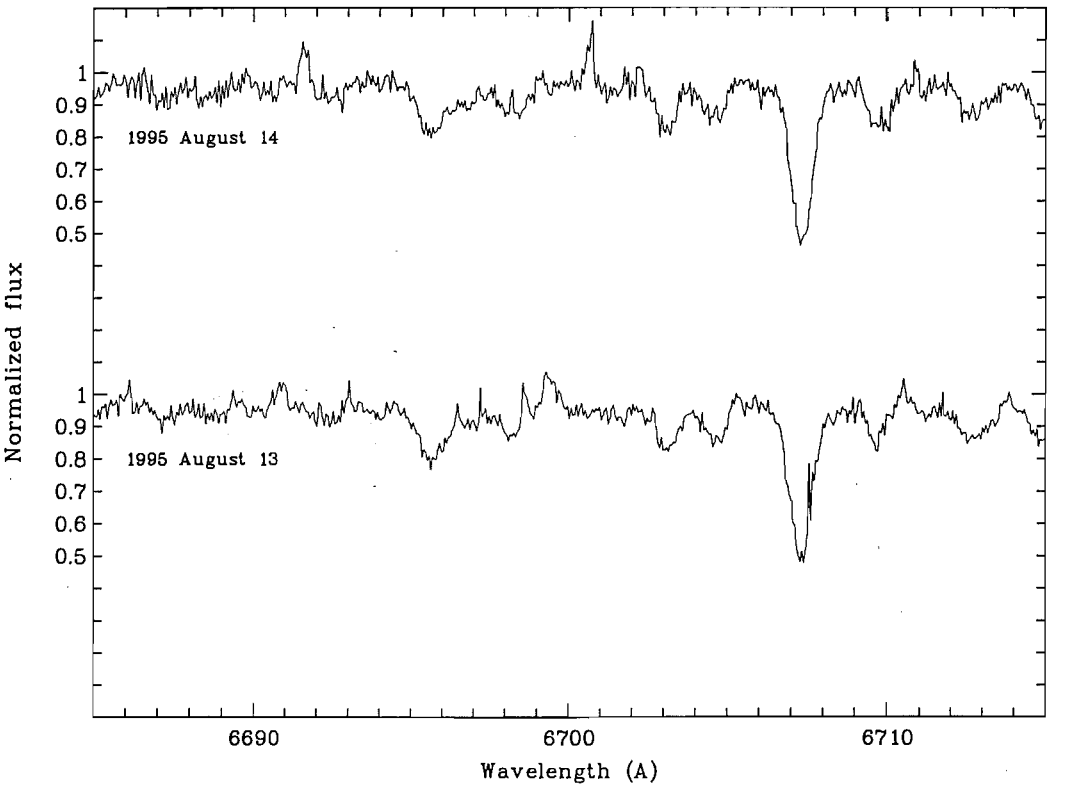

Figure 6.3: Li λ6708 spectra of HD 219025 obtained 1995 August 13 and 14. Tick marks represent one tenth of the normalized continuum flux.

The Doppler images presented by Kürster[20] show some spotting visible at all phases of the orbit and can thus explain the filling of the Hα absorption line at all observed phases. Kürster's large spot at phase 0·8 could account for the possibly stronger emission visible in the spectrum obtained at orbital phase 0·726, and, since the larger part of it would be on the approaching limb at phase 0·726, it would also be somewhat blue-shifted. It is notable, however, that the imaged spot is located at a lower latitude than the spot produced by the BINARY-MAKER program, which is presumably a consequence of part of the light variation being accounted for by a polar spot which is not present in the BINARY-MAKER image.

[20]Kürster, 1996, *op cit*

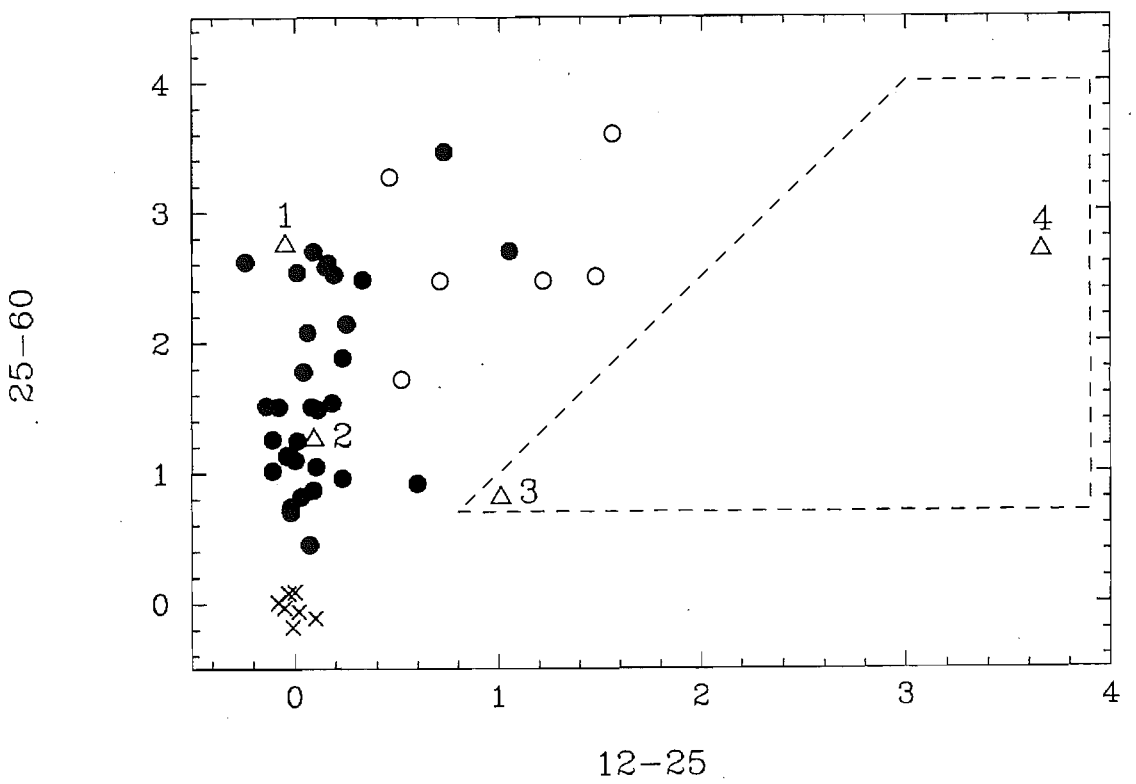

Figure 6.4: IRAS colour-colour diagram of IR-excess giants, after Fekel and Watson, *op cit.* The dashed line defines the region in which most giants are lithium-rich.

6.2 Observations of HD 219025

The star HD 219025 (SAO 255433, IRAS F23107 −6833, HIP 114678) is a K2 giant[21] with an infrared excess,[22] and a large lithium abundance,[23] and it was identified as a member of the class of rapidly rotating, single, chromospherically active giants by Fekel *et al.*[24] Such stars might provide confirming examples of both the Fekel & Balachandran[25] and de la Reza *et al*[26] hypotheses connecting fast rotation, lithium excess and infrared excess in early giants.

The work to which the present author contributed is reported in Fekel & Watson.[27] A measurement of the lithium abundance of HD 219025 was required, and on 1995 August 13 and 14 two échelle spectra of the λ6708 Li I doublet shown in Figure 6.3 were obtained. Measurements of the equivalent widths of the two Li lines as 485 mÅ in the upper spectrum

[21] Houk and Cowley, *op cit*
[22] Stencel R. E. and Backman D. E., 1991, *ApJS*, **75**, 905
[23] Randich S., Gratton R. and Pallavicini R., 1993, *Astron. Astrophys.*, **273**, 194
[24] Fekel F. C., Webb R. A., White R. J. and Zuckerman B., 1996, *ApJ*, **462**, L95
[25] *op cit*
[26] *op cit*
[27] Fekel F. C. and Watson L. C., 1998, *AJ*, **116**, 2466

and 486 mÅ in the lower spectrum were made and, for the purpose of calculating rotational $v \sin i$, the FWHM of Fe I lines at λ6323, λ6335, λ6337 and λ6704 was also measured

The principal investigator, using his own measurements of the Li I equivalent width, calculated the lithium abundance of HD 219025 as $\log N(\mathrm{Li}) = 3{\cdot}3$ (where $\log N(\mathrm{H}) = 12$) which is in excess of the limiting abundance, $\log N(\mathrm{Li}) < 1{\cdot}5$ predicted for normal red giants by Iben.[28] The rotational velocity was estimated at $v \sin i = 25\,\mathrm{km/s}$, also confirming that this is a fast-rotating giant. As discussed in Section 1.8, De la Reza *et al*[29] have proposed an evolutionary model wherein every star with a mass between 1 and $2{\cdot}5\,M_{\odot}$ becomes lithium-rich while a K giant, and the internal mechanism responsible for the enrichment also initiates a mass-loss event which produces an infrared excess. They plotted evolutionary tracks for detached circumstellar shells in an infrared colour-colour diagram in which the stars move anticlockwise around the diagram from the lower left corner, the most extended tracks being followed by stars which have the greatest mass-loss rates. In Figure 6.4, taken from Fekel and Watson, HD 219025 is labelled with the number 3: it falls within the region, marked by a dashed line, in which the theory predicts most giants will be lithium-rich, in a position which suggests that it has experienced a mass-loss event which was both relatively small (because of the tight radius of its evolutionary track) and recent (because of its small angular displacement from the starting point).

[28] *op cit*
[29] *op cit*

Chapter 7

Summary of conclusions

In addition to the three stars mentioned individually below, of the southern stars selected for observation from the ROSAT Bright Source Catalogue,[1] HD 147633 was found to be a double-lined spectroscopic binary with moderate H and K emission, and a clear photometric period (2·8 days, probably a spot-wave) could be seen to persist for several years in the observations of HD 222259 which has also been shown[2] to be an active star.

7.1 CS Ceti

It has been shown that CS Cet is a binary system with a period of 27·332±0·008 days and an orbital eccentricity of 0·293±0·026. Hα spectra show emission of a strength sufficient to more than fill the Hα absorption lines of both stars of the system. If there is any periodicity in the brightness of the system it must have a timescale of less than 60 days.

Based on the fitting of a model Hα line to a single spectrum, it is concluded that the CS Cet system consists of a late F-type dwarf secondary and a chromospherically active G5-K1 III-IV primary having an absolute visual magnitude of $M_V \approx 2{\cdot}4$ and a mass $M \approx 1{\cdot}45\,M_\odot$. Based on this analysis, an upper limit for the rotation period of the active star has been calculated as 11·5±1·3 days, a period less than half the orbital period of the system which suggests that the photosphere of the active star has been spun up by a transfer of angular momentum from a fast-spinning core. Assuming co-rotation, the rotational velocities of the Hα emission show that the source of that emission is located in, and varies within, a range of distance of up to 5·8±1·1 times the radius of the active star from the centre of the star.

7.2 BB Sculptoris

It has been shown that the B component of the A+B visual binary system in BB Scl is an eclipsing binary system with an orbital period of 0·476525±0·000013 days.

[1] Pounds *et al, op cit*

[2] Soderblom, King and Henry, *op cit*

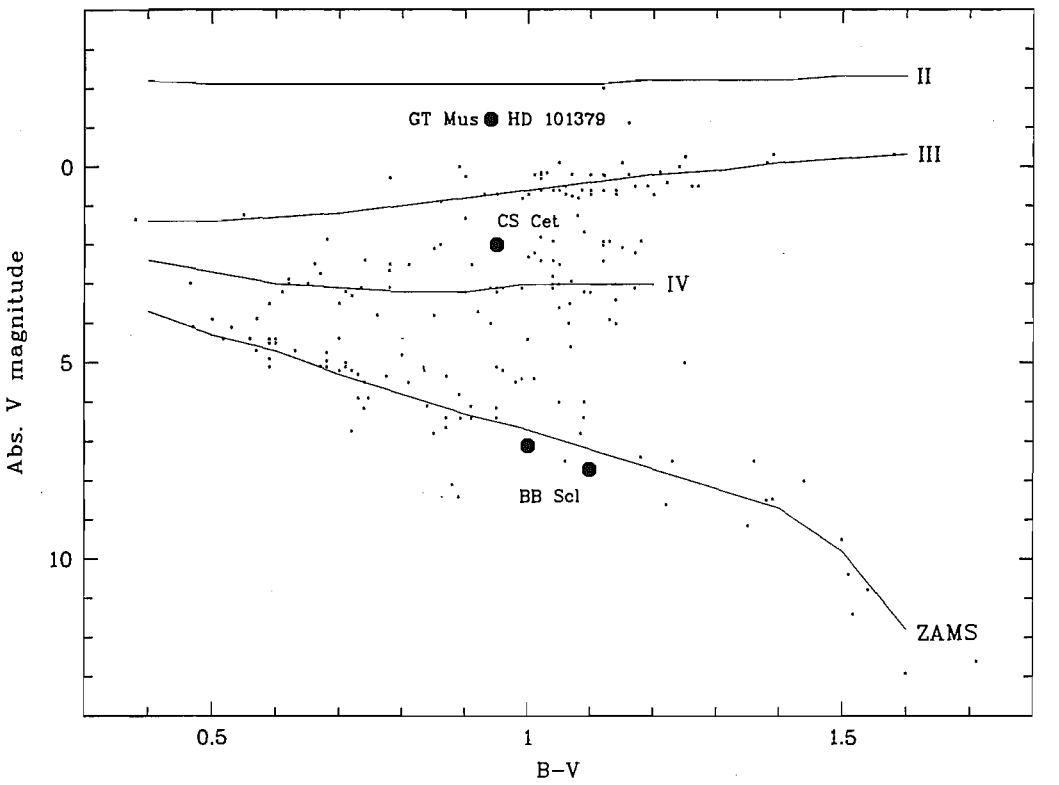

Figure 7.1: The positions of the active stars of BB Scl, CS Cet and GT Mus, as calculated in this work, superimposed on the H-R diagram of Figure 1.3.

There is a well-defined difference of 105 ± 20 K between the effective temperatures of the two eclipsing stars. While their relative radii are not defined with high precision, the total surface area of the two eclipsing stars is better determined and, with the colour photometry, is consistent with the system consisting of a pair of K3 to K5 dwarfs. Échelle spectra of the Hα line indicate that both stars of the eclipsing binary system are active, the secondary being more strongly active, at least in Hα, than the primary. The light curve in V shows short-period variability characteristic of fast-rotating spotted stars, and it is concluded that the eclipsing binary system is a BY Dra-type system consisting of two K-type dwarfs and having the shortest orbital period of any known system of that type. The inclination of the system obtained from the light curve analysis is $i = 86° \pm 4°$.

On the basis of the measured magnitudes and colour index, the published orbital parameters and the *Hipparcos* parallax, it is concluded that the A component of BB Scl is probably also a binary system, consisting of K1 and K3 V stars, possibly with a small angle of inclination. The whole BB Scl system thus comprises five stars, two of them in the active BY Dra system B, two in the non-active system A, and the (presumed) single star C of type M2 V.

7.3 GT Muscae

The period of the eclipsing binary system HD 101380 has been yet more precisely determined as 2·754591±0·000003 days. The eclipsing binary light curve has been analysed to show that the two stars have a magnitude difference of ~0·5 mag. and that they are of approximate spectral types A0 V and A2 V.

Analysis of the light of GT Muscae after subtracting the flux of an A0 V star and an A2 V star shows that the starlight is reddened in a manner consistent with extinction by dust grains, and that colours are consistent with reddened light from a late G bright giant, and that the active star cannot be later in spectral type than K0 II and is probably a G5/8 bright giant.

Spots are distributed around the active star in longitude with no stellar hemisphere presenting an immaculate photosphere. The spot patterns decay on a time scale of less than 10 orbital periods of the HD 101379 system. The power spectra of the spot modulations disclose dominant periods always slightly longer than the orbital period of the HD 101379 system, which may indicate that the active star has differential surface rotation which increases in period with increasing latitude.

The HD 101379 system emits strongly in Hα with an asymmetrical Doppler shift which implies that the emission is stronger on one side of the star or that a principal emission region is situated in magnetic field lines in the space between the active star and its companion and rotates relative to the companion with the active star. Since the rotation period is at least similar to the orbital period, it is not possible to distinguish between the two possibilities.

References

Abetti, G., 1969,*The Sun*, Faber and Faber, London.

Allen C. W., 1976, *Astrophysical Quantities*, 3rd edition corrected, London.

Armado P. J. and Byrne P. B., 1997, *Astron. Astrophys.*, **319**, 967.

Banks T. and Budding E., 1990, *Ap&SS*, **167**, 221.

Barnes T. G., Evans D. S. and Parsons S. B, 1976, *MNRAS*, **174**, 503.

Barnes T. G., Evans D. S. and Moffett T. J., 1978, *MNRAS*, **183**, 285.

Bessell M. S., 1990, *Astron. Astrophys. Supp.*, **83**, 357.

Biermann P. and Hall D. S., 1976, in *Proc. IAU Symp. 73, Structure and Evolution of Close Binary Systems*, eds Eggleton P. *et al*, Reidel, Dordrecht, p. 381.

Bopp B. W. and Fekel F. C., 1977, *AJ*, **82**, 490.

Bopp B. W., Noah P. V. and Klimke A., 1980, *Stellar Surface Phenomena: Stellar Rotation and the BY Draconis Syndrome in the High-Eccentricity Binary BD +24°692*, pub. Ritter Astrophys. Research Center.

Bopp B. W. and Rucinski S.M., 1981, in *Proc. IAU Symp. 93, Fundamental Problems in the Theory of Stellar Evolution*, eds Sigimoto D., Lamb D. Q. and Schramm D. N., Reidel, Dordrecht, p. 177.

Bopp B. W. and Stencel R. E., 1981, *ApJ*, **247**, L131.

Bopp B. W. and Talcott J. C., 1978, *AJ*, **83**, 1517.

Bowyer S., Lieu R. Lampton M., Lewis J., Wu X., Drake J. J. and Malina R. F., 1994, *ApJS*, **93**, 569.

Bowyer S., Lampton M., Lewis J., Wu X., Jelinsky P., and Malina R. F., 1996, *ApJS*, **102**, 129.

Bromage G. E., Buckley D. A. H., Gilmore A. C., Hearnshaw J. B., Kilmartin P. M. and Watson L. C., 1996, *IBVS* No. 4400.

Brown J., Sneden C., Lambert D. L., and Dutchover E., 1989, *ApJS*, **71**, 293.

Buchholz B. and Ulmschneider P., 1994, in *Cool Stars, Stellar Systems and the Sun VIII*, ed. Caillaut J.-P., ASPCS, p. 363.

Budding E., 1985, *IBVS* No. 2779.

Budding E., Burgess A., Chan S. and Slee O. B., 1992, in *Surface inhomogeneities on late-type stars*, eds Byrne P. B. and Mullan D. J., Springer Lect. Notes Phys., **397**, at p. 253.

Budding E., Jones K. L., Slee O. B. and Watson L., 1999, *MNRAS*, **305**, 966.

Budding E. and McLaughlin E., 1987, *Ap&SS*, **133**, 45.

Budding E. and Zeilik M, 1995, *ApJ*, **319**, 827.

Butler C. J., 1996, in *Proc. IAU Symp. 176, Stellar Surface Structure*, eds Strassmeier K. G. and Linsky J. L., Kluwer, Dordrecht.

Carbon D. and Gingerich O, 1969, in *Theory and Observation of Normal Stellar Atmospheres* ed. Gingerich O., MIT Press.

Carlsson M. and Stein R. F., 1994, in *Chromospheric Dynamics*, ed. Carlsson M., Inst. Theor. Astrophys., Oslo, p. 47.

Castenmiller M. J. M., Zwaan C. and van der Zalm B. J., 1986, *Solar Physics*, **105**, 237.

Catalano S., Rodonò M., Frasca A. and Cutispoto G, 1996, in *Proc. IAU Symp. 176, Stellar Surface Structure*, eds Strassmeier K. G. and Linsky J. L., Kluwer, Dordrecht, p. 403.

Collier A., 1982, Ph.D. Thesis, Univ. Canterbury.

Collier Cameron A., 1987, *S. Afr. Astron. Obs. Circ.*, **11**, 57.

Collier Cameron, A., 1988, *MNRAS*, **233**, 235.

Collier Cameron A., 1996, in *Proc. IAU Symp. 176, Stellar Surface Structure*, eds Strassmeier K. G. and Linsky J. L.,Kluwer, p. 449.

Collier Cameron, A. and Robinson R. D., 1989, *MNRAS*, **236**, 57.

Collier Cameron A. and Woods J. A., 1992, *MNRAS*, **258**, 360.

Cutispoto G., Kürster M., Messina S., Rodonò M. and Tagliaferri G., 1997, *Astron. Astrophys.*, **320**, 586.

Cutispoto G., Pallavicini R., Kürster M. and Rodonò M., 1995, *Astron. Astrophys.*, **297**, 764.

Dempsey R. C., Bopp B. W., Henry G. W. and Hall D. S., 1993, *ApJS*, **86**, 293.

Dempsey R. C., Bopp B. W., Strassmeier K. G., Granados A. F., Henry G. W. and Hall D. S., 1992, *ApJ*, **392**, 187.

Dempsey R. C., Linsky J. L., Fleming T. A. and Schmitt J. H. M. M., 1993, *ApJSS*, **86**, 599.

Dobson A. K. and Radick R. R., 1989, *ApJ*, **344**, 907.

Dommanget, J., and Nys, O., 1982, *Second Catalogue d'Éphémérides*, Roy. Obs. Belgium Comm., Ser. B, No. 124.

Donahue R. A., Dobson A. K. and Baliunas S. L., 1996, *Harvard-Smithsonian Center for Astrophysics Preprint series* No. 4423.

Donati J.-F., 1996, in *Proc. IAU Symp. 176, Stellar Surface Structure*, eds Strassmeier K. G. and Linsky J. L., Kluwer, Dordrecht, p. 58.

Donati J.-F., Brown S., Semel M., Rees D., Dempsey R., Matthews J., Henry D. and Hall D. S., 1992, *Astron. Astrophys.*, **265**, 682.

Doyle J. G. and Collier Cameron A., 1990, *MNRAS*, **244**, 291.

Drake S.A., Simon T. and Linsky J. L., 1992, *ApJS*, **82**, 311.

Eaton J. A., Gregory W. H., Bell C. and Okorogu A., 1993, *AJ*, **106**, 1181.

Eaton J. A. and Hall D. S., 1979, *ApJ*, **227**, 907.

Edwards T. W., 1976, *AJ*, **81**, 245.

Eggen O. J., 1962, *Roy. Obs. Bull.* No. 51.

Eggen O. J., 1976, *ApJS*, **30**, 351.

Fekel F. C. and Balachandran S., 1993, *ApJ*, **403**, 708.

Fekel F. C. and Eitter J. J., 1989, *AJ*, **97**, 1139.

Fekel F. C., Moffett T. J. and Henry G. W., 1986, *ApJS*, **60**, 551.

Fekel F. C. and Watson L. C., 1998, *AJ*, **116**, 2466.

Fekel F. C., Webb R. A., White R. J. and Zuckerman B., 1996, *ApJ*, **462**, L95.

Feldman P. A., Taylor A. R., Gregory P. C., Seaquist E. R., Balonek T. J. and Cohen N. L., 1978, *AJ*, **83**, 1471.

Fitzgerald M. P., 1970, *Astron. Astrophys.*, **4**, 234.

Flower P. J., 1996, *ApJ*, **469**, 355.

Fraquelli D. A., 1978, *AJ*, **83**, 1535.

Furenlid I. and Young A., 1978, *AJ*, **83**, 1527.

Gaizauskas V., Harvey K. L., Harvey J. W. and Zwaan C., 1983, *ApJ*, **265**, 1056.

García López R. J., Rebolo R., Beckman J. E. and McKeith C. D., 1993, *Astron. Astrophys.*, **273**, 482.

Gershberg R. E., Il'in I.V. and Sharkhovskaya N. I., 1991, *Sov. Astron.*, **35**, 479.

Giampapa M. S., 1984, *ApJ*, **277**, 235.

Gray D. F., 1986, *Adv. Space Res.*, Vol. 6 No. 8, 161.

Gray D. F., 1992, *The Observation and Analysis of Stellar Photospheres*, 2nd ed., Cambridge.

Grenon M., 1997, *The Hipparcos and Tycho Catalogues* vol. 12, ESA PublicationsDivision, Noordwijk.

Grevesse N., 1968, *Solar Phys.*, **5**, 159.

Güdel M., 1996, in *Proc. IAU Symp. 176, Stellar Surface Structure*, eds Strassmeier K. G. and Linsky J. L., Kluwer, Dordrecht, p. 485.

Gurzadyan G. A. and Cholakyan V. G., 1995, *Ap&SS*, **229**, 185.

Haisch B. and Schmitt J. H. M. M., 1994, *ApJ*, **426**, 716.

Hall D. S., 1976, in *Proc. IAU Coll. 129, Multiply Periodic Phenomena in Variable Stars*, ed. Fitch W. S., Reidel, Dordrecht, p. 287.

Hall D. S., 1991, in *Proc. IAU Coll. 130, The Sun and Cool Stars: activity, magnetism, dynamos*, eds Tuominen I., Moss D. and Rüdiger G., Springer-Verlag, Berlin.

Hall D. S. and Henry G. W., 1994, *IAPPP Comm.*, **55**, 51.

Hearnshaw J. B., 1977, *Proc. ASA*, **3(2)**, 102.

Hearnshaw J. B., 1978, *AJ*, **83**, 1531.

Hearnshaw J. B. and Oliver J. P., *IBVS* 1342.

Hickman M. A., Sloan G. C. and Canterna R., 1995, *AJ*, **110**, 2910.

Hirshfeld A., and Sinnott R. W., 1985, *Sky Catalogue 2000.0*, Cambridge University Press and Sky Publishing Corporation, Vol. 2.

Hobbs R. W., Kondo Y. and Feibelman W. A., 1978, *AJ*, **83**, 1525.

Hodgkin S. T. and Pye J. P., 1994, *MNRAS*, **267**, 840.

Hoffleit, D., and Jaschek, C., 1982, *The Bright Star Catalogue*, Yale University Observatory, Conn., 4th Revised Ed.

Houk N., 1982, *Univ. Michigan Catalog of Two-dimensional Spectral Types for the HD Stars*, vol. 3, Univ. Michigan, Ann Arbor.

Houk N., Cowley A. P., 1975, *Univ. Michigan Catalog of Two-dimensional Spectral Types for the HD Stars*, vol. 1, Univ. Michigan, Ann Arbour.

Hünemörder D. P., Ramsey L. W., Buzasi D. L. and Nations H. L., 1993, *ApJ*, **404**, 316.

Iben I., 1967, *ApJ*, **147**, 624.

Iben I., 1967, *ApJ*, **147**, 650.

Jeffries R. D., 1993, *MNRAS*, **262**, 369.

Jeffries R. D., 1996, in *Proc. IAU Symp. 176, Stellar Surface Structure*, eds Strassmeier K. G. and Linsky J. L., Kluwer, Dordrecht, p. 461.

Jenkins, L. F., 1963, *Supplement to the General Catalogue of Trigonometric Stellar Parallaxes*, Yale University Observatory, Conn.

Jetsu L., Huovelin J, Savanov I. and Tuominen I, 1991, *Astron. Astrophys.*, **248**, 574.

Johnson H. L., 1966, *Ann. Rev. Astron. Astrophys.*, **4**, 193.

Jordan C. and Linsky J. L., 1987, in *Exploring the Universe with the IUE Satellite*, ed. Kondo Y., Reidel, Dordrecht, p. 259.

Joy A. H., 1930, *ApJ.*, **72**, 41.

Katsova M. M. and Tsikoudi V., 1992, *Sov. Astron.*, **36**, 421.

Kreysing H.-C., Brunner H., and Staubert R., 1995, *Astron. Astrophys.*, **114**, 465.

Kürster M., 1994, in *Proc. Eighth Cambridge Workshop, Cool Stars, Stellar Systems, and the Sun*, ed. Caillaut J. P., *PASPC*, **64**, p. 658.

Kürster M., 1996, in *Proc. IAU Symp. 176, Stellar Surface Structure*, eds Strassmeier K. G. and Linsky J. L., Kluwer, Dordrecht, p. 477.

Kürster M. and Dennerl K., 1993, in *Physics of Solar and Stellar Coronae*, eds Linsky J. L. and Serio F., Kluwer, Dordrecht, p. 443.

Kürster M. and Schmitt J. H. M. M., 1996, *Astron. Astrophys.*, **34**, 211.

Kurucz, R. L., 1993, *New Atmospheres for Modeling Binaries and Disks* in *Light Curve Modeling of Eclipsing Binary Stars*, ed. E. F. Milone, Springer-Verlag, Berlin.

Kurucz R. L., 1994, Kurucz CD-ROM No. 19, *Solar Abundance Model Atmospheres for 0,1,2,4,8 km/s*, Smithsonian Astrophysical Observatory.

Lambton M., Lieu R., Schmidt J. H. M. M., Bowyer S., Voges W., Lewis J. and Wa X., 1997, *ApJS*, **108**, 545.

van Leeuwen F., Lindegren L., and Mignard F., 1997, *The Hipparcos and Tycho Catalogues*, vol. 3, ESA Publications Division, Noordwijk.

Lomb, N. R., 1976, *A&SS*, **39**, 447.

Mason K. O., Hassall B. J. M., Bromage G. E., Buckley D. A. H., Naylor T., O'Donoghue D., Watson M. G., Bertram D., Branduardi-Raymont G., Charles P. A., Cooke B., Elliott K. H., Hawkins M. R. S., Hodgkin S. T., Jewell S. J., Jomaron C. M., Sekiguchi K., Kellett B. J., Lawrence A., McHardy I., Mittaz J. P. D., Pike C. D., Ponman T. J., Schmitt J., Voges W., Wargau W, and Wonnacott, D. 1995, *MNRAS*, **274**, 1194.

Mathioudakis M. and Doyle J. G., 1992, *Astron. Astrophys.*, **262**, 523.

Mathioudakis M., Fruscione A., Drake J. J., McDonald K., Bowyer S. and Malina R. F., 1995, *Astron. Astrophys.*, **300**, 775.

McGale P. A., Pye J. P., Barber C. R., and Page C. G., 1995, *MNRAS*, **275**, 1232.

Middlekoop G. and Zwaan C, 1981, *Astron. Astrophys.*, **101**, 26.

Mitrou C. K., Mathioudakis M., Doyle J. G. and Antonopoulou E., 1997, *Astron. Astrophys.*, **317**, 776.

Mullan D. J., 1974, *ApJ*, **192**, 149.

Mullan D. J. and Johnson M., 1995, in *IAU Symp. 176, Poster Proceedings*, ed. in Strassmeier K. G., Institut für Astronomie, Vienna, p. 206.

Mullis C. L. and Bopp B. W., 1994, *PASP*, **106**, 822.

Murdoch K. A., Hearnshaw J. B., Kilmartin P. M., Gilmore A. C., 1995, *MNRAS*, **276**, 836.

Narain U. and Ulmschneider P, 1990, *Space Sci. Rev.*, **54**, 377.

Nolthenius R., 1991, *IBVS* No. 3589.

Odenwald S. F., 1986, *ApJ*, **307**, 711.

Olah K., Budding E., Butler C. J., Houidebine E. R., Gimenez A. and Zeilik M., 1992, *MNRAS*, **259**, 302.

van den Oord G. H. J. and Zuccarello F., 1996, in *Proc. IAU Symp. 176, Stellar Surface Structure*, eds Strassmeier K. G. and Linsky J. L., Kluwer, Dordrecht, p. 433.

Pallavicini R., Cerruti-Sola M. and Duncan D. K., 1987, *Astron. Astrophys.*, **174**, 116.

Pallavicini R., Cutispoto G., Randich S. and Gratton R., 1993, *Astron. Astrophys.*, **267**, 145.

Pallavicini R., Randich S and Giampapa M, 1992, *Astron. Astrophys.*, **253**, 185.

Parker E. N., 1955, *ApJ*, **122**, 293.

Perryman, M. A. C., 1997, *The Hipparcos and Tycho Catalogues* Volume 1, ESA Publications Division, Noordwijk.

Petit M., 1980, *IBVS* No. 1788.

Pinsonneault M. H., Kawaler S. D., Sofia S. and Demarque P., 1989, *ApJ*, **338**, 424.

Popper D. M., 1978, *AJ*, **83**, 1522.

Popper D. M. and Ulrich R. K., 1977, *ApJ.*, **212**, L131.

Pounds K. A., Allan D. J., Barber C., Barstow M. A., Bertram D., Branduardi-Raymont G., Brebner G. E. C., Buckley D., Bromage G. E., Cole R. E., Courtier M., Cruise A. M., Culhane J. L., Denby M., O'Donoghue D., Dunford E., Georgantopoulos I., Goodall C. V., Gondhalekar P. M., Gourlay J. A., Harris A. W., Hassall B. J. M., Hellier C., Hodgkin S., Jeffries R. D., Kellett B. J., Kent B. J., Lieu R., Lloyd C., McGale P., Mason K. O., Matthews L., Mittaz J. P. D., Page C. G., Pankiewicz G. S., Pike C. D., Ponman T. J., Puchnarewicz E. M., Pye J. P., Quenby J. J., Ricketts M. J., Rosen S. R., Sansom A. E., Sembay S., Sidher S., Sims M. R., Stewart B. C., Sumner T. J., Vallance R. J., Watson M. G., Warwick R. S., Wells A. A., Willingale R. R., Willmore A. P., Willoughby G. A., and Wonnacott D., 1993, *MNRAS*, **260**, 77.

Pye J. P., McGale P. A., Allan D. J., Barber C. R., Bertram D., Denby M., Page C. G., Ricketts M. J., Stewart B. C., and West R. G., 1995, *MNRAS*, **274**, 1165.

Randich S., Gratton R. and Pallavicini R., 1993, *Astron. Astrophys.*, **273**, 194.

Reader J. and Corliss C. H., 1982, *Line Spectra of the Elements* in *CRC Handbook of Chemistry and Physics*, 63rd ed., ed. Weast R. C., CRC Press, Boca Raton.

de la Reza R., Drake N. A. and da Silva L., 1996, *ApJ*, **456**, L115.

Rodonò M., 1986, in *Cool Stars, Stellar Systems and the Sun, Fourth Cambridge Workshop*, eds Zeilik M. and Gibson D. M., Springer-Verlag, Berlin, p. 475.

Rutten, R. G. M., Schrijver C. J., Lemmens A. F. P. and Zwaan C., 1991, *Astron. Astrophys.*, **252**, 203.

Scargle, J. D., 1982, *ApJ*, **263**, 835.

Schmidt-Kaler Th., 1965, in *Landolt-Börnstein Tables*, New Series, Group VI, Volume 1, ed. Voigt H. H., Springer-Verlag, Berlin.

Schrijver C. J., 1987, *Astron. Astrophys.*, **172**, 111.

Schrijver H., 1997, *The Hipparcos and Tycho Catalogues* vols 5 and 10, ESA Publications Division, Noordwijk.

Simon T., 1986, in *New Insights in Astrophysics*, ed. Rolfe E. J., E.S.A., p. 53.

Simon T., 1988, in *A decade of UV astronomy with the IUE satellite*, ed. Rolfe E. J., E.S.A., vol. 1, p. 279.

Simon T. and Drake S. A., 1989, *ApJ*, **346**, 303.

Simon T. and Fekel F. C., 1987, *ApJ*, **316**, 434.

Sitterly B. W., 1930, *Contr. Princeton Univ.*, **11**, 21.

Slee O. B., Nelson G. J., Stewart R. T., Wright A. E., Innis J. L., Ryan S. G., and Vaughan A. E., 1987, *MNRAS*, **229**, 659.

Snodgrass H. B., 1992, in *The Solar Cycle*, ed. Harvey K. L., *ASP Conf. Ser.*, **27**, p. 205.

Soderblom D. R., Jones B. F., Balachandran S., Stauffer J. R., Duncan D. K., Fedele S. B., and Hudon J. D., 1993, *AJ*, **106**, 1059.

Soderblom D. R., King J. R. and Henry T. J., 1998, *AJ*, **116**, 396.

Söderhjelm S., 1999, *Astron. Astrophys.*, **341**, 121.

Stawikowski A. and Głębocki R., 1994, *A.A.*, **44**, 393.

Stencel R. E. and Backman D. E., 1991, *ApJS*, **75**, 905.

Stępień K., 1994, *Astron. Astrophys.*, **292**, 191.

Strassmeier K. G., 1994, *Astron. Astrophys.*, **281**, 395.

Strassmeier K. G., Hall D. F., Fekel F. C., and Scheck M., 1993, *Astron. Astrophys.*, **100**, 173.

Strassmeier K. G., Hall D. S., Zeilik M., Nelson E., Eker Z. and Fekel F. C., 1988, *Astron. Astrophys.*, **72**, 291.

Strassmeier K. G., Handler G, Paunzen E. and Rauth M., 1994, *Astron. Astrophys.*, **281**, 855.

Strassmeier K. G. and Olah K, 1992, *Astron. Astrophys.*, **259**, 595.

Strassmeier K. G., Rice J., Wehlau W., Vogt S., Hatzes A., Tuominen I., Piskunov N., Hackman T. and Poutanen M., 1991, *Astron. Astrophys.*, **247**, 130.

Tagliaferri G., Covino S., Cutispoto G., and Pallavicini R., 1999, *Astron. Astrophys.*, **345**, 514.

Taylor B. J., 1986, *ApJS.*, **60**, 577.

Traub W. and Roesler F. L., 1971, *ApJ*, **163**, 629.

Tuominen I., Moss D. and Rüdiger G., eds, 1991, *Proc. IAU Coll. 130, The Sun and Cool Stars: activity, magnetism, dynamos*, Springer-Verlag, Berlin.

Vogt S. S., 1981, *ApJ*, **250**, 327.

Vogt S. S. and Fekel F. C., 1979, *ApJ*, **234**, 958.

Vogt S. and Hatzes A., in *Proc. IAU Coll. 130, The Sun and Cool Stars: Activity, Magnetism, Dynamos*, eds Tuominen I., Moss D. and Rüdiger G., Springer-Verlag, Berlin, p. 297.

Weiler E. J., Owen F. N., Bopp B. W., Schmitz M., Hall D. S., Fraquelli D. A., Piirola V., Ryle M. and Gibson D. M., 1978, *ApJ*, **225**, 919.

Welty A. D., Ramsey L. W., Iyengar M., Nations H. L. and Buzasi D. L., 1993, *PASP*, **105**, 1427.

Wilson R. E., 1979, *ApJ*, **234**, 1054.

Wilson R. E., 1994, *PASP*, **106**, 921.

Wood B. E., Brown A., Linsky J. L., Kellet B. J., Bromage G. E., Hodgkin S. T. and Pye J. P., 1994, *ApJS*, **93**, 287.

Woolley R., Epps, E. A., Penston M. J., and Pocock S. B., 1970, *Roy. Observ. Ann.*, No. 5.

Wolstencroft R. D., Savage A., Clowes R. G., MacGillivray H. T., Leggett S. K. and Kalafi M., 1986, *MNRAS*, **223**, 279.

Worley C. E., 1989, *Publ. U.S. Naval Obs.*, **24**, Part 3.

Zahn J. P., 1977, *Astron. Astrophys.*, **57**, 383.

Zeilik M. and Smith E. v P., 1987, *Introductory Astronomy and Astrophysics*, Saunders, Philadelphia.

Appendix A

```
! Procedure rvfit2.prg
!   Fits a pair of gaussian or cauchy functions to an absorption-line
!   which has been doubly doppler-shifted and directly gives the two
!   barycentrically-corrected radial velocities.
!   Initial values for the functions are set using the graphics cursor.
!
!   Requires a normalised reduced spectrum in MIDAS .bdf format.  The
!   descriptor BARCOR/r/1/1 containing the heliocentric barycentric
!   correction must be present.
!
! Use:
!   @@ rvfit2 [name of spectrum]
!
! Written by Lyndon Watson, 1996 July,
! Last modified 1998 January.

! Initialise and collect name of spectrum if not given.

define/local barcor/r/1/1 0
define/local length/r/1/1 0
define/local blueend/r/1/1 0
define/local redend/r/1/1 0
define/local wavestep/r/1/1 0
define/local linid/r/1/1 0
define/local subblue/r/1/1 0
define/local subred/r/1/1 0
define/local answer/c/1/1 " "
define/local A/r/1/1 0.
define/local B/r/1/1 0.
define/local C/r/1/1 0.

set/format F20.12

write/out " "
define/parameter P1 ? I "Enter name of spectrum: "
```

```
copy/dk {P1} BARCOR barcor
copy/dk {P1} NPIX length
copy/dk {P1} START blueend
copy/dk {P1} STEP wavestep
compute/keyword redend = {blueend}+(({length}-1)*{wavestep})

GETLINE:
inquire/keyword linid "Rest wavelength (A) of line: "

compute/keyword subblue = {linid} - 4
if {subblue} .LT. {blueend} compute/keyword subblue = {blueend}
compute/keyword subred = {subblue} + 8
if {subred} .GT. {redend} compute/keyword subred = {redend}
extract/image {P1}sub = {P1}[{subblue}:{subred}]

compute/keyword A = ({subblue}-linid)*299792.458/linid + barcor
copy/kd A {P1}sub START
compute/keyword A = {wavestep}*299792.458/linid
copy/kd A {P1}sub STEP
write/descr {P1}sub CUNIT "flux              km/s      "

set/graph pmode=1 ltype=1 stype=0 colour=1 xaxis=auto yaxis=0.6,1.1,.2,.1
plot/row {P1}sub

GETVAL:
! delete/table rvfit2_fit NO
! create/table rvfit2_fit 31 24
! create/column rvfit2_fit :FUNCTIONS "" A60 C*60
! create/column rvfit2_fit :PARAMETERS "" A60 C*60

write/keyword IN_A/c/1/60 " " ALL
write/keyword OUT_A/C/1/60 " " ALL
IN_A = "rvfit2"

INPUTI = 0

RUN APP_EXE:fittable

rvfit2_fit,:FUNCTIONS,@1 = "POLY(X;A,B,C)"
rvfit2_fit,:PARAMETERS,@1 = "A=1. B=0. C=0."

! Collect initial values for the fit

! write/out " "
```

```
! inquire/keyword answer "Fit a gaussian (G) or cauchy (C) function (G/C)? "

! if "{answer}" .eq. "G" then
rvfit2_fit,:FUNCTIONS,@2 = "GAUSS(X;A2,B2,C2)"
rvfit2_fit,:FUNCTIONS,@3 = "GAUSS(X;A3,B3,C3)"
! endif

! if "{answer}" .eq. "C" then
! rvfit2_fit,:FUNCTIONS,@2 = "CAUCHY(X;A2,B2,C2)"
! rvfit2_fit,:FUNCTIONS,@3 = "CAUCHY(X;A3,B3,C3)"
! endif

write/out " "
write/out "Define the first absorption line:"
write/out "First mark the centre, then the FWHM, left then right"
write/out " "

get/gcurs {P1}sub
A(1) = {{P1}sub,:X_COORD,@2}
B(1) = {{P1}sub,:X_COORD,@3}
compute/keyword C = {B}-{A}
B(1) = {{P1}sub,:VALUE,@1}
compute/keyword A = {B}-1
B(1) = {{P1}sub,:X_COORD,@1}

rvfit2_fit,:PARAMETERS,@2 = "A2={A}  B2={B}  C2={C}"

write/out " "
write/out "Define the second absorption line:"
write/out "First mark the centre, then the FWHM, left then right"
write/out " "

get/gcurs {P1}sub
A(1) = {{P1}sub,:X_COORD,@2}
B(1) = {{P1}sub,:X_COORD,@3}
compute/keyword C = {B}-{A}
B(1) = {{P1}sub,:VALUE,@1}
compute/keyword A = {B}-1
B(1) = {{P1}sub,:X_COORD,@1}

rvfit2_fit,:PARAMETERS,@3 = "A3={A}  B3={B}  C3={C}"

read/table rvfit2_fit
```

```
! fit the function to the spectrum and display

write/key outputi/i/1/1 0
compute/keyword IN_A = "rvfit2"
compute/keyword OUT_A = "rvfit2_fit"
RUN APP_EXE:tablefit

set/fit method=MGN

fit/image 50,0.0001,0.2 {P1}sub rvfit2

set/graph colour=2
select/fun rvfit2 1,2
compute/fit fit1 = rvfit2
overplot/row fit1
select/fun rvfit2 1,3
compute/fit fit2 = rvfit2
overplot/row fit2

write/out " "
write/out "Enter - R to re-examine this line"
write/out "      - L to examine another line in this spectrum"
write/out "      - or any other key to end"
inquire/keyword answer "    : - "

if "{answer}" .eq. "R" then
goto GETVAL
endif

if "{answer}" .eq. "L" then
goto GETLINE
endif

delete/fit rvfit2 NO
delete/image {P1}sub NO
delete/table {P1}sub NO
delete/table rvfit2_fit NO
```

Appendix B

```
! Procedure perstep.prg
!  Computes a phase column for a table of photometric or radial-velocity
!  data and plots phased V photometry or radial velocities for periods
!  starting with a specified period in specified increments.
!
!  The table must have columns labelled either :HJD and :V or :DATE and :RADVEL.
!  Set graphics parameters before invoking this program.
!
! Use:
!  @@ perstep [name of table]
!
! Written by Lyndon Watson, 1997 October.

! Initialise and collect name of table if not given.

define/local sper/r/1/1 0.5
define/local peri/r/1/1 0.00001
define/local perm/r/1/1 10.0
define/local kind/c/1/1 " "
define/local answer/c/1/1 " "

write/out " "
define/parameter P1 ? I "Enter name of table: "

! Collect kind of data

GETKIND:
inquire/keyword kind "Photometric or radial-velocity data (p/r)? "
if kind .ne. "p" then
  if kind .ne. "P" then
    if kind .ne. "r" then
      if kind .ne. "R" then
        goto GETKIND
      endif
    endif
```

```
  endif
endif

! Collect mode of operation

GETMODE:
inquire/keyword answer "Run automatically or under manual control (a/m)? "
if answer .ne. "a" then
  if answer .ne. "A" then
    if answer .ne. "m" then
      if answer .ne. "M" then
        goto GETMODE
      endif
    endif
  endif
endif

! Collect periods and increment

GETPER:
inquire/keyword sper "Starting period: "
if answer .eq. "a" then
  inquire/keyword perm "Ending period: "
endif
inquire/keyword peri "Period increment: "
write/out " "

! Compute phase column and plot phased data

PHASER:
compute/table {P1} :PERIOD = {sper}
if kind .eq. "p" then
  compute/table {P1} :PHASE = (mod(:HJD,:PERIOD))/:PERIOD
  plot/table {P1} :PHASE :R
endif
if kind .eq. "r" then
  compute/table {P1} :PHASE = (mod(:DATE,:PERIOD))/:PERIOD
  plot/table {P1} :PHASE :RADVEL
endif
write/out "Period: {sper}"

! Collect next instruction or plot next period

if answer .eq. "a" then
```

```
  sper(1) = sper(1) + peri(1)
  if {sper} .gt. {perm} then
    goto GETOUT
    else
    goto PHASER
  endif
else
  write/out " "
  write/out "Enter N for next period."
  write/out "Enter C to change period and increment."
  write/out "Enter Q to quit."
  GETANS:
  inquire/keyword answer "> "
  if answer .eq. "N" then
    sper(1) = sper(1) + peri(1)
    goto PHASER
  elseif answer .eq. "C" then
    goto GETPER
  elseif answer .eq. "Q" then
    goto GETOUT
  elseif answer .ne. "Q" then
    goto GETANS
  endif
endif
GETOUT:
```

Appendix C

```
      implicit real*8 (a-h,o-z)
      implicit integer (i-n)
c
      dimension h(0:93),v(93),X(0:94),y(0:94),z(0:94)
      dimension b(0:93),c(0:94),d(0:93)
      dimension deltang(0:94),resid(0:94),flux(0:1500)
      dimension sflux(1500),vels(1500),splinepoint(1500)
c
      character*15 bmodelfile,specfile,scanfile
      character*1 ans
c
      bluelimit = -0.0
      redlimit = 4.0
c
      print*
      print*,'ScanKurucz program for creating a cubic spline'
      print*,'interpolation of a Kurucz model Balmer line and scanning'
      print*,'it across a normalized, reduced spectral order to find'
      print*,'the position of best fit in radial velocity space.'
      print*
      print*,'Enter name of file containing the Kurucz model line.'
      read(5,'(a15)') bmodelfile
1000  print*,'Enter spectrum filename.'
      read(5,'(a15)') specfile
1010  print*,'What is the desired line core depth?'
      read*,sdepth

c Open and read the single-column spectrum file
      open(unit = 4, file = specfile, status = 'old')
      print*,'Reading file ',specfile
      read(4,*) startd,stepd,npixd
      read(4,*) barcor
      read(4,*) (sflux(i),i=1,npixd)
      close(unit=4)
```

```
c Open and read the Kurucz model line file
      open(unit = 4, file = bmodelfile, status = 'old')
      print*,'Reading file ',bmodelfile
      depth = 1.0
      read(4,*) refline
      do 1030 i = 0,94,1
        read(4,1020) deltang(i),resid(i)
        if (resid(i).lt.depth) depth = resid(i)
1020  format(f6.1,1x,f7.3)
1030  continue
      close(unit=4)

c Create a column of radial velocities
      vstart = (((startd - refline) * 299792.458)/refline) + barcor
      vstep = (stepd * 299792.458)/refline
      do 1040 i = 1,npixd,1
        vels(i) = vstart + (vstep * (i-1))
1040  continue

c Convert wavelength calibration to radial velocities
      do 1050 i = 0,94,1
        deltang(i) = (deltang(i) * 299792.458)/refline
1050  continue

c Set up an array of intervals between given points
      do 1060 i = 0,93,1
         h(i) = deltang(i+1)-deltang(i)
1060  continue

c Set up the solution vector
      do 1070 i = 1,93,1
        v(i) = (3*(resid(i+1)*h(i-1)-resid(i)*(deltang(i+1)-
     2  deltang(i-1))+resid(i-1)*h(i)))/(h(i-1)*h(i))
1070  continue

c Set up and solve the tridiagonal linear system
      x(0)=1
      y(0)=0
      z(0)=0
      do 1080 i = 1,93,1
        x(i) = 2*(deltang(i+1)-deltang(i-1))-(h(i-1)*y(i-1))
        y(i) = h(i)/x(i)
        z(i) = (v(i)-h(i-1)*z(i-1))/x(i)
1080  continue
```

```
      x(94)=1
      y(94)=0
      c(94)=0
      do 1090 j = 93,1,-1
        c(j) = z(j)-y(j)*c(j+1)
        b(j) = ((resid(j+1)-resid(j))/h(j))-(h(j)*(c(j+1)+2*c(j))/3)
        d(j) = (c(j+1)-c(j))/(3*h(j))
1090  continue
        c(0) = z(0)-y(0)*c(1)
        b(0) = ((resid(1)-resid(0))/10.0)-(10.0*(c(1)+2*c(0))/3)
        d(0) = (c(1)-c(0))/(30.0)

c Interpolate on cubic spline from bluelimit to redlimit
      i = 0
      j = 0
      startp = (bluelimit*299792.458)/refline
      endp = (redlimit*299792.458)/refline
1100  splinepoint(i) = startp + (i * vstep)
      if (splinepoint(i).le.endp) then
1110    if (splinepoint(i).ge.deltang(j+1)) then
          j = j + 1
          go to 1110
        endif
        abscis =  splinepoint(i) - deltang(j)
        flux(i) = resid(j)+b(j)*abscis+c(j)*abscis**2+d(j)*abscis**3
        i = i + 1
        go to 1100
      endif
      icount = i-1

c Scale the interpolated line according to companion's share of light
        scalefactor = (1-sdepth)/(1-depth)
        do 1120 i = 0,icount,1
          drop = (1 - flux(i))*scalefactor
          flux(i) = 1 - drop
1120    continue

c Start scanning across stellar spectrum
      rmserr = 1.0
      bestvel = 0.0
      do 1140 i = 1,(npixd-icount),1
        sqerr = 0.0

c Compute rms error in fit at each spectral data-point
```

```
        do 1130 j = 0,icount,1
          sqerr = sqerr + (sflux(i+j) - flux(j))**2
1130    continue

c Test for best fit, and next scan
        rooterr = sqrt(sqerr/icount)
        if (rooterr.lt.rmserr) then
          rmserr = rooterr
          bestvel = vels(i)
          bestpos = i
        endif
1140  continue

c Compute best-fit velocity for whole and half model lines
      if ((abs(bluelimit).ge.stepd).and.(redlimit.ge.stepd)) then
        bestvel = bestvel + (startp + endp)/2
      endif
      if (redlimit.lt.stepd) bestvel = bestvel + abs(startp)

c Display results
      print*
      print*,'Best-fit radial velocity: ',bestvel,' km/s'
      print*,'RMS error in fit: ',rmserr

c Keep a graphics source file?
      print*
      print*,'Keep a graphics record of the fit (Y/N)?'
      read(5,'(a1)') ans
      if ((ans.eq.'Y').or.(ans.eq.'y')) then
        do 1150 i = 1,bestpos-1,1
          splinepoint(i) = 0.0
1150    continue
        do 1160 i = bestpos,bestpos+icount-1,1
          splinepoint(i) = flux(i-bestpos)
1160    continue
        do 1170 i = bestpos+icount,npixd,1
          splinepoint(i) = 0.0
1170    continue
        print*,'Enter output filename.'
        read(5,'(a16)') scanfile
        open(unit=10,file=scanfile,status='new')
        do 1190 i = 1,npixd,1
          write(10,1180) vels(i),sflux(i),splinepoint(i)
1180  format(f8.3,1x,e12.5,1x,e12.5)
```

```
1190     continue
         close(unit=10)
       endif

c Try a different scale?
       print*
       print*,'Rescan with a different spectral line depth (Y/N)?'
       read(5,'(a1)') ans
       if ((ans.eq.'Y').or.(ans.eq.'y')) go to 1010

c Scan another spectrum or end
       print*
       print*,'Scan another spectrum with the same model line (Y/N)?'
       read(5,'(a1)') ans
       if ((ans.eq.'Y').or.(ans.eq.'y')) go to 1000

       end
```

Appendix D

```
      implicit real (a-h,o-z)
      implicit integer (i-n)
c
      dimension tcalib(0:1279),tflux(0:1279),ccalib(0:1279)
      dimension cflux(0:1279),acalib(0:1279),aflux(0:1279)
      dimension scalib(1:1280),sflux(1:1280),tsflux(1:1280)
      dimension ctsflux(1:1280),actsflux(1:1280),flux(1:1280)
c
      character*1 ans,alpha
      character*3 ext
      character*12 filename
      character*16 specfile,tfile,cfile,afile,subfile
c
      print*
      print*,'SubStars program for isolating emission profile of an'
      print*,'active-chromosphere star by subtracting from its spectrum'
      print*,'scaled Kurucz model or real stellar spectra representing'
      print*,'any one or more of third light and binary companion stars'
      print*,'and the active star itself.'
      print*
      print*,'The spectrum to be operated on is assumed to be an ASCII'
      print*,'ASCII data file made from a MIDAS image and consisting of'
      print*,'three header lines followed by the spectral fluxes, one'
      print*,'to a line.  The header lines contain (1) the MIDAS START'
      print*,'and STEP descriptors, (2) the barycentric correction and'
      print*,'the radial velocity of the active star, and (3) the HJD.'
      print*,'The filename is presumed to have a .dat extension which'
      print*,'must NOT be typed in.  The results file will have the'
      print*,'same name with the extension .em'
      print*
      print*,'The spectra to be subtracted are assumed to be either'
      print*,'identical in form with the subject spectrum, or to be'
      print*,'model spectra, the files consisting of a single line'
      print*,'header specifying the central wavelength of the model'
      print*,'followed by fluxes, one to each line.  Stellar spectra'
```

```
      print*,'MUST be contained in files with the extension .dat;'
      print*,'model spectra MUST be in files with the extension .mod.'
c
1000  itstar = 0
      icstar = 0
      iastar = 0
      tscale = 0.0
      cscale = 0.0
c
      print*
      print*,'What is the reference wavelength for radial velocity?'
      read(5,*) refline
      print*,'What is the system radial velocity (gamma)?'
      read*,sysgamma

c Collect third light's stellar or model spectrum
      print*,'Do you wish to subtract third light (Y/N)?'
      read(5,'(a1)') ans
      if ((ans.eq.'Y').or.(ans.eq.'y')) then
        itstar = 1
1010    print*,'Enter name of file containing third light spectrum.'
        read(5,'(a16)') tfile
        do 1020 i = 1,13
          alpha = tfile(i:i)
          if (alpha.eq.'.') go to 1030
1020    continue
        go to 1010
1030    ext = tfile(i+1:i+4)
        if ((ext.eq.'DAT').or.(ext.eq.'dat')) then
          call GetStar(tfile,tstart,tstep,npixt,tbarcor,trvel,thjd,
     2    tflux)
          tstart = tstart-((trvel-tbarcor)*refline)/299792.458
          do 1040 i = 0,npixt-1
            tcalib(i) = tstart + (tstep * i)
1040      continue
          goto 1050
        endif
        if ((ext.eq.'MOD').or.(ext.eq.'mod')) then
          call GetModel(tfile,refline,npixt,tflux)
          go to 1050
        endif
        go to 1010
1050    print*,'What fraction of the total light does it contribute?'
        read*,tscale
```

```
      endif

c Collect companion's stellar or model spectrum.
      print*,'Do you wish to subtract a companion star (Y/N)?'
      read(5,'(a1)') ans
      if ((ans.eq.'Y').or.(ans.eq.'y')) then
        icstar = 1
1060    print*,'Enter name of file containing the companion spectrum.'
        read(5,'(a16)') cfile
        do 1070 i = 1,13
          alpha = cfile(i:i)
          if (alpha.eq.'.') go to 1080
1070    continue
        go to 1060
1080    ext = cfile(i+1:i+4)
        if ((ext.eq.'DAT').or.(ext.eq.'dat')) then
          call GetStar(cfile,cstart,cstep,npixc,cbarcor,crvel,chjd,
     2    cflux)
          cstart = cstart-((crvel-cbarcor)*refline)/299792.458
          do 1090 i = 0,npixc-1
            ccalib(i) = cstart + (cstep * i)
1090      continue
          goto 1100
        endif
        if ((ext.eq.'MOD').or.(ext.eq.'mod')) then
          call GetModel(cfile,refline,npixc,ccalib,cflux)
          go to 1100
        endif
        go to 1060
1100    print*,'What fraction of the total light does it contribute?'
        read*,cscale
        print*,'Enter the mass ratio of active star to companion star.'
        read*,rmass
        print*,'Enter the half-amplitude of the active star radial'
        print*,'velocity variations.'
        read*,hamp
        print*
      endif

c Collect absorption spectrum of the active star
      print*,'Do you wish to subtract the active star spectrum (Y/N)?'
      read(5,'(a1)') ans
      if ((ans.eq.'Y').or.(ans.eq.'y')) then
        iastar = 1
```

```
1110    print*,'Enter name of active star absorption spectrum.'
        read(5,'(a16)') afile
        do 1120 i = 1,13
          alpha = afile(i:i)
          if (alpha.eq.'.') go to 1130
1120    continue
        go to 1110
1130    ext = afile(i+1:i+4)
        if ((ext.eq.'DAT').or.(ext.eq.'dat')) then
          call GetStar(afile,astart,astep,npixa,abarcor,arvel,ahjd,
     2    aflux)
          astart = astart - ((arvel - abarcor) * refline)/299792.458
          do 1140 i = 0,npixa-1
            acalib(i) = astart + (astep * i)
1140      continue
          goto 1150
        endif
        if ((ext.eq.'MOD').or.(ext.eq.'mod')) then
          call GetModel(afile,refline,npixa,acalib,aflux)
          go to 1150
        endif
        go to 1110
      endif

c Collect the stellar spectrum which is to be subtracted from
1150  print*
      print*,'Enter spectrum filename WITHOUT extension.'
      read(5,'(a12)') filename
      specfile = filename//'.dat'
      subfile = filename//'.em'
      call GetStar(sfile,sstart,sstep,npixs,sbarcor,srvel,shjd,sflux)

c Interpolate, scale and subtract the third light
      if (itstar.eq.1) then
        startp = sstart + (sysgamma*refline)/299793.458
        call SubLine(npixt,tcalib,tflux,startp,npixs,sstep,tscale,
     2  sflux,tsflux)
      else
        do 1160 i = 1,npixs
          tsflux(i) = sflux(i)
1160    continue
      endif

c Interpolate, scale and subtract the companion's light
```

```
      if (icstar.eq.1) then
        cvel = sysgamma + (rmass * (hamp - (srvel - sysgamma)))
        startp = sstart + (cvel*refline)/299792.458
        call SubLine(npixc,ccalib,cflux,startp,npixs,sstep,cscale,
     2  tsflux,ctsflux)
      else
        do 1170 i = 1,npixs
          ctsflux(i) = tsflux(i)
1170    continue
      endif

c Renormalize the subject spectrum
      if (itstar.eq.1) then
        rescale = 1 - tscale
        do 1180 i=1,npixs
          flux(i) = tsflux(i)/rescale
1180    continue
      endif
      if (icstar.eq.1) then
        rescale = 1 - cscale
        do 1190 i = 1,npixs
          flux(i) = flux(i)/rescale
1190    continue
      endif

c Interpolate and subtract the active star's absorption spectrum
      if (iastar.eq.1) then
        call SubLine(npixa,acalib,aflux,sstart,npixs,sstep,1,flux,
     2  actsflux)
      else
        do 1200 i = 1,npixa
          actsflux(i) = flux(i)
1200    continue
      endif

c Create a column of radial velocities for spectrum
      do 1210 i = 1,npixs,1
        scalib(i) = ((sstart+((i-1)*sstep)-refline)/refline)*299792.458
1210  continue

c Write output file
      open(unit = 10, file = subfile, status = 'new')
      print*,'Writing file ',subfile
      do 1230 i = 1,npixs,1
```

```
        write(10,1220) scalib(i),sflux(i),tsflux(i),ctsflux(i),
     2  actsflux(i)
1220  format(f8.3,1x,e12.5,1x,e12.5,1x,e12.5,1x,e12.5)
1230  continue

c Next spectrum, restart or end
      print*
      print*,'Subtract from another spectrum of the same star (Y/N)?'
      read(5,'(a1)') ans
      if ((ans.eq.'Y').or.(ans.eq.'y')) go to 1150
      print*,'Restart (Y/N)?'
      read(5,'(a1)') ans
      if ((ans.eq.'Y').or.(ans.eq.'y')) go to 1000
      end

c-----------------------------------------------------------------------

      SUBROUTINE GetStar(starfile,start,step,npix,barcor,rvel,hjd,flux)

      implicit real (a-h,o-z)
      implicit integer (i-n)

      dimension flux(0:1279)

      character*16 starfile

c Read in stellar spectrum
      print*,'Reading file ',starfile
      open(unit = 4, file = starfile, status = 'old')
      read(4,*) start,step
      read(4,*) barcor,radvel
      read(4,*) hjd
      npix = 1
2000  read(4,*,end=2010) flux(npix)
      npix = npix + 1
      go to 2000
2010  npix = npix - 1
      close(unit=4)

      end

c-----------------------------------------------------------------------

      SUBROUTINE GetModel(filename,refline,deltang,resid)
```

```
      implicit real (a-h,o-z)
      implicit integer (i-n)

      dimension deltang(0:1279),resid(0:1279)

      character*16 modelfile

c Open Kurucz model line file and collect its data
      open(unit = 4, file = modelfile, status = 'old')
      print*,'Reading file ',modelfile
      read(4,3000) topline
3000  format(f8.3)
      print*,refline,topline
      if (topline.ne.refline) then
        print*
        print*,'ERROR: model wavelength differs from given wavelength.'
        stop
      endif
      npix = 0
3010  read(4,3020,end=3030) deltang(npix),resid(npix)
        npix = npix + 1
      go to 3010
3020  format(f6.1,1x,f7.3)
3030  npix = npix - 1
      close(unit=4)

c Convert wavelength calibration to absolute values
      do 3040 i = 0,npix,1
        deltang(npix) = deltang(npix) + refline
3040  continue
      return

      end

c-----------------------------------------------------------------------

      SUBROUTINE SubLine(nfit,calib,fluxspline,startp,npix,step,scale,
     2fluxin,fluxout)

      implicit real (a-h,o-z)
      implicit integer (i-n)

      dimension calib(0:1279),fluxspline(0:1279)
```

```
      dimension b(0:1278),c(0:1279),d(0:1278)
      dimension h(0:1278),v(1:1278),x(0:1279),y(0:1278),z(0:1279)
      dimension fluxsub(1:1280),fluxin(1:1280),fluxout(1:1280)

c Set up an array of intervals between wavelength points
      do 4000 i = 0,nfit-2,1
         h(i) = calib(i+1)-calib(i)
4000  continue

c Set up the solution vector
      do 4010 j = 1,nfit-2,1
        v(j) = (3*(fluxspline(j+1)*h(j-1)-fluxspline(j)*(calib(j+1)-
     2         calib(j-1))+fluxspline(j-1)*h(j)))/(h(j-1)*h(j))
4010  continue

c Set up and solve the tridiagonal linear system
      x(0)=1
      y(0)=0
      z(0)=0
      do 4020 i = 1,nfit-2,1
        x(i) = 2*(calib(i+1)-calib(i-1))-(h(i-1)*y(i-1))
        y(i) = h(i)/x(i)
        z(i) = (v(i)-h(i-1)*z(i-1))/x(i)
4020  continue
      x(nfit-1)=1
      y(nfit-1)=0
      c(nfit-1)=0
      do 4030 j = nfit-2,1,-1
        c(j) = z(j)-y(j)*c(j+1)
        b(j) = ((fluxspline(j+1)-fluxspline(j))/h(j))-(h(j)*(c(j+1)+2*
     2         c(j))/3)
        d(j) = (c(j+1)-c(j))/(3*h(j))
4030  continue
        c(0) = z(0)-y(0)*c(1)
        b(0) = ((fluxspline(1)-fluxspline(0))/10.0)-(10.0*(c(1)+2*c(0))
     2         /3)
        d(0) = (c(1)-c(0))/(30.0)

c Interpolate on cubic spline
      i = 0
      do 4050 j = 1,npix,1
        splinepoint = startp + ((j-1) * step)
        if (splinepoint.lt.calib(1)) fluxsub(j) = 1.0
4040    if (splinepoint.ge.calib(i+1)) then
```

```
          i = i + 1
          go to 4040
        endif
        abscis =  splinepoint - calib(i)
        fluxsub(j) = fluxspline(i)+b(i)*abscis+c(i)*abscis**2+d(i)*
     2               abscis**3
        if (splinepoint.gt.calib(npix-1)) fluxsub(j) = 1.0
4050  continue

c Scale the interpolated line according to share of total light
      do 4060 j = 1,npix
        fluxsub(j) = fluxsub(j)*scale
4060  continue

c Subtract the interpolated line fluxes from the spectral fluxes
      do 4070 j = 1,npix,1
        fluxout(j) = fluxin(j) - fluxsub(j)
4070  continue
      return

      end
```

Acknowledgements

I thank my supervisor, Professor John Hearnshaw, for guidance, advice, and innumerable acts of practical assistance, and my mentors, Professors Jack Baggaley and Philip Butler, for their vital help in the later stages of this project.

I thank our observers at Mt John, Alan Gilmore and Pam Kilmartin, for their enthusiasm, for the data which they obtained for me, and for their generous advice whenever I needed it. I thank Mike Clark and John Baker for keeping the instruments working, and Mike and June for their hospitality on the mountain. I thank Bob Donahue of CfA Harvard for providing me with useful papers and ideas. I thank David Buckley of SAAO for his data and advice, and for conceiving this project in the first place.

I thank Karen Pollard, John Pritchard and Frank Fekel for insightful discussion and criticism of my work and practical assistance in the preparation of papers for publication. I thank my fellow students for their companionship and the exchange of ideas and experience, and I particularly thank Irene Cummings, Ed Savage and Ljiljana and Jovan Skuljan for providing me with valuable computer programs and programming advice.

I thank all of those people and organizations who made it possible for me to attend IAU Symposium No. 176 in Vienna: the Wood Fund, the Royal Society of New Zealand, the University of Canterbury and the Department of Physics and Astronomy, the Kingdon-Tomlinson Fund, and the IAU itself.

And I thank my parents who made it possible.

This research made use of the *Simbad* database, operated at CDS, Strasbourg, France, the valuable assistance of which is acknowledged.

This research has made use of data obtained through the High Energy Astrophysics Science Archive Research Center Online Service, provided by the NASA/Goddard Space Flight Center.